IMPROVEMENTS IN ULTRASONICALLY ASSISTED TURNING OF TI 15V3AI3Cr3Sn

by

Agostino Maurotto

A Doctoral Thesis

Submitted in partial fulfilment of the requirements for the award of Doctor of Philosophy of Loughborough University

December 2012

Abstract

Titanium alloys have outstanding mechanical properties such as high hardness, a good strength-to-weight ratio and high corrosion resistance. However, their low thermal conductivity and high chemical affinity to tool materials severely impairs their machinability with conventional techniques. Conventional machining of Ti-based alloys is typically characterized by low depth of cuts and relatively low feed rates, thus adversely affecting the material removal rates (MRR) during the machining process. Ultrasonically assisted turning (UAT) is an advanced machining technique, in which ultrasonic vibration is superimposed on a cutting tool. UAT was shown to improve machinability of difficult-to-machine materials, such as ceramics, glass or hard metals. UAT employment in the industry is, however, currently lacking due to imperfect comprehensive knowledge on materials' response and difficulties in obtaining consistent results.

In this work, significant improvements in the design of a UAT system were performed to increase dynamic and static stiffness of the cutting head. Concurrent improvements on depth-of-cut controls allowed precise and accurate machining operations that were not possible before. Effects of depth of cut and cutting speed were investigated and their influence on the ultrasonic cutting process evaluated. Different cutting conditions -from low turning speeds to higher recommended level- were analysed. Thermal evolution of cutting process was assessed, and the obtained results compared with FE simulations to gain knowledge on the temperatures reached in the cutting zone. The developed process appeared to improve dry turning of Ti-15-3-3-3 with significant reduction of average cutting forces.

Improved surface quality of the finished work-piece was also observed. Comparative analyses with a conventional turning (CT) process at a cutting speed of 10 m/min showed that UAT reduced the average cutting forces by 60-65% for all levels of a_p considered. Temperature profiles were obtained for CT and UAT of the studied alloy. A comparative study of surface and sub-surface layers was performed for CT- and UAT-processed work-pieces with notable improvements for the UAT-machined ones. Two- to three-fold reductions of surface roughness and improvements of other surface parameters were observed for the UAT- machined surfaces. Surface hardness for both the CT- and UAT-machined surfaces was investigated by micro-indentation. The intermittent cutting of the UAT-process resulted in reduction of hardening of the sub-surface layers. Optical and electronic metallographic analyses of cross-sectioned work-pieces investigated the effect of UAT on the grain structure in material's sub-surface layers. Backscatter electron microscopy was also used to evaluate the formation of α-Ti during the UAT cutting process. No grain changes or α-precipitation were observed in both the CT- and UAT-machined work-pieces.

Keywords: *ultrasonic, machining, titanium, turning, cutting force, hybrid machining, surface quality, dry cutting, aerospace alloy, vibration assisted machining.*

Acknowledgements

I would like to thank my supervisor Prof. Vadim V. Silberschmidt, for his help and guidance in the completion of this work. His encouragement, motivation, patience and help in presentation skills had an invaluable effect on the completion of this work.

I would like to express my gratitude to my supervisor Prof. Vladimir I. Babitsky for his consistent encouragement, useful suggestions and clear explanations which worked toward the improvement of my research methods ultimately allowing the completion of this thesis.

I would like to express my sincere thanks to my supervisor Dr. Anish Roy, for his advices and support on improving my writing and presenting skills on all levels. His help and suggestions helped in the timely writing of this work.

I acknowledge with much appreciation the academic and technical staff of the Wolfson School of Mechanical and Manufacturing Engineering. I would like to thank the workshop staff for their help and suggestions in manufacturing the setup, the metrology lab and the microscopy lab staff for their practical help and assistance in evaluating surface profilometry and metallography.

Support of the MaMiNa academic and industrial partners is also much appreciated, in particular Herr. Carsten Siemers and Prof. Hans-Werner Hoffmeister for their help and guidance in understanding better material behavior and machining characteristics.

I am thankful to MaMiNa and office colleagues for their collaboration and advice on

many different issues.

Special thanks to Prof. Alexander Korsunsky of Oxford University for his help and support in understanding the sub-surface effects of ultrasonic vibration.

Finally, I would like to appreciate my wife, Dr. Maulina Sharma, and my parents for their support and enthusiasm toward the completion of this work.

Publications

Maurotto, A., Roy, A., Babitsky, V.I., Silberschmidt, V.V.

Ultrasonically-assisted turning of advanced alloys summary of results for Ti and Ni based alloys. 20th International Workshop on Computational Mechanics of Materials, 8-10 September 2010 Loughborough, UK

Maurotto, A., Roy, A., Babitsky, V.I., Silberschmidt, V.V.

Recent developments in ultrasonically assisted machining of advanced alloys. Proceedings of the 4th CIRP International Conference on High Performance Cutting HPC2010, 24-26 October, 2010, Gifu, Japan. T. Aoyama, Y. Takeuchi (eds.), Vol. 2, pp. 81-84

Muhammad, R., **Maurotto, A.**, Demiral, M., Roy, A., Silberschmidt, V.V.

3D finite element analysis of ultrasonically assisted turning of modern alloys. Proceedings of the International Conference on Computational and Experimental Engineering and Sciences (ICCES'11), Nanjing, China. 19/3, pp. 95-96.

Muhammad, R., **Maurotto, A.**, Roy, A., Silberschmidt, V.V.

Analysis of forces in vibro-impact and hot vibro-impact turning of advanced alloys. Applied Mechanics and Materials Vol. 70 (2011), pp. 315-320. doi:10.4028/www.scientific.net/AMM.70.315

Maurotto, A., Roy, A., Babitsky, V.I., Silberschmidt, V.V.

Analysis of machinability of Ti- and Ni-based alloys. Solid State Phenomena Vol. 188 (2012),pp. 330-338. doi:10.4028/www.scientific.net/SSP.188.330

Maurotto, A., Muhammad, R., Roy, A., Babitsky, V.I., Silberschmidt, V.V.

Comparing machinability of Ti 15-3-3-3 and Ni-625 alloys in UAT. Procedia CIRP 1 (2012), 5th CIRP International Conference on High Performance Cutting, pp. 347-352. doi:org/10.1016/j.procir.2012.04.059

Muhammad, R., **Maurotto, A.**, Roy, A., Silberschmidt, V. V.

Hot Ultrasonically Assisted Turning of Ti Alloy. Procedia CIRP 1 (2012),

5th CIRP International Conference on High Performance Cutting, pp.336-341.

doi:org/10.1016/j.procir.2012.04.060

Muhammad, R., **Maurotto, A.**, Roy, A., Silberschmidt, V.V.

Ultrasonically assisted turning of Ti-6Al-2Sn-4Zr-6Mo. Journal of Physics, Conference Series accepted and awaiting publication

Maurotto, A., Muhammad, R., Roy, A, Silberschmidt, V.V.

Enhanced ultrasonically assisted turning of a β-titanium alloy. Ultrasonics, in press. http://dx.doi.org/10.1016/j.ultras.2013.03.006

Symbols and abbreviations

a	amplitude of vibration
a_p	dept-of-cut (DOC)
f	feed rate [mm/rev]
f_q	frequency of vibration
n	rotational speed
t_x	chip thickness
D	diameter
D_c	length between tool fixation and cross-slide middle point
E	Young's modulus
$\underline{F}$	friction force
F_c	cutting force
F_a, F_f	cutting force, axial component
F_r	cutting force, radial component
F_t	cutting force, tangential component
L_c	contact length
$\underline{N}$	normal-to-rake face force vector
P3z	mean of the third point height
PSm	mean spacing at mean line
PV	peak to valley parameter
$\underline{R}$	resultant cutting force vector
R_a	arithmetic average heigth
R_n	tool nose radius

R_{max}	maximum roughness
R_q, R_{rms}	root-mean square roughness
R_{ku}	kurtosis of the profile
R_{sk}	skewness of the profile
R_z	ten-point height of the profile
S	specific pressure
S_a	average absolute deviation of the surface
S_{ku}	kurtosis of the surface
S_{pd}	surface peak density
S_{sk}	skewness of the surface
V	cutting velocity
V_c	critical cutting velocity
V_t	chip-flow velocity
α	rake angle
γ	relief (chamfer) angle
λ	friction angle
μ	average friction coefficient
σ	surface height values
φ	shear plane
Φ	shear angle
1D	mono-dimensional
2D	two-dimensional
AVG	average
CT	conventional turning
CVD	chemical vapour deposition

EBSD	electron backscatter diffraction
EMF	electro-magnetic field
EPSRC	Engineering and Physical Sciences Research Council
FE, FEA	finite elements, finite elements analysis
FEGSEM	field emission scanning electron microscopy
MosFet	metal–oxide–semiconductor field-effect transistor
MRR	material removal rate
PCD	poly-crystalline diamond
PTFE	polytetrafluoroethylene
PVD	phisical vapour deposition
RPM	revolution per minute
SEM	scanning electron microscopy
SMA	shape memory alloy
STD	standard deviation
UAM	ultrasonically assisted machining
UAT	ultrasonically assisted turning
VAM	vibration assisted machining

Contents

Abstract 1

Acknowledgements 3

Publications 5

Symbols and abbreviations 7

1 Introduction 18

Aims and objectives 19

2 Mechanics of machining 22

2.1 Lathe and parameters of turning 22

2.2 Cutting forces 24

2.3 Cutting tools 32

2.4 Evolution of vibro-assisted machining 35

Parallel developments of VAM 37

3 Ultrasonically assisted machining 61

3.1 Methods of generation of the ultrasonic vibration 62

3.2 Ultrasonically assisted turning 67

4 Test rig 74

4.1 Introduction 74

4.2 UAT lathe 75

4.3 Second prototype (Stage II) 76

4.4 Third prototype (Stage III) 80

4.4.1 Finite element analysis (FEA) 88

4.4.2 Power characterization 98

4.4.3 Summary 101

5 Experimental analyses 103

5.1 Titanium 15V3Al3Cr3Sn 103
5.2 Experimental results with Stage II prototype 104
5.3 Stage III UAT system 111
5.3.1 Force sensors 111
5.3.2 Signal generator and power circuit 115
6 Force measurements 120
6.1 Cutting parameters 120
6.2 Low-speed cutting force measurements 123
6.3 Variable-speed cutting force measurements 128
6.4 Impulsive force measurements 131
6.5 Summary 135
7 Thermal analysis 137
7.1 Thermal imaging equipment 139
7.2 Thermal measurements 142
Comparative thermal analysis 145
8 Surface quality 149
8.1 Parameters and instruments 150
8.1.1 Laser interferometry 153
8.1.2 Surface analysis 154
8.2 Evaluation of surface hardness 158
9 Metallographic tests 164
10 Discussion 173
10.1 Force reduction 173
10.2 Cutting temperature 176
10.3 Surface quality 177
11 Conclusions 182

Future works 184
Appendices 186
A1 Methodology 186
A1.2 Operations before machining 186
A1.2.1 Mechanical checklist 187
A1.2.2 Vibration checklist 189
A1.2.3 Sensors checklist 191
A3 Surface analysis 193
References 198

Table of figures

Figure 1-1: Thesis flowchart 21

Figure 2-1: Lathe schematics. [Boothroyd & Knight, 1989] 22

Figure 2-2: Schematic process of turning. [Trent & Wright, 2000] 23

Figure 2-3: Other cutting parameters [Childs *et al.*, 2000] 24

Figure 2-4: Main forces acting on the cutting tool [Childs *et al.*, 1972] 25

Figure 2-5: Merchant's force circle [Merchant, 1945] 27

Figure 2-6: Projected contact length and chip-rake face contact 31

Figure 2-7: Main vibration directions. 39

Figure 2-8: Schematic of tool with embedded thermocouple 42

Figure 2-9: Ultrasonic two axis vibrator using piezoelectric actuators 48

Figure 2-10: Inclined direction of vibration for ultrasonically assisted turning tool 50

Figure 2-11: Chatter suppression for UAT cutting (simulations) 51

Figure 2-12: Micro-photography of work-piece cross-section showing crack damage 53

Figure 2-13: Comparison of cut surfaces: b) conventional turning, c) UAT 54

Figure 3-1: Schematic of Langevin concentrator head used in UAT [Maurotto *et al.*, 2000] 61

Figure 3-2: Magnetostrictive and piezo transducers schematic comparison [Thoe *et al.*, 1998] 64

Figure 3-3: Industrial piezoelectric transducer [Brehl & Dow, 2008] 66

Figure 3-4: Rear view of the cutting head 68

Figure 3-5: Simplifier model of transducer [Voronina *et al.*, 2008] 73

Figure 4-1: Early prototype [Voronina *et al.*, 2008] 75

Figure 4-2: Stage II prototype 77

Figure 4-3: Stage II schematic 78

Figure 4-4: Stage III prototype 80
Figure 4-5: Stage III mounting post 81
Figure 4-6: Stage III prototype close up 82
Figure 4-7: Stage III schematic 85
Figure 4-8: Drawing of Stage III prototype 87
Figure 4-9: Optimization process of cutting assembly 88
Figure 4-10:Schematic of simple mass attached to spring with coefficient k and applied harmonic force F(t) 89
Figure 4-11: Model of cutting head with mesh 91
Figure 4-12: Modal shape computed for frequency slightly below resonance frequency of transducer 94
Figure 4-13: Modal shape computed for frequency slightly above resonance frequency of transducer 95
Figure 4-14: Modal shape for frequency of 18111 Hz showing large deformations of cutting assembly 96
Figure 4-15: Vibrational modes for first four natural frequencies 97
Figure 4-16: Characteristics of transducer around resonance frequency of 17.8 kHz 99
Figure 4-17: Block diagram with power footprint of vibration system. 101
Figure 5-1: Head displacement vibration in radial direction in CT and UAT, a_p=0.1 mm, V=10 m/min, f=0.1 mm/rev [Maurotto *et al.*, 2000] 105
Figure 5-2: Zygo interferometer and its control equipment 107
Figure 5-3: SEM image of conventionally cut chip (a) and ultrasonically cut one (b) (cross section), a_p = 0.5 mm,V = 10 mm/rev, f = 0.1 mm/rev 108
Figure 5-4: Stage II surface analysis of finished work-piece (a_p = 100, 200, 300 µm, f = 0.1 mm/rev, V = 10 m/min) 110
Figure 5-5: Kistler dynamometer 9257 [Kistler, 2011] 110
Figure 5-6: Kistler 5001 charge amplifier [Kistler, 2011] 113

Figure 5-7: Matchbox 117

Figure 5-8: Block diagram of connections in power circuit 118

Figure 6-1: Evolution of force components signals during single run, a_p=0.2 mm, V=10 m/min, f=0.1 mm/rev 122

Figure 6-2: Lathe Inverter ACS150 by ABB..... 123

Figure 6-3: Cutting forces for CT and UAT at various depths of cut, V=10 m/min, f=0.1 mm/rev 124

Figure 6-4: Movement of the tool during the cutting process..... 125

Figure 6-5: Reduction of tangential and radial components in UAT, V=10 m/min, f=0.1 mm/rev 126

Figure 6-6: Cutting forces for CT and UAT for a_p=0.2 mm at different cutting speeds, f=0.1 mm/rev 128

Figure 6-7: Percent reduction of tangential and radial components at variable cutting speeds for a_p=0.2 mm, f=0.1 mm/rev 130

Figure 6-8: Dimensions of piezoceramic ring 132

Figure 6-9: Schematics of peak force sensor 132

Figure 6-10: Peak force sensor, first prototype with Teflon insulators; mounted on the cutting head [see Figure 6-9]..... 133

Figure 6-11: Peak force signal during UAT cutting (UAT in red) and with tool disengaged (ES in blue), in green the difference of signals (Sub in green)..... 134

Figure 7-1: Band resistance heater and work-piece 140

Figure 7-2: SC3000 camera mounted on cross slide 141

Figure 7-3: Thermal image of UAT cutting process, a_p=0.2 mm, V=10 m/min, f=0.1 mm/rev 142

Figure 7-4: Temperature plot for a_p=0.1 mm in CT, dashed line denote end of transient, V=10 m/min, f=0.1 mm/rev 145

Figure 7-5: Comparison of chip maximum temperatures for a_p=0.1 mm in CT (blue) and UAT (red), V=10 m/min, f=0.1 mm/rev 146

Figure 7-6: Comparison of chip maximum temperatures for a_p=0.2-0.5 mm in CT (blue) and UAT (red), V=10 m/min, f=0.1 mm/rev 146

Figure 8-1: Definition of Ra 150

Figure 8-2: Definition of Rz 151

Figure 8-3: Skewness of surface profile 152

Figure 8-4: Kurtosis of surface profile 152

Figure 8-5: Surface plot for a_p=0.2 mm in CT a) and UAT b), V=10 m/min, f=0.1 mm/rev 154

Figure 8-6: Roughness Ra for varying a_p, V=10 mm/rev, f=0.1 mm/rev 156

Figure 8-7: Micro-impact traces for a_p=0.2 mm, V=10 m/min, f=0.1 mm/rev 157

Figure 8-8: Spd for CT and UAT machined surfaces, V=10 m/min, f=0.1 mm/rev . 158

Figure 8-9: NanoTest NTX^3 160

Figure 8-10: Indentation sample preparation 161

Figure 8-11: Surface hardness for CT and UAT machined surfaces at different a_p, V=10 m/min, f=0.1 mm/rev 162

Figure 9-1: Embedding hot press and etched samples 164

Figure 9-2: Etched cross sections of work-pieces: (a) virgin-state bulk sample; (b, d) machined with CT; (c, e) machined with UAT. Note different scales, a_p=0.5 mm, V=10 mm/rev, f=0.1 mm/rev 166

Figure 9-3: Carl Zeiss electronic microscope 167

Figure 9-4: EMTECH Au-Pd sputter coater coating sample 169

Figure 9-5: SEM images of gold-coated etched sample (a_p=0.5 mm): left CT, right UAT, V=10 m/min, f=0.1 mm/rev 170

Figure 9-6: Backscatter images of CT (a) and UAT (b) machine work-pieces (a_p=0.5 mm, V=10 m/min, f=0.1 mm/rev) 171

Figure 9-7: SEM images of uncoated etched sample (a_p=0.5 mm, V=10 m/min, f=0.1 mm/rev) for CT (a) and UAT (b) 172

Figure 10-1: Schematics of the cutting areas: front a), side b) 174

Figure 10-2: Specific cutting pressure at various cutting depths in CT and UAT at V=10 m/min, f=0.1 mm/rev. 175

Figure 10-3: Distribution of temperature in cutting zone for CT and UAT (a_p = 0.2 mm, V = 10 m/min) [Muhammad *et al., 2012]* 177

Figure 10-4: α-casing formations in Ti alloy..... 180

1 Introduction

Machining of titanium alloys was identified as one of the most important manufacturing processes since broad adoption of these alloys in aerospace, automotive, chemical and biomedical industries [Arrazola *et al.,* 2009]. β-titanium alloys offer high tensile strength due to their enhanced inherent hardness, with increased fatigue strength and better forming properties in comparison to near-α-or α+β-titanium alloys. Various mission-critical components in the aerospace industry require removal of up to 90% of the total material to obtain finished work-pieces. Conventional turning (CT) of such hard alloys causes high cutting forces imposed by a tool on a work-piece, ultimately leading to high stresses, strains and temperatures in the machined material. Poor thermal conductivity and high chemical affinity of such alloys to traditional tool materials severely impair their machinability [Sun & Guo, 2009]. Machining processes of titanium alloys are characterized by low cutting feeds and speeds, typically in the range between 12 to 38 m/min for aged alloys [Donachie, 2004]. Use of cutting fluids for cooling and lubrication is typically recommended in the machining of titanium alloys to avoid rapid tool wear. Their primary goal is to dissipate generated heat thus avoiding localized thermal expansions at the tool tip. Also, the lubricant reduces friction at the tool-work-piece interface improving machining efficiency [Chandrasekaran, 1972; Ezugwu *et al.*, 2003]. Sustainability is negatively affected by large volumes of coolant and lubricant needed to limit thermal excursions in the machined work-piece. That and the relatively low MRR when compared to other ferrous and non-ferrous alloys increase machining costs. Dry machining methods address current needs for environmentally

friendly manufacturing techniques by removing flood cutting-fluid supply [Weinert *et al.,* 2004; Mativenga & Rajemi, 2011]. Dry machining compared with these using coolant flow methods reduces the energy footprint of machined products, since a significant power is spent on pumping high pressure coolants. Elimination of lubricants and coolants presents some additional challenges in machining of difficult-to-cut materials. High cutting temperatures and high cutting forces together with rapid tool wear ultimately require several finishing steps to be incorporated into a manufacturing process in order to obtain the desired component quality, increasing the overall machining cost. Ultrasonic assisted turning was used to improve the machining process of difficult-to-machine alloys, however, so far has it not been industrially employed. Drastic changes of elastic-plastic behaviour of the work-piece material and of contact conditions, with dry friction in the region of interactions between two surfaces transformed into quasi-viscous friction in the presence of ultrasonic vibration [Astashev & Babitsky, 1998], are the desirable effects observed in ultrasonically assisted machining. In this study, a conventional lathe was converted into one for ultrasonically assisted machining by a modular system.

Aims and objectives

The aim of the project is to improve the machining of difficult-to-machine alloys in dry turning and to investigate the effects of ultrasonically assisted turning on the work-piece material. Enhanced modularity and design improvements of the cutting head will be evaluated for future industrial application of the technique.

Objectives:

1) To study and suggest design improvements by evaluation of design

modularity for possible future conversions of industrial machines and increase in accuracy, precision and ease of operation.

2) To analyze the power response of the UAT system by power characterizations of driving circuit and transducer in attempt to improve stability and amplitude of the vibration.
3) To study cutting forces by evaluation of its reduction at different depths of cut and cutting velocities to characterize the response of the system to load-variations.
4) To analyze the response of the system toward cutting parameter by studying the stability of the cutting force reduction at cutting speeds close to critical velocity while evaluating cutting temperatures in CT and UAT.
5) To investigate the response of material to the ultrasonic vibration by surface quality, surface hardness, material's grains and structure analyses in surface and sub-surface layers.
6) To understand the effects of CT- and UAT-dry-cutting by evaluating intra-grain and surface precipitation of α-titanium.

This work is organized in chapters [Figure 1-1], with chapters 2 to 4 discussing the mechanics of the process and the state of the art. Chapter 5 details the design improvements that were implemented in the early prototype and the reasons behind them. Chapters 6 to 10 deal with the cutting tests, measurements and experimental equipment employed in this work. In chapters 10 to 12 the results are discussed and the final conclusions drawn.

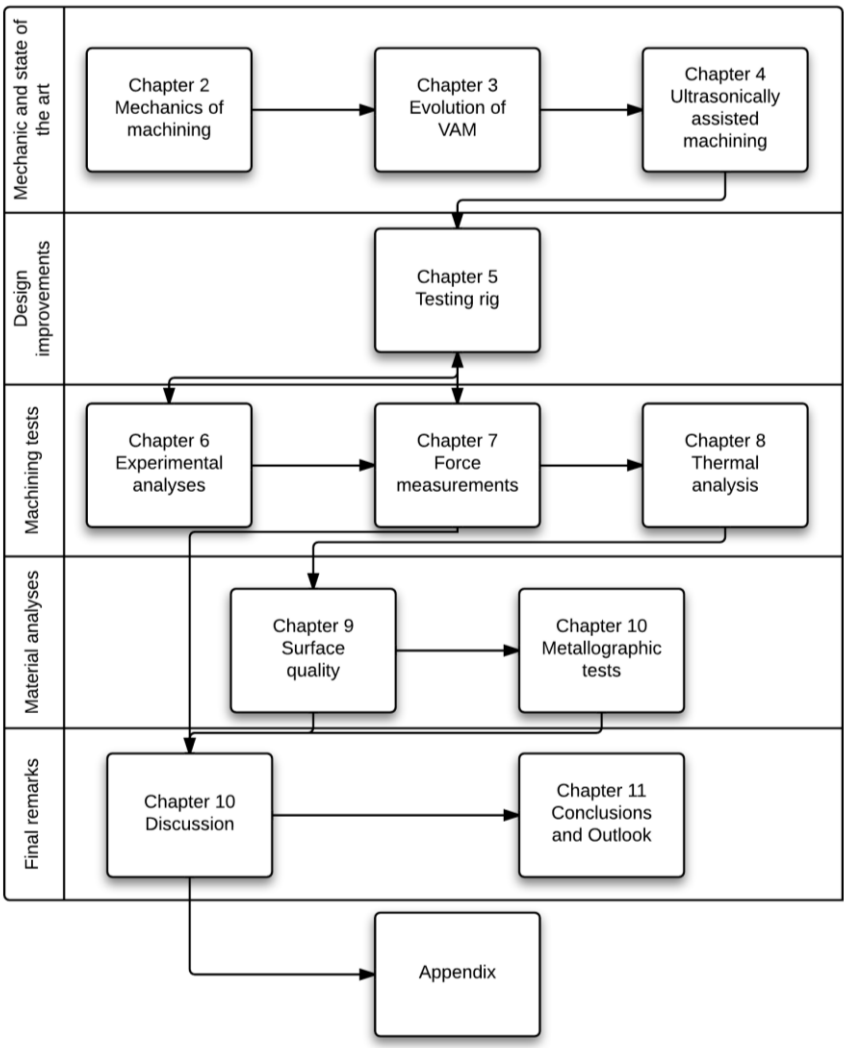

Figure 1-1: Thesis flowchart

2 Mechanics of machining

2.1 Lathe and parameters of turning

Metal turning is a chip formation process in which a work-piece is formed by a tool that deforms the material and generates a chip. A lathe [Figure 2-1] is a machine used to remove metal from a surface in rotation thus forming a cylindrical surface. In a modern commercial lathe, the tool is kept static and the work-piece is locked in the chuck and rotated against the tool.

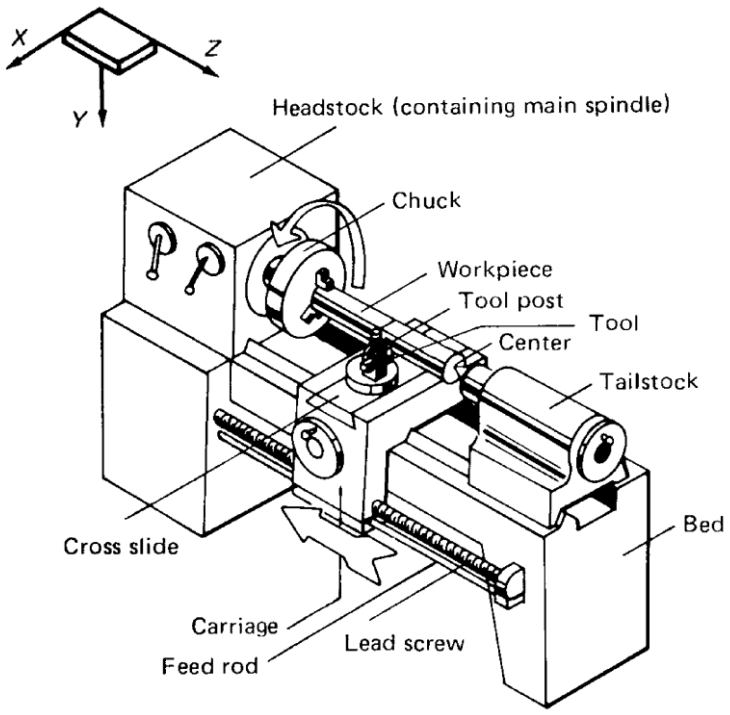

Figure 2-1: Lathe schematics. [Boothroyd & Knight, 1989]

The tool itself is moved at a constant rate (feed rate) along the axis of the work-piece cutting away material thus forming a surface.

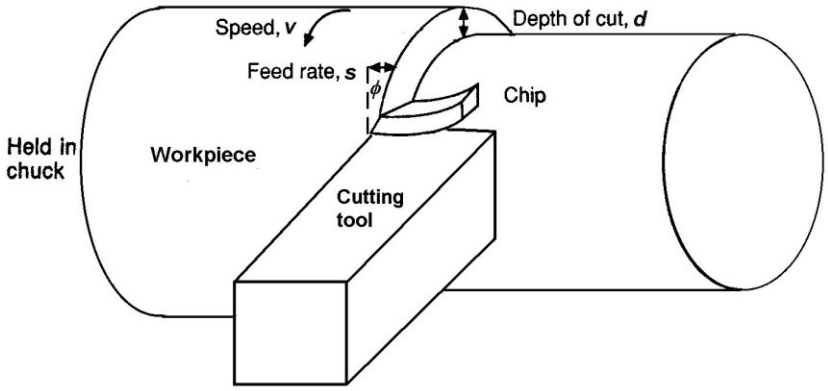

Figure 2-2: Schematic process of turning. [Trent & Wright, 2000]

The main cutting parameters that can be influenced by the operator are: the rotational speed of the chuck (n, usually in rev/min); the depth of cut a_p (the thickness of the removed layer during the cutting process) and the feed rate f (the distance travelled by the tool along the axial direction for every revolution of the work-piece)[Figure 2-2].

Among these, the parameter that has the most influence above the cutting process is the cutting speed V. It is directly linked to the rotation speed:$\mathrm{V} = \frac{1}{2}\mathrm{nD}$, where D is the diameter of the work-piece usually expressed in m/min and has to be adjusted according to a_p, f, type of tool used and material to be machined in order to achieve the optimum cutting conditions.

The cutting tool geometry deeply influences the cutting performances and has to be adjusted accordingly to the type of cut that is to be performed. The face of the tool that is in contact with the chip is called rake face, and is inclined in respect to the axis of the work-piece of an angle α that usually vary from 10° to 30°. Larger positive values of α render the cutting edge sharper, however more prone to wear or damage; while zero or negative values of the rake angle are generally used when a longer tool life is required at the price of decreasing the stability and ease of cut.

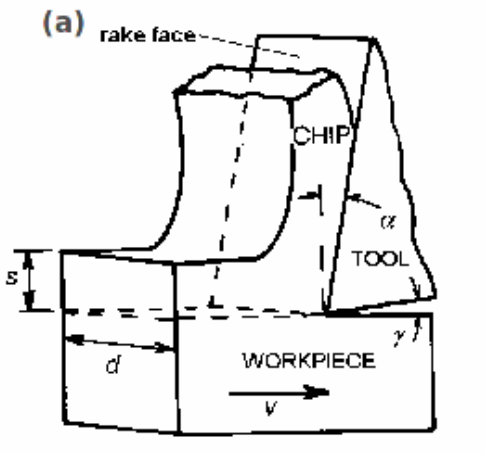

Figure 2-3: Other cutting parameters [Childs *et al.*, 2000]

The lower face of the tool is called clearance face, and is continuously in contact with the work-piece. In order to reduce the wear and prevent contact against the freshly cut surface, the clearance face is inclined of an angle γ (relief angle) generally in the range of 0° to 10°. It is generally possible to make adjustments in the position of the tool in order to change the rake/clearance angles and achieve the optimal performances for a particular tool-material couple [Figure 2-3].

The side faces of the tool are also inclined to prevent contact with the freshly cut surface and the intersection of these planes generates a surface called nose of the tool. The radius of curvature of this surface between the two side clearance faces is called nose radius (R_n) and is an important parameter of the cutting tool, directly influencing the cutting performances.

2.2 Cutting forces

Chip formation is a power intensive process needing large amount of energy to form and separate the chip from the work-piece. The desirable fast machining rates of today's machining equipment require careful design of cutting edge in order to limit the cutting force.

The cutting force is one of the the key measureable parameter in the analysis of turning. High pressure and friction force in the cutting process generate force components active in different directions. The forces on the cutting tool have a direct influence on tool edge wear but they play a more important role in the generation of residual stresses in the finished work-piece. Large compressive stresses are generated during the chip formation process by the cutting edge coupled with smaller shear stresses; these stresses are partially retained in the finished work-piece as residual stresses and for many applications are best if kept to a minimum.

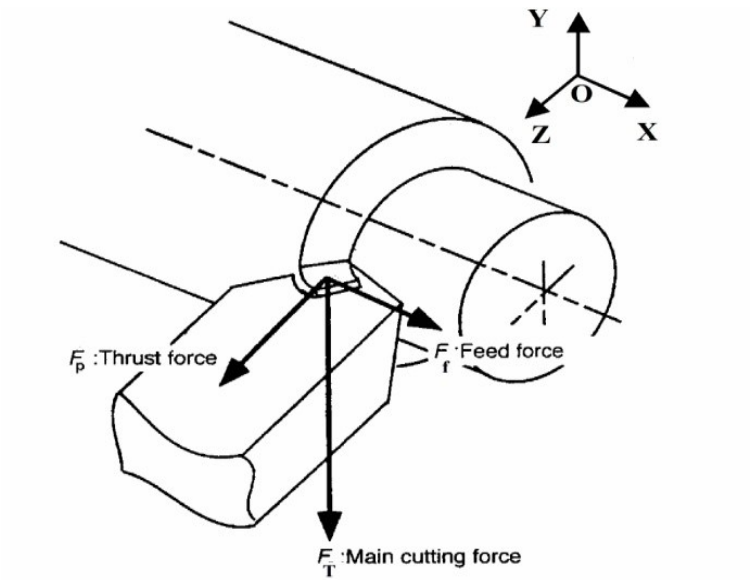

Figure 2-4: Main forces acting on the cutting tool [Childs *et al.*, 1972]

The cutting force can be divided into three orthogonal components [Figure 2-4] : the component of the force acting on the rake face of the tool, along the direction of the cutting velocity, is called “main cutting force” or “tangential force”, being tangent to the surface of the machined work-piece, and it can be called it F_t. This component is directly dependent on the compressive stresses and friction stresses acting between the chip and the rake face of the tool. The magnitude of the tangential component directly contributes to the needed torque for the cutting operations, thus directly

influencing the power needed for the chip formation process. It also influences the stability of the system with higher tangential components rendering the system more prone to vibrations and chatter. The second component is directed along the direction of the normal to the machined surface, and is called “thrust force” or “radial force”, F_r; the third components is acting along the rotational axis of the machined work-piece in a direction parallel to the feed velocity, this component is called “feed force” or “axial force”, F_a. The largest of the three components is, in common cutting conditions, the tangential force, or F_t, several times larger than the smallest of the group: the axial force F_a. The axial force is generally small enough to be neglected in normal cutting conditions.In general, during the cutting process, the contact area between the cutting edge of the tool and the work-piece is quite small, so the magnitude of the stresses in the contact area between the tool and the work-piece is very large even for a cutting force in the range of 10-2000 N. This magnitude is dwarfed when compared to the one of forces in metal forging or pressure forming, which are several thousands of Newton. [Trent & Wright, 2000].

Cutting forces models

In order to find correlations between the cutting force components and the chip formation process in orthogonal cutting the Merchant's model is generally used. Even though this model simplifies far too much the influence of the contact area between tool and chip [Shaw, 2005; Trent & Wright, 2000] and discounts the complexity of the friction model, it allows for finding easily relations between the various components of the forces in the orthogonal cutting model. In the classic model [Merchant, 1945], all the shears are limited to the shear plane and the newly formed chip slides on the rake face of the tool with an average friction coefficient μ.

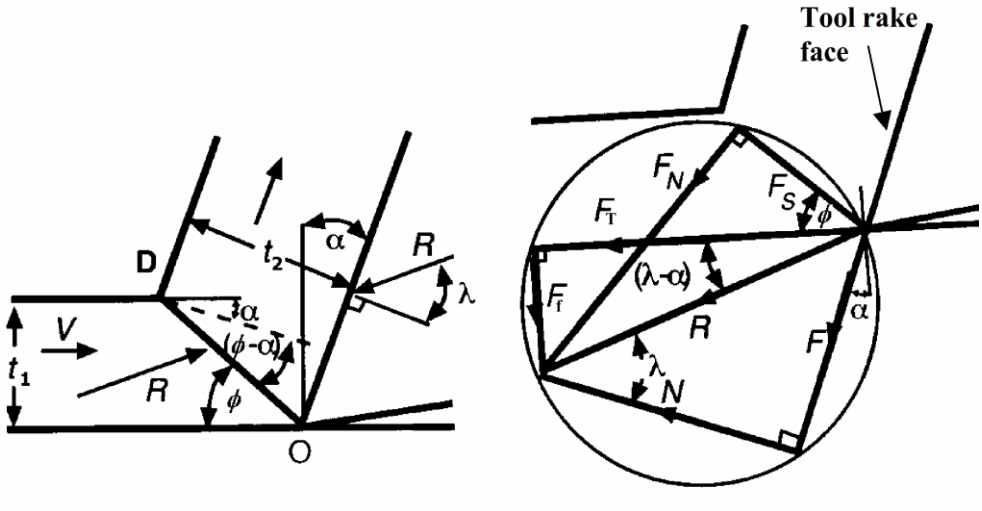

Figure 2-5: Merchant's force circle [Merchant, 1945]

The resultant cutting force $\vec{R}$ can be decomposed into different components [Figure 2-5] namely the main cutting force $\overrightarrow{F_T}$ and the feed force $\overrightarrow{F_f}$. It can also be considered as the resultant between the friction force $\vec{F}$ in a direction parallel to the tool rake face and the force normal to the rake face $\vec{N}$.

Given that $\mu = \frac{\vec{F}}{\vec{N}} = \tan \lambda$, the resultant $\vec{R}$ is inclined of an angle λ (friction angle) to the normal at the rake face of the cutting tool. Eventually, it is possible to consider $\vec{R}$ a combination of two forces, $\overrightarrow{F_S}$ and $\overrightarrow{F_N}$, acting respectively, in a direction parallel to the shear plane and normal to it.

With the aid of a dynamometer it is possible to experimentally determine the magnitude of the components F_T and F_f. By the relations is then possible to link analytically the shear and friction components:

$$F_S = F_T \cos\phi - F_f \sin\phi \qquad 2.6$$

$$F_N = F_f \cos\phi + F_T \sin\phi = F_S \tan(\phi + \lambda - \alpha) \quad 2.7$$

$$F_C = F_T \sin\alpha + F_f \cos\alpha \quad 2.8$$

However, the stresses acting in the shear plane are, obviously, equal to the shear strength of the material (k_S), so it is possible to define:

$$N = k_S a_S = \frac{k_S dt_1}{\sin\phi} \quad 2.9$$

Where a_S is the area of the shear plane and d is its width.

From this it is obtained:

$$R = \frac{k_S dt_1}{\sin\phi\cos(\phi + \lambda - \alpha)} \quad 2.10$$

$$F_T = \frac{k_S dt_1 \cos(\lambda - \alpha)}{\sin\phi\cos(\phi + \lambda - \alpha)} \quad 2.11$$

$$F_f = \frac{k_S dt_1 \sin(\lambda - \alpha)}{\sin\phi\cos(\phi + \lambda - \alpha)} \quad 2.12$$

by imposing $\frac{dF}{d\phi} = 0$ and a φ which minimizes the F_T (and the cutting labour) is found:

$$\phi = \frac{\pi}{4} - \frac{1}{2}(\lambda - \alpha) \quad 2.13$$

Merchant equation

The [2.13] is also known as Merchant's equation, which minimizes the labour needed for cutting. Substituting this value in the 2.11 and 2.12 it is obtained:

$$F_T = 2k_S dt_1 \cot\phi \quad 2.14$$

$$F_f = k_S dt_1[(\cot \phi)^2 - 1] \quad 2.15$$

From [Figure 2-5] it is obtained:

$$F_S = F_T \cos \phi - F_f \sin \phi \quad 2.16$$

$$F_N = F_T \sin \phi + F_f \cos \phi \quad 2.17$$

And:

$$k_S = \frac{F_S}{A_S} = \frac{(F_T \cos \phi - F_f \sin \phi)}{dt_1} \quad 2.18$$

$$\sigma = \frac{(F_T \sin \phi + F_f \cos \phi)}{dt_1} \quad 2.19$$

where σ is the normal stress.

Eventually:

$$\mu = \frac{F}{N} = \frac{F_T \sin \alpha + F_f \cos \alpha}{F_T \cos \alpha - F_f \sin \alpha} \quad 2.20$$

In this simplified model, the friction force and the normal force (F and N), are considered as uniformly distributed along the contact boundary between the chip and the rake face of the tool, and that F is proportional to N. However this model predicts unrealistic high contact pressures between the chip and the rake face along with extremely high friction forces, moreover it cannot describe the transient condition on the interface, this model is good as a first approximation since it is simple and thus request limited computational power.

The shear angle φ is not directly controlled by the operator, and changes greatly during the cutting process for different cutting conditions (cutting forces increase

proportionally with the feed rate and depth of cut, but the shear force F_S is greatly dependent on φ and for small values of φ can be over five times higher than for larger values). An additional force, due to the pressure of the work-piece against the small contact area on the clearance face of the cutting tool, has to be kept into account if the tool is not sharp enough (thus rubbing the freshly cut surface) and if the contact area on the clearance face can't be neglected (in turning large diameters).

Since the knowledge of cutting forces in determinant in machining to select the appropriate cutting tool, various empirical methods were historically used to determine a relationship between the cutting forces and the parameters of cutting. It is generally possible to obtain good agreement between predicted and measured cutting components, by a simple proportional relation which for the main cutting component can be written:

$$\mathrm{F_t = A a_p^x V^y f^z} \qquad 2.21$$

where F_t is the tangential component of the cutting force, A is a proportionality constant which together with x,y,z depends on the tool geometry and the mechanical properties of the work material [Armarego and Brown, 1969].

Successively, Kronenmberg proposed a more accurate empirical formula:

$$\mathrm{F_t = B_t (1000 A_0)^r} \qquad 2.22$$

where B_t and r are constant depending on the material and the rake face of the tool, and A_0 is the area of cut [Armarego and Brown, 1969]. These empirical relations predict the cutting force in conventional turning but do not agree with the experimental results when measuring cutting forces in ultrasonically assisted turning.

Generally, when trying to apply the models based on the fundamentals of cutting in ultrasonically assisted machining, it is found that the shear angle is hard to define due to the particular thermodynamic process and mechanics of the deformation involved. All attempts to apply the conventional machining relations to UAT have failed: for example, Oxley's shear zone analysis cannot be properly applied due to the continuous changing strain rate at the shear plane during normal cutting operation in Ultrasonically Assisted Turning.

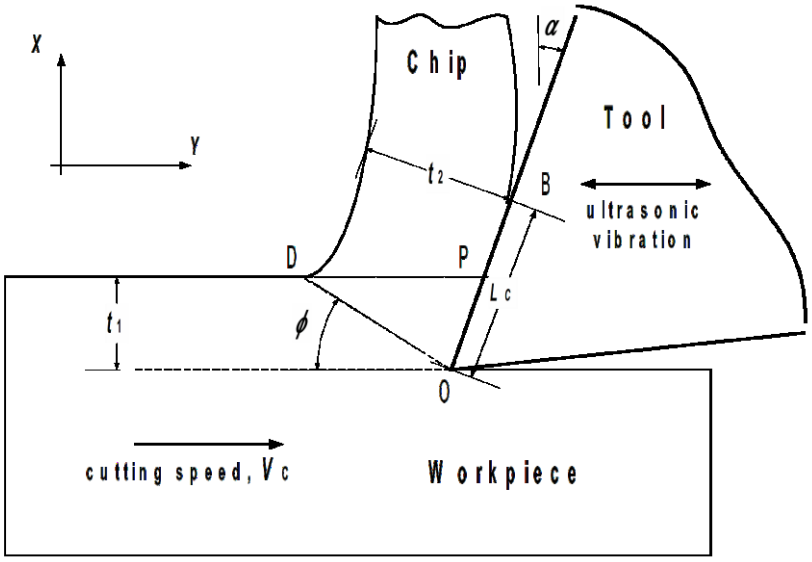

Figure 2-6: Projected contact length and chip-rake face contact

Another model, based on the minimization of the total energy (both energy spent in the shear plane and on the rake face), proposed by Rowe and Spick [Rowe and Spick, 1967] links the proportion of sliding/seizure on the tool-chip interface with the chip-rake face contact length divided by the projected contact length OB [Figure 2-6]. In this case the contact length L_C in Ultrasonically Assisted Cutting mode, is variable from zero to L_C for every cycle, thus the model is rendered useless to describe the cutting conditions in UAT.

2.3 Cutting tools

Cutting tool materials are the direct product of a technological advancement during the last century. The advancements in sintered materials has allowed for the production of extremely hard and durable cutting insert. The present day manufacturing is experiencing the beneficial effects of these advanced materials in the cutting process of high strength materials: micro grained carbides, differential grains carbides, cermets, new coating materials and techniques (as is possible to see from any supplier catalogue). It must be remembered in fact, that a cutting tool is cutting metal because it is harder than the metal itself and has a sharp edge that is mostly retained during the cutting operations.

In UAT, due to the transducer assembly geometry and the influence on the vibration tuning, small and light cutting inserts need to be fixed on the transducer; for that, carbides are the natural choice, inserts being small and readily available commercially. Tungsten carbide inserts are generally recommended by the industry in cutting high strength and heat resistant alloys, especially if given an active coat via the latest physical vapour deposition, chemical vapour deposition (PVD, CVD) techniques, which further improve the insert characteristics. Ability to stand up wear, allowing for faster cutting speed and longer life, keeping the flank wear to a minimum, is one of the desirable characteristics offered by modern cutting sintered materials.

In cutting heat resistant alloys high cutting temperatures are generated and high temperatures cause the cutting edge to degrade faster. Hot hardness of the carbide

insert is a crucial parameter for modern cutting conditions. The nickel-cobalt matrix in which the tungsten carbide particles are sintered cannot resist high temperatures. In fact, even if the fusion temperature of tungsten carbide is over 2700 °C, by a temperature of 900-1000 °C the nickel-cobalt binder starts to soften, and the solubility of tungsten carbide in the matrix starts to became important, leading to an abrupt loss of structural integrity [Sandvik Coromant, 2009].

The tungsten carbide insert, due to its high thermal conductivity (K=60 W/mK), effectively removes the heat generated during the cutting operations from the high strain region thus acting as a thermal well. However, the thermal conductivity of the coat is generally different than the one of the carbide core, often creating dangerous tensile stresses at cutting temperatures outside the optimal range.

At very high temperatures, even oxidization becomes important, in fact, in most sintered inserts, for temperatures over 550 °C, the chances of superficial oxidization with changes in the surface properties became noticeable. Moreover, due to the nature of UAT cutting, the rake face of the tool gets exposed to air at every cycle, even in this case, the chance of catastrophic oxidization are remote and not critical for failure.

The Young's modulus of tungsten carbide is very high as compared to the cutting materials; this allows considering the cutting insert as rigid during the cutting operations. The coating of the inserts is increasing the hardness of the cutting edge, reducing the friction rate, and increasing the structural integrity of the whole tool. In short, the coat will increase greatly the resistance to wear of the tool and improve the performances in the most severe cutting conditions. Toughness of the insert, namely its bending and transverse rupture strength, is an important parameter to keep into

account especially when selecting a cutting insert for UAT.

Today, nearly all turning carbide inserts are coated. Modern coating offer not only hard surfaces with limited wear, they also provide a chemically inert surface suitable with the most chemically reactive modern alloys. Only coated tools are used in all experiments in order to study cutting conditions as close as possible to the industrial cutting conditions.

2.4Evolution of vibro-assisted machining

From the beginning of history, metals have always played a key role in most industrial applications, and their manufacture has thus been of strategic importance for the human technological advancement. New manufacturing techniques have been developed in the modern age in order to improve the manufacture of metal pieces; metal cutting technology such as turning, milling, drilling, and metal forming have been extensively improved over the decades to improve the outcome of the processes.

Machining is one of the most whole spread metal shaping process. Along with drilling it is used to produce complex shaped components that cannot be produced by casting or forging processes. Turning, in particular, is used in industry for the production of axial symmetrical work-pieces by removal of material. It has been in use for several decades so far and a substantial experience was gathered. Advanced automated processes were developed with the aid of computer control, such as computer numerical controlled (CNC) machines, capable of achieving high precision and complete automation of the process. With the technological advancement in composite and ceramic materials, new materials for cutting inserts have come into use, such as carbides and ceramics. New advanced coatings were developed, leading to a substantial increase in the permitted cutting speed ranges and material removal rate (MRR). The continuous technological demand for better materials has led to the development of high-strength and super-alloys. These materials are in widespread use in the aerospace and all applications that require advancedchemical and mechanical properties. However, when machined with conventional machining techniques these alloys are difficult to machine thus

requiring the development of new techniques. The machining of these alloys requires expensive specialized cutting inserts. Their high hardness generates high cutting forces which result in high parasitic stresses in the finished work-piece [Ezugwu *et al,* 2003]. High surface temperatures during machining are also common, as well as chatter leading to poor surface finish and dimensional inaccuracy. Their strong abrasive properties accelerate tool wear, damaging the cutting edge of the insert quickly even when made from an advanced material [Ezugwu, 2005]. With advancements in materials, new non-metallic materials have come into use. The need to machine non-metal materials, which often are not even possible to machine by conventional machining, such as glass, glass-metals, ceramics, cermets or other brittle materials, has lead to the development of new machining techniques, which reduce the expensive post-processing operations needed in rotational finished components.

In the 1960's a new technique was developed for the machining of intractable materials, namely Ultrasonically Assisted Machining (UAM). The earlier techniques developed were similar to grinding: a hard metal shaped tool (sonotrode) is vibrated against the work-piece in the presence of abrasive slurry. In this process the abrasive particles remove the work-piece material until the desired shape is obtained (a negative image of the hard sonotrode).

Attempts to introduce a direct cutting technique were started soon after the first experiences with abrasive slurry with the first experiments in vibration assisted turning. In conventional turning, the work-piece is constantly in contact with the cutting tool, the work-piece being held and rotated by the chuck of the lathe. In Ultrasonically Assisted Turning (UAT), the tool is vibrated at ultrasonic frequencies (15-30 kHz) thus transforming the cutting process from a continuous one to a micro-

chipping multiple-impact process based on the interaction between the tool and the formed chip. Ultrasonic vibrations are used in many different applications in metal manufacturing: while ultrasonic welding is in widespread use in the welding of thin metal foils or the embedding of fibre or metal wires into a metal or plastic matrix [Kong *et al.*, 2004]; ultrasonic cutting is particularly beneficial in brittle or difficult to cut materials. At the same time ultrasonic grinding is widely used in the polishing of metals and ceramics [Suzuki *et al.*, 2010].

Several improvements in the cutting process have been observed such as decrease in cutting force, improvement in the surface finish and dimensional accuracy of the finished work-piece. However, the introduction of UAT techniques into industrial production is still being debated today due to the lack of consistent vibration control. This leads to instability of the vibration during the cutting process, it should be noted that most UAT machines operate in resonation, the cutting force variation during machining pose the danger of interfering with the resonating frequency, ultimately moving it far from the exciting one, bringing the system to operate in unfavourable conditions. This ultimately brings uncertainties in the quality of the finished work-pieces (it should be noted that DMG has recently introduced an Ultrasonically assisted milling machine) [DMG, 2010]. To summarize, at today the thermo-mechanics and the complex dynamics of UAT have not yet been completely understood nor studied due to the difficulties in accessing the cutting zone.

Parallel developments of VAM

From the initial works on ultrasonically assisted machining in the 1960, many

developments have taken place. Some early attempts to employ ultrasonic vibration to improve the machinability of hard or brittle materials were made in parallel by Japanese [Kubota *et al*., 1977; Kumabe, 1979] and Russian [Isaev & Anochin, 1961; Markov, 1966] researchers.

In his extensive work, Kumabe [Kumabe, 1979] pointed out that even in conventional turning (CT), the force acting on cutting tool is not completely static, but oscillates with a variable pattern of frequencies and amplitudes in dependency of the machining process. He advocated the idea of superimposing ultrasonic vibration to forcefully stabilize these random patterns. In his study in theory and techniques of turning axial symmetrical components, he developed an innovative high precision cylindrical machining chuck by combining a zero-vibration cutting assembly with a spindle system using an air bearing. While the work-piece was fixed on the main spindle it was machined using a periodic pulsating cutting force, this attempt was one of the firsts examples of applied vibration assisted machining (VAM) [Kumabe, 1979].

This system evolved into one using a torsional vibrational-mode with high-amplitude vibration of the cutting tool. Encouraging results were achieved, by the generation of finished work-pieces of high precision roundness in the range of 0.1-0.2 μm and a maximum surface roughness R_{max} of 0.03-0.09 μm by using carbon, stainless and hardened steels. Kumabe used magnetostrictive transducers in all his experiments, specially designed for the generation of ultrasonic vibrations, which was the current technology of the time. These generators are not efficient in the conversion of electric energy into mechanical energy thus requires extensive cooling during operations. The large water cooling system needed was bulky, ultimately limiting the diffusion of the technique. He studied three different vibrational modes in order to

summarize the peaks and flaws of the different modes, and these findings are summarized in one of his work [Kumabe & Hachisuka, 1984]. He found that while the ultrasonic vibration was active a reduction of the average cutting force was observed for all the three direction of vibration (having the maximum percent reduction in the tangential mode and the minimal in the axial or feed mode). Further tests showed that only tangential and axial modes demonstrated promising results in improving the mechanics of the process such to justify the additional expenses in the use of ultrasonically assisted cutting.

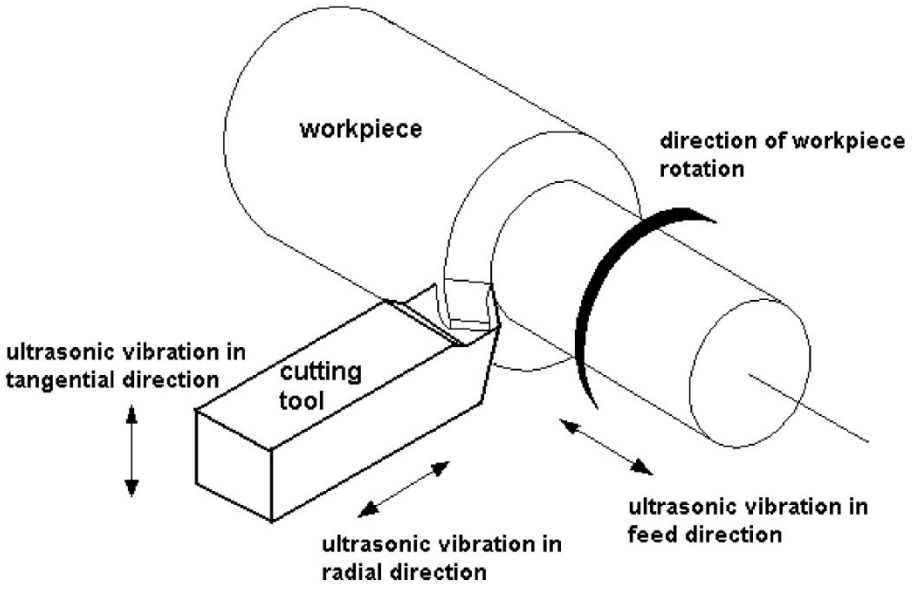

Figure 2-7: Main vibration directions.

Markov observed that when the vibration was superimposed in the axial or feed direction, there was a minimal reduction in the average cutting force. A sharpening of the cutting edge due to the apparent increase in the equivalent rake angle was observed along with fast wear of the cutting edge due to increased friction on the cutting insert tip and consequent quick thermal damage of the insert [Markov, 1966]. When the vibration was imposed in the radial direction a noticeable reduction in the average cutting force was observed, along with the formation of a very thin chip.

During the machining operations it was observed that the rake and clearance face of the cutting tool showed an accelerated wear rate. Valuable results were obtained for vibration superimposed in the tangential direction: an excellent reduction in the average cutting force was obtained as well as lower temperatures during the cutting process. A marked improvement in the lubrication of the cutting zone was observed as well as a very strong resistance to built-up edge formation on the cutting tool. The precision of machining was in general greatly increased [Kumabe, 1979; Markov, 1966]. To summarize, vibration applied in the tangential direction showed the maximum effect in the reduction of the average cutting force while axial direction vibration showed maximum improvement over surface quality of the finished work-pieces.

Heat resistant alloys were suddenly into interests being difficult to machine by conventional means, and they were machined extensively by Markov [Markov, 1966; Markov, 1996]. He used magnetostrictive transducers to generate ultrasonic vibration applied in an innovative radial-tangential direction to the cutting tool. In his book “Ultrasonic machining of intractable materials” [Markov, 1966] he studied the effect on surface finish, tool life, and residual stresses of the cutting layer. He calibrated the tool vibrational amplitude under different static loads, and found that the cutting force significantly dampens the amplitude of displacement of the cutting tool and lowers its vibrational resonance frequency. The effect of the dampening force on the vibrational resonance frequency is one of the most important particularities of UAT with resonating heads. A large variation of the vibrational resonance frequency of the head against a fixed driving frequency would bring the system out of resonance effectively reducing of orders of magnitude the vibration amplitude.

Further works characterized the effect of ultrasonic vibration on the cutting process. The influence of ultrasonic vibrations on tool life was studied for the heat-resistant nickel alloy E1437B for fixed cutting conditions of: cutting velocity V=10m/min, feed-rate f=0.2 mm/rev, depth of cut a_p=0.5 mm and high speed steel tools. It was observed that a high amplitude of the vibration (over 13 μm peak to peak) reduced noticeably the tool life while low amplitude ones (less than 8 μm) increased it. While low amplitude axial vibration seemed to increase the tool life, any kind of ultrasonic vibration was proven to shorten the tool life for hard inserts (VK8 or greater) [Markov, 1996]. This finding showed there is a complex relationship between work-piece material, cutting parameters, tool material and maximum amplitude of the displacement in UAT.

The very complex interaction between ultrasonic vibrations and tool life suggested that the cutting process itself it is regulated by many variables. Different work-piece materials and cutting inserts would respond in different ways to the superimposition of ultrasonic vibration. In particular, the shortened tool life in the case of high amplitude vibration could be explained as a change in the friction conditions of the interface between the work-piece and the cutting insert, due to the harmonically varying additional friction force introduced.

Markov advised the use of high fatigue resistance tools, considering not beneficial the use of hard-alloy cutters due to their negative response to fatigue cracking. He also studied the difference in surface finish of the machined work-pieces: heat-resistant alloys showed mirror-like finish when machined in Conventional Turning, while when machined with high amplitude vibration it became matt, and roughness was improved during UAT machining up to three times especially at low cutting speed [Markov, 1996].

Additional observations on the influence of other cutting parameters were studied by Markov in his extensive work. Very wide rake angle variations (from -40° to +30°) while machining in UAT showed negligible effects on the cutting force, chip properties and surface finish. As regarding the chips, it was noted that the micro-hardness and deformed surface layer were much thinner in CT as compared to UAT. The most interesting result was in the reduction of the cutting force by 5-6 times at slow cutting speeds when cutting steel [Markov, 1996]. The very low sensitivity of UAT to rake angle as compared to CT suggested that large process differences were involved in machining with superimposed vibration in comparison with conventional machining.

An approximate temperature measurement during the machining operations was attempted using a tool-work-piece thermocouple method, which unfortunately was not completely reliable under dynamically loading conditions. The concentration of stresses in the tool caused by the hole for the thermocouple was sufficient to render the tool so fragile that it lasted only for a fraction of the time when subject to the ultrasonic vibration. The method reported higher temperature for UAT as compared to CT and this was later explained by the energy dissipation of the ultrasonic vibration [Markov, 1966]. This was also observed in the experimental tests performed in this work, and is later discussed in details in the chapter dedicated to the thermal imagery.

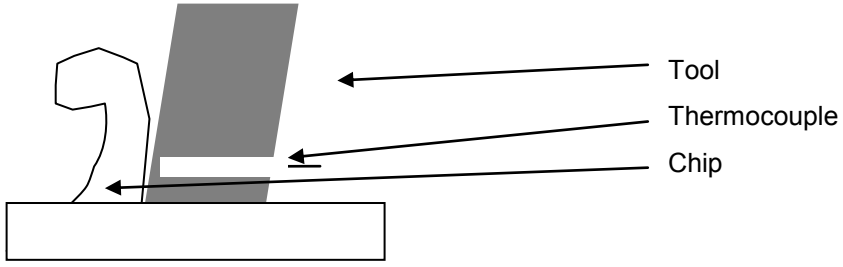

Figure 2-8: Schematic of tool with embedded thermocouple.

More and more details of the process were coming into study resulting in a steady improvement of the ultrasonic machining condition and of the machined outcome. Static and dynamic stiffness of the system is of great importance when cutting in UAT. The micro-chipping cutting process which is observed in UAT is highly sensitive to the elasticity of the cutting system: if the rigidity of the system is not high enough, the ultrasonic energy will be dissipated, tool life will suffer and in general the observed advantages are small. Markov's explanation for the effects of ultrasonic vibrations was based mainly on the thermal effect, which supposedly caused micro-melting and softening in the region of the impacting points between the cutting insert and the work-piece. In a more recent publication still on the ultrasonic subject [Markov, 1996] he found that it is possible to identify optimal amplitude of ultrasonic vibration, which has a complex dependence on tool dimensions as well as the visco-elasto-plasto-thermo-mechanical properties of the work-piece and the tool material itself. He also observed in many experimental tests that tangential vibrations were more effective than radial ones, and that the friction coefficient was changing its form from quasi-static to dynamic one when ultrasonic vibration was superimposed on the cutting insert during the machining operations.

He also observed that an amplitude of the ultrasonic vibration exceeding a threshold value accelerated the diffusion of dislocations and increased the ratio of formation of new dislocations in the material of the work-piece, thus permitting plastic flow with lower stresses. However, when ultrasonic vibrations with very high amplitude were applied to the cutting insert, they showed not to effectively improve the cutting process. It was observed that their energy was diverted toward the heat generation thus worsening the tool wear ratio. Choosing optimal amplitude of the vibration showed to offer the maximal friction reduction without the unwanted effects [Markov,

1996].

An excellent survey of the available methods was offered by Babikov [Babikov, 1960], who critically summarized and analyzed some of the available researches dealing with the machining of hard and brittle materials with ultrasonic vibration superimposed on the cutting tool. He concluded that, not only the cutting process was made easier by the ultrasonic vibrations but also the finished work-piece surface quality was greatly improved. The beneficial effects of ultrasonic vibration in the machining of both hard and ductile materials were also assessed and summarized by Frederick in his book [Frederick, 1965]. He concluded that not only cutting force reduction was observed (and partially explained by friction reduction), but also lower residual stresses due to the lower parasitic forces in the machining of hard materials. Great improvements were observed in the surface finish during the machining of ductile materials, which readily form a built-up edge on the cutting tool under certain cutting conditions in CT. It must be noted how ultrasonic vibration offered several advantages which were no longer restricted to the cutting force reduction.

The arrival of new cutting tool materials has opened a new experimentation wave among researchers with the aim of characterizing the response of these new materials in UAT. Carbide sintered tools were used together with a magnetostrictive transducer in turning, showing a significant reduction of the cutting forces especially at low cutting speeds [Skelton, 1969]. In these tests, tangential and axial mode vibrations were used and consistently resulted in reduction in cutting forces and reduction in built-up edge formation. It was attempted also to explain the force reduction as a reduction of the mechanical properties (yield) of the machined material due to the vibration. This was hiding a more subtle change in the theory of ultrasonic vibrations, the effect of force reduction was no longer supposed to be only

a thermal effect but it was suggested that the ultrasonic vibration could have a more deep effect on the work-piece material, to the point of changing its mechanical properties.

General reduction of cutting force, improvement of surface finish, elimination of built-up edge and in general longer tool life were observed on different materials such as carbon steel (C1010, C1045) and aluminium alloy (2024-T6), in the extensive study of Devine [Devine, 1979] which covered also ultrasonically assisted drilling (demonstrating an increase in the drilling speed). Drilling in fact, was to become the field in which most of the industrial efforts to implement UAT were spent, with several Japanese companies offering ultrasonic drills in the following decades.

The effects of tangential ultrasonic vibrations in the machining of difficult to machine alloys, such as C60 steel and X5CrNiMo18.11 alloy, were also studied, showing significant improvement on the surface roughness of the finished work-piece for cutting velocity below the critical limit (V_c) [see eq. 3.5 on chapter 3] [Weber & Piltz, 1984]. However, the most interesting finding was the complete abolition of formation of the built-up edge, which was typically observed in the turning of these alloys in CT.

A cutting process using tangential mode vibration and a velocity $V>V_c$ was studied. In this case, complete separation between work-piece and tool did not happen, however a considerable number of advantages were identified. Among these were chatter elimination and a reduction in the build-up edge formation [Wang, 1992]. His interesting findings further elucidate the complex interaction between the tool and work-piece during Ultrasonically Assisted Machining. The elimination of chatter is an important observed feature of UAT.

In further experiments, involving the machining of very difficult-to-machine ceramics, such as magnesium based glass ceramic (VKB-MgO), he showed that superimposition on the tool of ultrasonic vibration (frequency 20 kHz) in tangential-radial (a_p=8 to 12 μm, 2 to 6 μm) mode extended the cutting tool life by several times (up to 20 times) for a carbide tool. These interesting results started a new research interest for UAT in the machining of very brittle and difficult to machine materials.

Tests to assess the machinability of glass and stainless steel (grade SU303Se-JIS) were also attempted in a ultra-precision single-crystal diamond turning and tangential vibration superimposition (f_q=40 kHz, a_p=3 μm) [Moriwaki *et al.*, 1992; Moriwaki & Shamoto, 1991; Shamoto & Moriwaki, 1999]. The higher frequency was believed to reduce the vibration marks on the finished work-piece and improve the surface roughness.

A roughness R_{max} of 0.026 μm was obtained with a mirror-like finished surface of the stainless steel work-piece; general increase in resistance to crater and flank wear in the used tool was also observed. Grooving (i.e. deep notch cutting) experiments were carried out to assess the effect of ultrasonic vibration on brittle non turnable materials: a glass work-piece was machined with an increasing depth of cut until it was observed the transition from ductile cutting mode to brittle mode. The critical value of the depth of cut was then identified for both conventional and ultrasonically assisted turning. It was observed that the critical depth of cut at which the transition from ductile cutting mode to brittle one occurred was seven times greater in UAT as compared to CT. It was hence demonstrated that in principle the material removal ratio is far greater in UAT [Moriwaki *et al.*, 1992].

Advantages of UAT did not stop at the machining of conventional materials, carbon-

fibre reinforced aluminium composite machinability was also studied with single-crystal diamond tools. A four time increase in the quality of the surface finish was reported as well as a five time increase in the life of the tool [Yang *et al.*, 1998]. Due to the widespread use of composite materials, a great interest was aroused around the improved machinability of composite materials in UAT ultimately giving the impulse to some valuable studies on the effects of ultrasonic vibration on the surface finish and cutting force. Carbon-fibre reinforced plastics machinability was investigated for tangential vibration of 19.5 kHz frequency and amplitude of 15 μm. The average cutting force generated while cutting in UAT was constantly observed to be smaller than the one observed in the CT operations. Moreover, the quality of the finished surface in UAT was several times better than the one in CT when the cutting speed was kept below the critical limit. An interesting point observed was a strong dependence from cutting speed and feed rate of the surface quality of the finished work-piece [Kim & Lee, 1996].

Ultrasonically assisted machining was investigated as a valuable substitute for the micro-surface machining of optical parts made of brittle optical plastics (CR-39). Generally expensive micro-machining processes have to be used for an acceptable surface finish of these machined parts. With the aid of UAT (f_q=20 kHz, a_p=26.4 μm) it was possible to cut in ductile mode up to a depth of 2.7 μm (depth of cut) still observing an improvement in the surface finish of the machined work-piece. Thus, UAT was proved as an effective and valuable substitute for high-precision micro-surface machining [Kim & Choi, 1997]. Extremely low cutting speeds were also investigated during the precision machining of optical parts in CR-39 in order to maximize the non-contact period between the work-piece and the tool cutting edge. It was observed an effect of induced aerodynamic lubrication, which consistently

reduced the friction and the average cutting force. The obtained chips demonstrated ductile-mode cutting for cutting velocities up to V=1/40 V_c [Kim & Choi, 1998]. The cutting process was analysed using a vibrational wavelength spectrum analysis in comparison with the one in CT, and it was found that brittle fracture was almost completely removed by the UAT process. Production by tungsten carbide aspherical moulds for miniaturized glass lenses for DVD pick-ups and digital cameras has also shown great improvements when the moulds were polished using two-axis ultrasonic polishing. The specially designed vibrator [Figure 2-9] was able to generate axial vibrations with a frequency of 27.81 kHz and flexural ones at 21.54 kHz with the result of a complex pseudorandom motion of the polishing tool on the work-piece surface. Experimental tests coupled with numerical simulation were used to optimize the process which ultimately resulted in a surface roughness of 8 nm in the finished mould surface [Suzuki *et al.*, 2010].

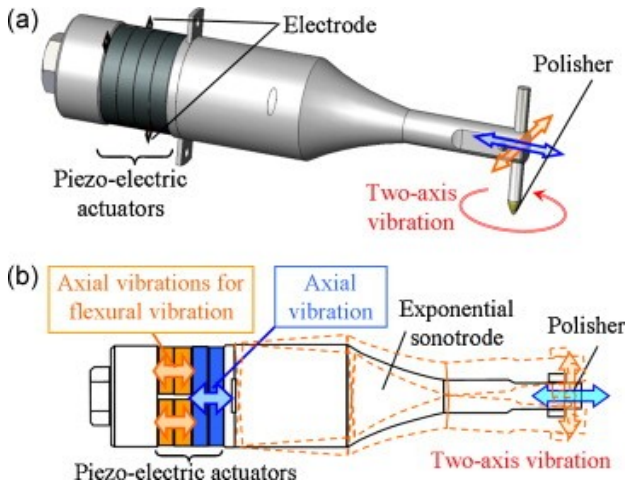

Figure 2-9: Ultrasonic two axis vibrator using piezoelectric actuators

The technological advancements in optical technologies gave the possibility for fine optimization of the vibrational performances of the whole cutting system by the means of a vibrational analysis using Laser Doppler Vibrometry and Electronic Speckle Pattern Interferometry. The subsequently developed model was studied for

various excitation conditions and design parameters eventually obtaining a full-parametric picture of the system. It was found that further improvements could be obtained by improving the tuning and quality of the driving signal and by redesigning the key component of the system (the transducer and tool holder) [Lucas *et al.*, 1996].

The advancement in technology for piezoelectric element ultimately opened the possibility of a built-in tool-piezoelectric material. For increasing the precision of the machined work-piece a hybrid cutting tool was developed: the cutting tool integrated the piezoelectric transducer, which was working at fixed vibrational parameters (f_q=20 kHz, a_p=10 μm). Experimental tests showed that this solution was effective in increasing the finished work-piece roundness and roughness. An active error compensation closed loop was also developed to control the non-linear dynamics of the system [Han *et al.*, 1998].

Investigations on improving the tool life were also performed in UAT. Several studies apparently conflicted about the effects of UAT on tool life. Brittle carbide tools generally showed a reduced life when compared with tougher steel cutting tools. Cutting tool edge chipping is the most common type of damage while cutting hardened steels by ultrasonically assisted turning, which ultimately brings the cutting process to a halt. It was proposed that the problem could be caused by the micro-impacts between the flank face of the cutting insert and the machined surface of the work-piece. In order to address this, it was attempted to increase the stability and rigidity of the ultrasonic system and to use a vibrational mode inclined by 10-30°[Figure 2-10] from the direction of the cutting velocity [Jin & Murakawa, 2001], so that the tool would not rub on the freshly machined surface.

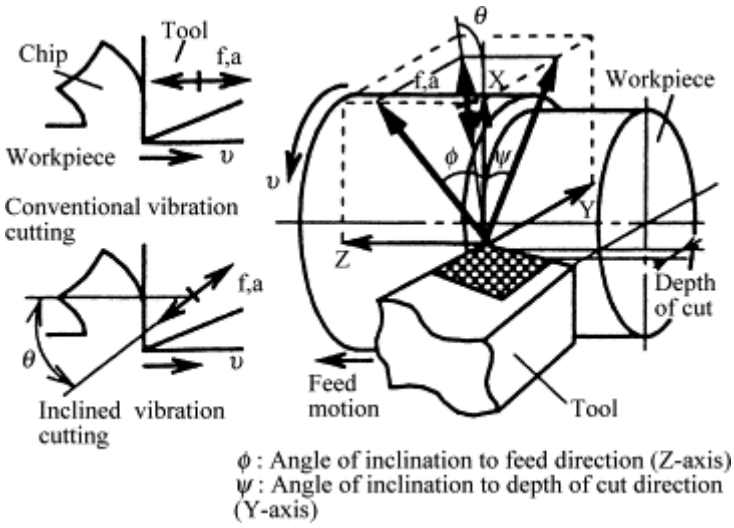

Figure 2-10: Inclined direction of vibration for ultrasonically assisted turning tool

Further investigations were performed in order to gain information on the dimensional influence of tool nose radius on chatter, cutting force and surface roughness. Inconel 600 and stainless steel SUS304 machining was investigated by a dynamic model and later experimentally. It was concluded that a larger nose radius of the tool could be successfully used in UAT, without triggering unwanted chatter vibrations as compared to CT. Larger nose radius are more resistant to fatigue cracking and chipping of the cutting edge due to the reduced tension concentration factor. An optimal nose radius was assessed with an experimental setup involving 5 different tool nose radii (R_n=0.02, 0.1, 0.2, 0.5, 1 mm), the results showed that a larger nose radius was preferred during UAT ensuring greater resistance to tool fracture and improving the surface finish [Xiao *et al.*, 2003]. Strong chatter suppression and increased accuracy were observed when ultrasonic vibration was engaged [Figure 2-11]. In Figure 2-11 simulated conventional and vibration-assisted process are compared at the same cutting conditions. Due to the irregularities in the work-piece resonant vibration (chatter) is excited during the conventional process, at each revolution the amplitude of displacement of the cutting head is increased.

During UAT, the intermittent cutting force prevents the system to resonate therefore effectively greatly reducing the displacement of the cutting head.

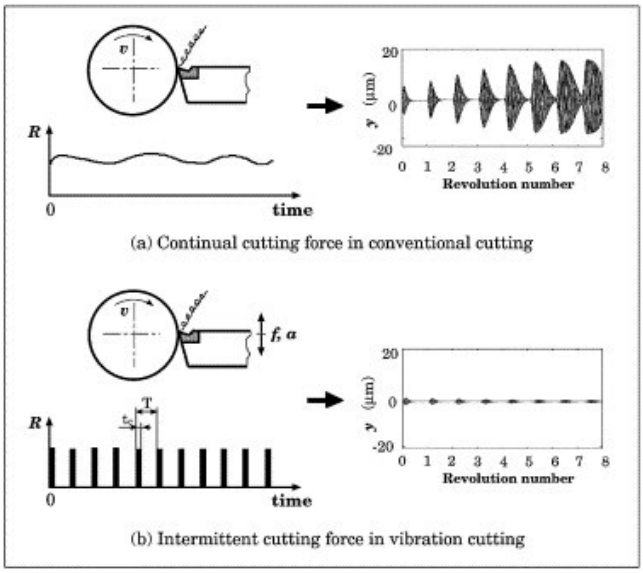

Figure 2-11: Chatter suppression for UAT cutting (simulations)

An extensive study on Inconel 718 was performed using both ultrasonics and high-temperature aided cutting in order to identify the machining parameter and tool materials which would ultimately giving the best results in machining this hard alloy. Depth of cut, cutting speed, feed rate, temperature, ultrasonic power and tool material were investigated experimentally in order to obtain a parametric Taguchi model characterization of the machinability of Inconel 718 in UAT. Cermet cutting tools were demonstrated to achieve the best surface roughness keeping the built edge formation to a minimum while increasing the working temperature to over 190 °C increased the cutting force due to precipitation of Ni_3Nb hard gamma phase. Ultrasonic vibration superimposition showed to decrease the cutting force and improve the surface quality of the finished work-piece significantly [Hsu *et al.*, 2008].

The technological improvements in the production of synthetic single diamond cutting tools shifted again the interest on the ultra-precision machining of C60 steel

for optical parts. The surface quality of the finished work-pieces was greatly limited by the rough polycrystalline structure of the cutting edges when using polycrystalline diamond, so a single crystalline diamond cutter was needed. Again, the chosen vibrational mode was the tangential one (f_q=40 kHz, a_p=3.5-5 μm), in an attempt to investigate a possible improvement of the tool life when compared to CT. A four to five times increase in the cutting tool life was reported in UAT when compared with CT, and it was proven that the tool wear in the machining of steel materials was mainly linked to the hardness of the material and not to its microstructure. With depth of cut and feed rate in the micron range the levels of accuracy experienced were mostly dependent on the size of material's grains (R_a<10 nm and PV<1 μm). Ductile mode machining was reported to be dependent on the vibration amplitude and it was proposed that the large delay in the application of UAT in industrial machining was mainly related to the fact that UAT processes are not completely understood and no "commercial" UAT system was available for industrial use [Klocke & Rubenach, 2000].

In recent times, the machinability of gamma-titanium aluminides has gained interest with the superimposition of ultrasonic vibration on the cutting tool: in fact, gamma-Ti-Al alloys are very difficult-to-machine titanium alloys due to their extremely high hardness as compared to other Ti alloys. An industrial (Rolls Royce) systematic study was performed by [Sharman *et al.*, 2001]. They machined the alloy using uncoated tungsten carbide insert tools (grade K10). It was observed that for the cutting conditions imposed (f_q=20 kHz and "load-free" a_p=15 μm) an abrupt failure of the cutting tool was to be expected due to the high fatigue load (several thousands cycles per seconds) imposed on the edge of the cutting insert causing chipping and micro-crack propagation, damage on the work-piece was also observed [Figure

2-12].

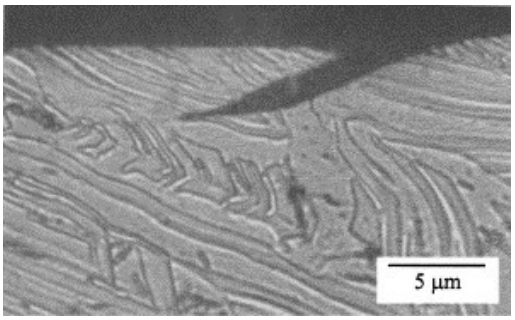

Figure 2-12: Micro-photography of work-piece cross-section showing crack damage

The tool life was generally reduced as compared with CT cutting operations. However, a beneficial effect was observed when V was increased in order to reduce and mitigate the time while the tool was not in contact with the work-piece, and increased depth of cut was found to be responsible for a visible reduction in the cutting tool life. These observations match the study by [Moriwaki, *et al.*, 1992] on ductile materials: completely different materials behave similarly when cut in UAT. The observed cutting force was several times less than the corresponding cutting force in CT and was explained by the reduction in the material's strength due to the formation and propagation of micro-cracks, also because changes in the rake angle had only non significant effects on the cutting force. It was found that the UAT process produced long helical chips (around 25 mm) as compared to the CT process (needle discontinuous chips), which was attempted to explain as a result of cutting force reduction preventing primary-cutting-edge crack propagation, and in general by the complex differences between the two cutting processes [Sharman *et al.*, 2001].

The influence of ultrasonic vibration superimposion on ultra-thin wall parts surface microstructure was assessed in [Gao *et al.*, 2002]. They compared results in ultrasonic cutting using a PCD (polycrystalline diamond) tool and a cemented carbide one [Figure 2-13]. It was found that the rigidity of the ultrasonic system

greatly influenced the surface finish of the work-piece: the surface roughness was improved for aluminium samples machined with the aid of ultrasonic vibration. In machining aluminium, the PCD tool performed far better than the cemented carbide one and in the study, a dedicated coolant for UAT was investigated: light-grade kerosene was suggested as one of the most suitable coolants for UAT.

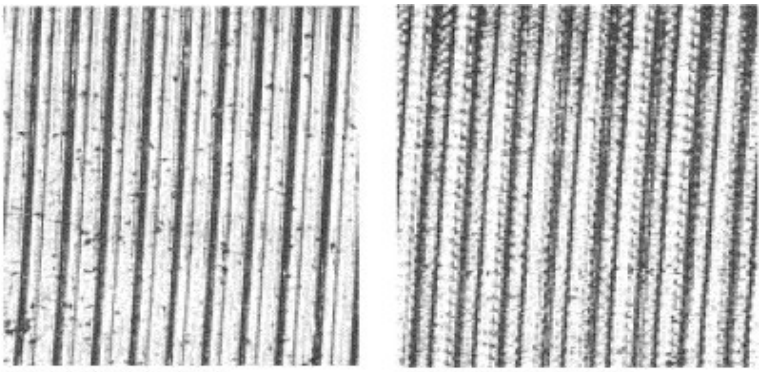

Figure 2-13: Comparison of cut surfaces: b) conventional turning, c) UAT

In several studies UAT was shown to reduce the average cutting force, elimination of chatter and built-up edge, and improving the dimensional accuracy and surface finish of the finished work-piece [Takeyama & Lijima, 1988; Devine, 1979; Kremer, 1995; Kumabe *et al.*, 1989] even for non metal composite materials such as glass-fibre reinforced plastic. Brittle materials were observed to undergo ductile machining even at higher than critical depth of cuts [Wang *et al.*, 2002]. A work-piece of fused silica was machined using a diamond tool with 0° rake angle and 11° clearance angle, tool nose radius of 0.8 mm and a feed rate of 5 μm/rev. The chosen vibration parameters were f_q=40 kHz and a=3 μm in tangential mode. The average cutting force was several times smaller in UAT than in CT, moreover, it was found that increasing the frequency of the ultrasonic vibration, further improved the surface quality obtained (R_a=100 nm for a depth of cut of 2 μm).This was also verified in precision machining of steel with a PCD tool [Zhou *et al.*, 2003]. It was demonstrated that improvements

in cooling and lubrication as well as reduced contact times during UAT were responsible for the lower temperature and average cutting force.

In more recent times, a new impulse in investigating advanced machining techniques was driven by the technological need of machining brittle materials or difficult to machine alloys [Guzzo *et al.*, 2004]. New materials, such as ceramic metal composites, showed improvements when machined in ultrasonically assisted rotary machining. In [Li *et al.*, 2005], ultrasonic machining is demonstrated to be a low-cost alternative to expensive hybrid machining methods in drilling of brittle ceramic. A twofold reduction of cutting force reduction was observed as well as a noticeable improvement of the quality of the drilled holes. Chipping of the entrance or exit surface of holes was reduced when ultrasonic vibration was superimposed on the diamond coated cutting tool.

New materials, such as adaptive composites, to be used in advanced aerospace applications became possible by the application of ultrasonic vibration in bonding techniques. Shape memory alloys (SMA) were able to be bonded in layered fabrication of aluminium components by the ultrasonic consolidation process. Absence of chemical reaction, low contact pressures and low temperatures were observed in the consolidation of SMA fibres in an aluminium matrix, high mechanical bonding was observed at the interface between the fibres and the aluminium matrix [Kong *et al.*, 2004].

Slurry machining of Ti 15 and Ti 31 alloys were investigated using a high speed tool to identify the optimal operating parameter critical to achieve acceptable productivity. It was demonstrated that given the rather low elastic modulus of the titanium alloy, ultrasonically assisted technique were optimal to obtain good surface and

dimensional quality in the finished work-pieces. Absence of chipping or cracking was generally observed in the drilled holes with a surprising better surface quality obtained with increased grit size [Singh & Khamba, 2006; Singh & Khamba, 2007]. The ultrasonically assisted drilling process was investigated extensively due to the large potential advantages which could offer to industry as compared to conventional drilling. Instabilities in the ultrasonic vibration during the drilling process have so far not allowed the industrial diffusion of ultrasonically assisted drills. Commercially available drill bit display strong vibration mode conversion characteristics and strong dependence on the correct frequency showing the need for specifically designed tool for ultrasonically assisted drilling [Thomas & Babitsky, 2007].

Dry ultrasonically assisted turning of Ti- and Ni- based super-alloys was also attempted to reduce the impact of machining waste on the whole machining costs. Turning of Ti 15-3-3-3 and Ni 625 with sintered carbide PVD coated tool showed large cutting force reduction and improvement on the surface finish of the machined work-pieces even in the absence of coolant or lubricant at low to medium cutting speeds (10 to 60 m/min). It was demonstrated a potential fivefold increase in MRR in UAT machining of these intractable alloys [Maurotto *et al.*, 2010; Maurotto *et al.*, 2012]. In the present work, carbide tools demonstrated a large variability in tool life when used in UAT. Damage of the tool was strongly dependant on the carbide grade and coating, on nose radius and chip breaker. I was understood therefore that increase or reduction in tool life in UAT showed a strong material dependence. Tougher tools with larger nose radiuses exhibited a longer life in UAT reducing the gap with conventional turning.

Compared to the large number of experimental studies few attempts have been made to explain theoretically and to model the ultrasonically assisted cutting

process.

Astashev [Astashev, 1992], was the first to propose an ultrasonic vibrational cutting model. These results were later confirmed by his experimental findings: tangential mode vibration, (f_q=20 kHz, a_p=10 μm) applied to the cutting tool during the cutting process, were proven to significantly reduce the cutting force. It was also proven experimentally the existence of the critical velocity V_c as the reduction of the cutting force F_c was approaching 0 for $V \to V_c$ ($\lim_{V \to V_c} F_c = 0$) since there was no longer any separation between the tool and the work-piece during the machining operations. Critical velocity for UAT is, in fact, the cutting speed at which there is no longer separation between tool and work-piece. For $V \geq V_c$ the ultrasonic vibration showed no effect on cutting force, which was considered as plastic deformation force of the cut-off layer and parasitic frictional force due to the contact of the working faces of the cutting tool with the chip material. In any case, the superimposition of vibration during the cutting process was proven to reduce the chatter, even for $V \geq V_c$, and this is beneficial for the cutting process. Further evolutions of the model, including non-linear dynamics, were explained within the framework of rheological models, and the accumulated experimental data explained theoretically [Astashev & Babitsky, 1998]. Under high-frequency vibration, dry friction undergoes a process of dynamic fluidization and the elasto-plasticity phenomena transform into visco-plasticity one. Almost complete dynamic characteristics of the machining process were obtained: the link between the magnitude of cutting force reduction and the vibration parameters; the non-linear response of the vibrating tool during the process of cutting was described. It was attempted to stabilize the non-linearities of the process with the aid of a closed-loop auto-resonant feedback system to stabilize the resonant conditions of ultrasonic excitation under the working load. An auto-resonant system

was designed and used to control the piezoelectric transducer accurately via a closed loop feedback, ensuring that the maximum efficiency of conversion was always achieved (thus a stable amplitude of the vibration). The auto-resonant system was built as a hybrid analog-digital system, involving a computer for the precise control of the excitation parameters. The control was tested under different vibrational modes, designs of tool holder, cutting inserts, parameters of cutting and materials, always showing significant improvements as compared to the manual control method. The auto-resonant system was tested [Babitsky *et al*., 2003; Babitsky *et al.*, 2004] during the cutting operations in order to stabilize the cutting conditions and has proven to improve the dimensional accuracy of the ultrasonic machined work-piece. Unfortunately it was also showing to be rather critical to be implemented correctly. Two nickel-based super-alloys (C263 and IN-718) were involved in the tests involving tangential and axial vibrational mode. It was shown that the feed direction vibrational mode overcomes the restrictions of the critical rotational velocity thus increasing greatly the productivity. Surface roughness was improved for UAT as well as roundness up to 40% for tangential and feed direction vibrational modes.

In order to understand the response of materials in UAT, finite element simulations are used as a numerical technique to predict the possible experimental outcomes. Residual stresses, strain of the finished work-piece were assessed in the surface layer and in the immediate sub-layers, in search for possible changes in the mechanical properties of the ultrasonically assisted machined work-pieces as well as the in-depth temperature profiles for different machining conditions [Mitrofanov *et al.*, 2003; Mitrofanov 2004; Mitrofanov *et al.*, 2005]. The effects of lubrication in the machining of Inconel 718 were also studied [Mitrofanov *et al.*, 2005]. It was found

that the cutting zone temperature shows a drop during UAT involving lubrication due to the reduction of frictional heating, and the cutting force drops up to 30% due to the reduction of friction in the interface work-piece cutting edge.

Finite element parametric studies of dry ultrasonically assisted turning of Ti- and Ni-based alloys also demonstrated the effect of vibration amplitude, frequency and cutting speed on cutting force [Muhammad *et al.*, 2011a; 2011d], eventually considering also the hybrid machining techniques by introducing temperature as a variable of the study [Muhammad *et al.*, 2011c] demonstrating that an increase in the working temperature is responsible for noticeable reduction in the cutting force.

Summary

Ultrasonically assisted cutting techniques were shown to reduce cutting forces during machining of different materials. Mixed elliptical vibration modes (2D) reduced cutting forces even more than single (1D) vibration modes; at the cost of a reduced cutting speed and depth of cut. Elliptical vibration modes were observed to be especially beneficial in the machining of brittle-non-metallic components such as optical lenses. In the machining these materials a large increase in the ductile-to-brittle depth of cut was also reported allowing for safer machining operations at increased a_p.

Generally, surface finish in UAM was improved when comparing with conventional cutting. Geometry accuracy improvements were also frequently reported in difficult-to-machine materials and metals.

Slight reductions on the residual deformations on the materials were observed. Concomitant reduction of dry friction on the rake face of the tool allowed for greatly

reducing or completely avoiding the employment of coolants and lubricants during the machining process. Inconsistent effects were observed on tool life, it was apparent that conventional cutting tools would respond in a completely different way when employed in UAM. Hard and brittle tool materials were especially sensitive to the effects of the micro-impacts observed during UAT. Longer tool life was observed to be strictly linked to increased toughness of the tool.

Micro-impact behaviour of UAT cutting was understood to produce highly variable cutting force components. Characterization of cutting force during the UAT cycle was attempted in several cases but generated results only when greatly reduced cutting speeds and vibration frequencies were employed due to technical limits of the sensing elements.

Effects of ultrasonic vibration on materials are not completely studied and understood as to day. Sub-surface layer effects, residual stress profiles after machining in UAT especially for non-metallic components are yet unavailable. Design of specialized tools for UAT was attempted only in recent times due to missing industrial interest. Lack of understanding of these processes could be one of the reasons that had kept low industrial interest in this promising technique; the other being the traditionally conservative approach of the industry toward innovative techniques.

3 Ultrasonically assisted machining

Vibration machining has been experimented for more than five decades now, infra-sonic, sonic and ultrasonic vibration in 1D and 2D has been used to improve the machinability of certain materials [Babikov, 1960]. The most important feature of ultrasonic vibration is its directionality; a comparatively large energy density can be achieved by focusing the waves to a small area of the cutting tool: the interface between tool and work-piece. By this means large localized strains rates are achieved effectively easing the manufacturing process [Shoh, 1975].

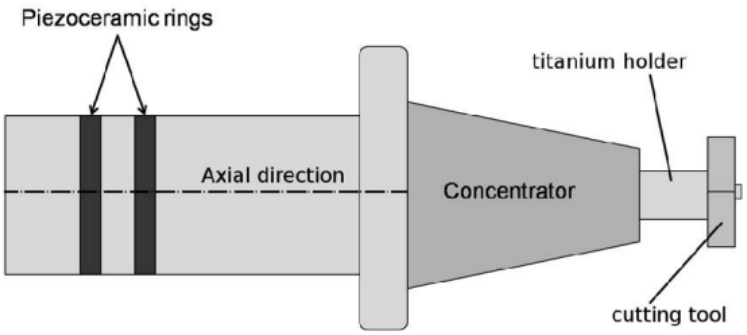

Figure 3-1: Schematic of Langevin concentrator head used in UAT [Maurotto *et al.*, 2000]

The manufacture of work-pieces using UAM can be divided into two distinct processes: one is ultrasonic erosion and another is ultrasonic cutting. In the former a hard tool is vibrated against the work-piece with abrasive slurry in between, forcing abrasive particles of fine grain against the work-piece material. The sonotrode (tool) is machined in a particular shape out of a hard material and is attached to the transducer which generates the ultrasonic vibrations. The sonotrode does not directly touch the work-piece material but causes the abrasive particles to erode the

work-piece material ultimately conforming it to the sonotrode shape.

The latter technique uses a vibrating cutting tool [Figure 3-1] that interacts directly with the work-piece without any abrasive interface. Such a technique may be applied to well known machining techniques such as drilling, milling and turning (dry or lubricated). Heat-resistant, brittle, ceramics and hard alloys are very difficult to cut by means of conventional machining techniques; ultrasonically assisted machining methods are then employed to improve the machining.

In conventional machining, vibrations are unwanted, so every possible precaution is taken to reduce them. However in vibration-assisted machining the presence of ultrasonic vibrations is purposely introduced in the cutting process so improving the surface finish, operational noise and dimensional accuracy.

For example, in ultrasonically-assisted drilling, a reduction in cutting forces, increase in drilling speed and in the quality of the finished holes have been observed in the tests in Wolfson School of Mechanical and Manufacturing Engineering in Loughborough University. Moreover, the technique has proven to be beneficial in the drilling of composite materials, in which de-lamination of materials components is greatly reduced, thus improving the quality of the finished product.

3.1 Methods of generation of the ultrasonic vibration

The earliest and most common method available for the generation of ultrasonic vibration is the magnetostrictive effect, or Joule effect, discovered by Joule in 1847. A ferromagnetic material, generally a nickel alloy, subjected to a strong magnetic

field changes shape, becoming smaller or larger, although the dimensional variations are extremely small and depends on the material, temperature, magnetic state. The strain generated by the magnetostrictive effect is generally very small, and its sign depends on the material used. Some cobalt and nickel alloy became shorter on magnetization, while iron and iron-cobalt alloys variation depends on the sign of the magnetization. When the temperature of the magnetostrictive alloy is raised the strain diminishes reaching zero at the curie point of the material effectively rendering null the effect. Beside this, the speed of sound in the material changes according to temperature, thus changing the position of the nodal points, ultimately making the design of a magnetostrictive driven cutting head a trial and error process [David & Cheeke, 2002].

The efficiency of these transducers is limited when compared to the more efficient piezoelectric ones. They require an active cooling to remove the heat generated because the poor conversion factor in mechanical energy of the magnetic energy supplied. The poor conversion efficiency between magnetic energy and mechanical energy that affect the magnetostrictive transducers made the much more efficient piezoelectric ones the preferred in ultrasonically-assisted machining.

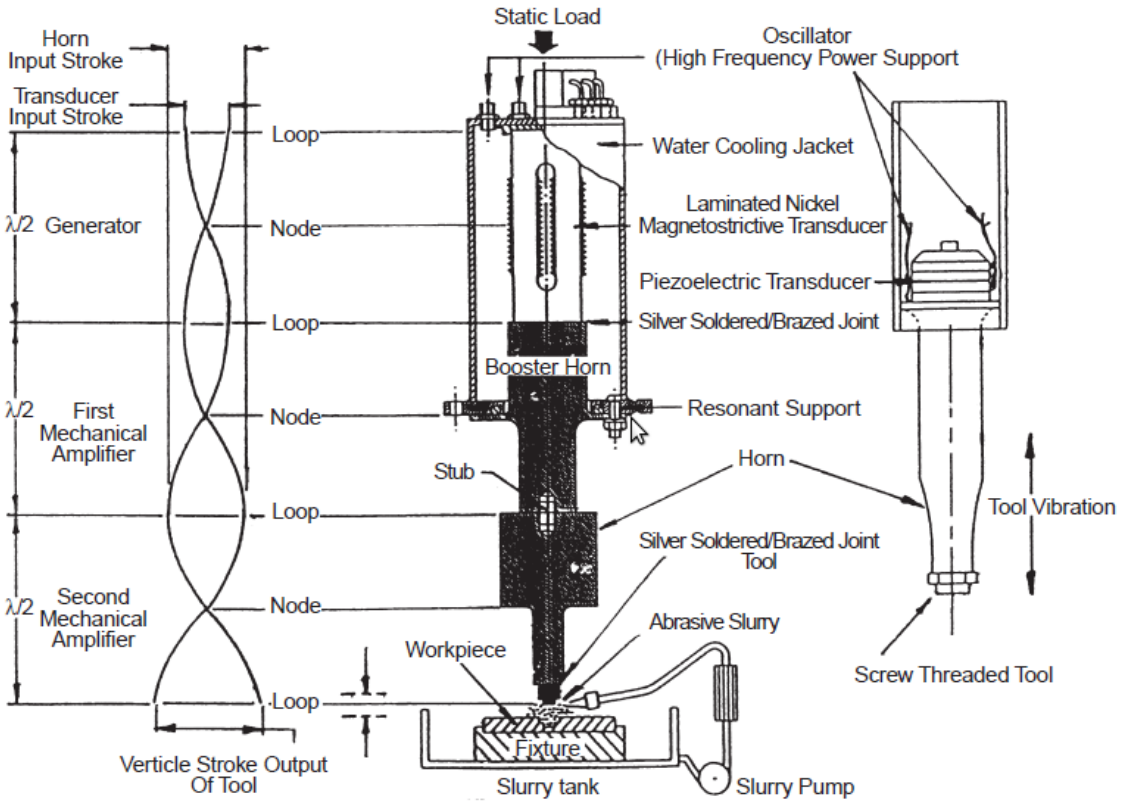

Figure 3-2: Magnetostrictive and piezo transducers schematic comparison [Thoe *et al.*, 1998]

Nowadays, the most used method for the generation of ultrasonic vibrations is the piezoelectric effect. This technique was discovered by the Curi brothers in 1880, who observed that some types of crystal under compressive stress produce free electric charges on their surface. This effect is extremely energy efficient, accounting for only 4% loss in the conversion of electric energy into mechanical energy. The piezoelectric materials are, in our case, in the form of ceramic disks which are squeezed between a high density base and a lower density front area, which is the tool face of the transducer. In fact, for momentum conservation, velocity and amplitude of vibration are higher in the lower density material. Beside this, since even at the resonant frequency the oscillation amplitude of such a transducer doesn't usually exceed 10 μm, it is necessary to concentrate the energy into a smaller volume by the use of a concentrator (a shaped wave-guide). The concentrator is the

link between the transducer and the cutting tool. It increases the vibration amplitude of the tool by increasing the particle velocity of the tool, and allow for matching to the different load conditions experienced during the cutting operations. The design of a concentrator is based on the plane wave assumption, where every vibration direction orthogonal to the axis of the concentrator is neglected. It is important to note that transverse vibration cannot be neglected when the lateral dimension of the transducer is comparable with the wavelength of the longitudinal waves. In the assumption that a perfectly sinusoidal plane wave is generated by the transducer and there is no transverse compression wave, it is possible to apply the laws of conservation of mass and force and obtain:

$$\frac{d^2u}{dx^2} + \frac{1}{F}\frac{dF}{dx} + \frac{\omega^2}{{v_s}^2} * u = 0 \qquad 3.1$$

It is possible to proficiently apply this equation to concentrators of any shape but its solution is beyond the scope of this work. The ceramic disks in the resonator have to be pre-loaded in compression in order to avoid separation of the assembly during the operations and to avoid the brittle ceramic to be loaded with tensile stresses [Figure 3-3]. This is generally achieved by a large screw between the concentrator and the resonator which applies a significant compressive stress to the piezoelectric elements, however it is not infrequent to encounter other methods. The generated mechanical energy, which is uniformly distributed over the whole cross surface of concentrator, becomes concentrated in smaller and smaller areas by tapering the concentrator.

Provided that the shape of the concentrator is such that the acoustic energy is not reflected back from the sides (i.e. its length to width ratio is high enough), the narrower end shows a greater oscillatory velocity and wider displacement amplitude

[Figure 3-2].

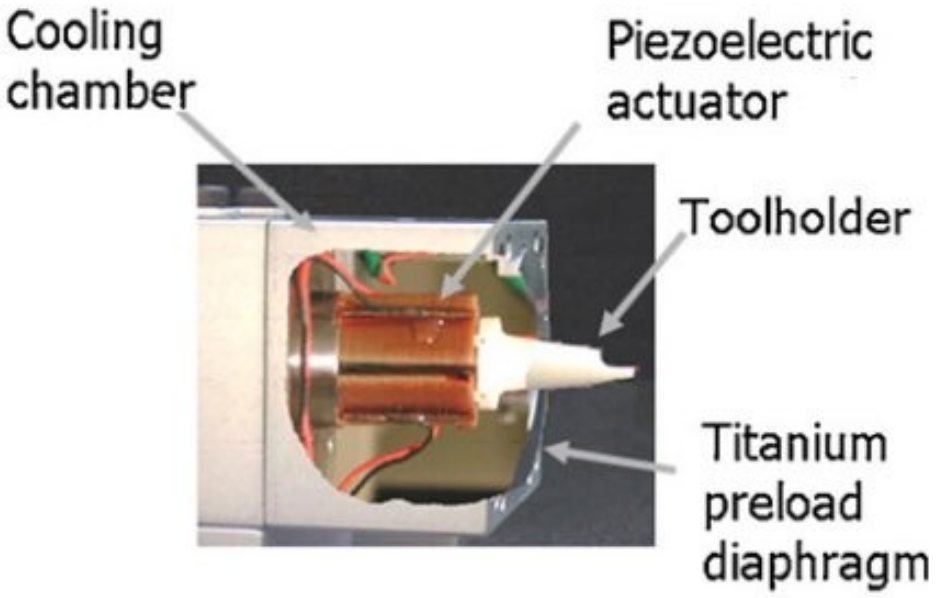

Figure 3-3: Industrial piezoelectric transducer [Brehl & Dow, 2008]

With a good shaped and well tuned concentrator, it is possible to increase the maximum amplitude up to 6 times according to the area factor (the ratio of the cross sectional areas at the junction with the transducer and at the end of the tapering), achieving the necessary range of displacement on the tool face. It is important to note that the larger the area factor the more suited for rough machining is the concentrator (due to the larger displacements achieved). However larger displacements accelerate the fatigue failure of the transducer material, so an optimal size has to be selected.

3.2 Ultrasonically assisted turning

When a sound wave propagating in a material reaches its boundary with another material of largely different acoustic impedance, it is reflected back in a direction parallel to the orthogonal direction of the interface surface. If the medium in which the wave is reflected has a length of N wavelengths a standing wave is formed. In this latter case, there are compression positions of minimum amplitude called nodes, and tension position of maximum amplitude called antinodes. In Vibration Assisted Machining (VAM), the position of the tool is always at an antinode. The movement of the cutting insert is periodic and can be approximated by the function of the harmonic oscillator:

$$u_0(t) = a\cos(\omega t) \qquad (3.2)$$

where a is the amplitude of the vibration and ω is the angular frequency in rad/sec. It is possible to write the formula in dependence of the relative speed of the cutter insert:

$$v_o(t) = -a\,\omega\,\sin(\omega t) \qquad (3.3)$$

It's possible to define Ultrasonically Assisted Turning as a process using a vibrational frequency of the cutting insert at the upper limit or outside the auditory capacity of the human ear (f≥15-18 kHz).

Taking as a reference the position of the work-piece central axis, the three independent principal direction in which ultrasonic vibration can be applied are the feed direction (or the direction along the axis), the radial direction (or the direction orthogonal to the work-piece surface) and the tangential direction (or the direction along the tangent to the work-piece surface) [**Error! Reference source not found.**].

In order to apply vibration in the feed direction a specially designed transducer is generally required, the large dimensions of the body of a normal sized transducer generally interfere with the machining operation due to the geometrical constrains of the machining process. The use of a normal size transducer would severely limit the range of application due to its large cross-section and length which would interfere with the machining operations [Figure 3-4].

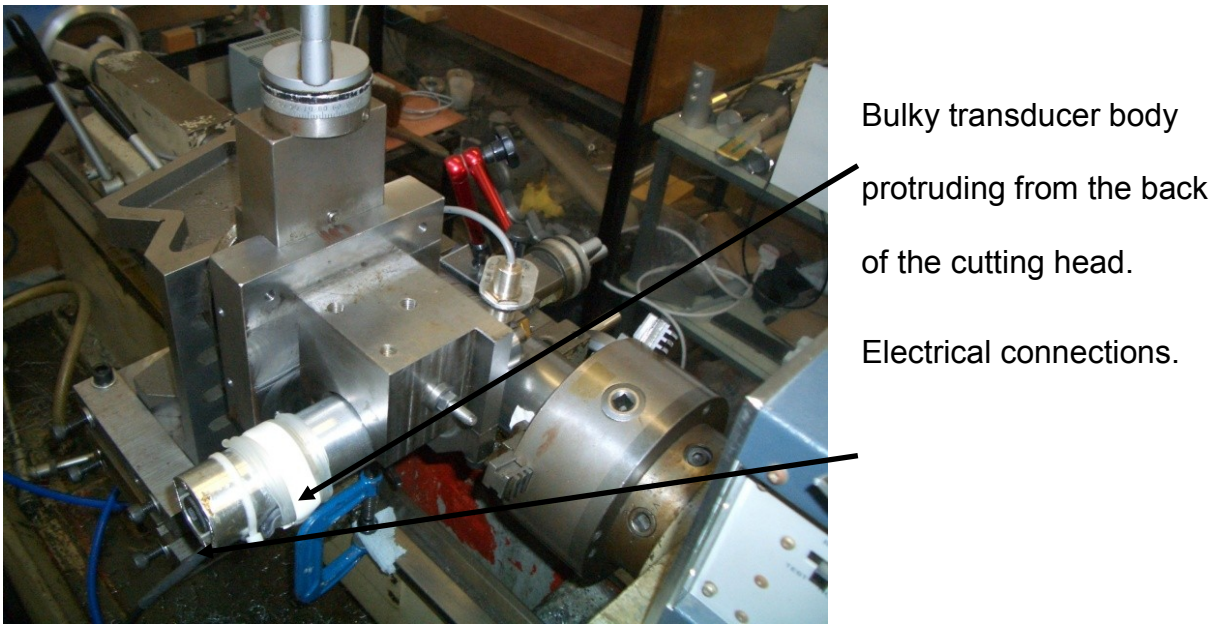

Figure 3-4: Rear view of the cutting head

For this reason, to apply vibration in the feed direction specially designed transducers are needed. The simplest of these designs uses 90° tool holders which are less efficient in the transmission of the vibration. Vibrations in the radial directions are not generally used because they result in a deterioration of the surface finish of the work-piece, it is interesting to notice that they still improve the dimensional quality of the finished work-piece [Markov, 1969].

Tangential vibration mode is thus the most used vibration mode [Brehl & Dow, 2008] because the technology needed is of relative ease of implementation. It also ensures the highest reduction of the cutting force as well as good improvement of surface

finish and dimensional accuracy of the finished work-piece, sparing from the need of time-expensive additional finishing operations. This vibrational mode also considerably reduces the chip shrinkage factor and the height of the surface defects on the finished work-piece [Markov, 1966].

In order to explain the force reduction observed in UAT of this alloy a rheological approach is used as suggested in [Astashev and Babitsky, 2007]. In this model the visco-elasto-plastic properties of real materials are used. The material undergoes deformation while subject to vibrational loading; hence, it was not possible to split the deformation process into an elastic part and a plastic (with hardening) one. The periodic motion of the cutting tool could be written as the one of a harmonic oscillator. It is possible to split the problem even further into three possible conditions: 1) the tool deforms the work-piece in the elastic region; no permanent deformation is observed (the tool could or could not lose contact with the work-piece); 2) the deformation imposed by the tool overcomes the yield point introducing plastic deformation on the work-piece, but the tool loses contact with the deformed work-piece during part of the cycles; 3) the tool introduces plastic deformation but never loses contact in any part of the cycle. In all the cases, in which the cutting speed is lower than the critical velocity, the tool and work-piece are in the second condition. For cutting speeds higher than the critical velocity, the third condition is expected. In the first condition it is possible to write the contact force as

$$F = \frac{ak_0}{\pi}\left[\sqrt{1-\left(1-\frac{h}{a}\right)^2} - \left(1-\frac{h}{a}\right)\cos^{-1}\left(1-\frac{h}{a}\right)\right], \qquad 3.4$$

where a is the amplitude of tool displacement, h is the maximum deformation over a period and k_0 is the static stiffness of the work-piece. More interesting is the second case where the impact force can be written as

$$F(t) = \begin{cases} k_0(vt + a\sin\omega t - \Delta) & t_1 \le t \le t_2 \\ D & t_2 \le t \le t_3 \\ D + k_0(vt + a\sin\omega t - u_m) & t_3 \le t \le t_4 \end{cases}, \qquad 3.5$$

where Δ is the distance between the centre line of the vibrating tool and the underformed work-piece, D is the force at which the work-piece starts to deform in plastic mode, u_m is the maximum displacement of the tool. The first, second and third intervals, represent respectively the period starting at the moment the tool contacts the work-piece up to the incipient beginning of plastic deformation (t_1-t_2), the period in which the work-piece undergoes plastic deformation (t_2-t_3), and the disengagement of the tool from the work-piece (t_3-t_4). It is interesting to notice that for deformation speeds $v \geq a\omega$ the deformation force $F=D$. In real ultrasonic cutting processes the velocity used are generally small and it is possible in these cases to simplify eq. 5.2 linking the static force with the speed of plastic deformation:

$$F = \frac{\pi}{2}\left(\frac{2D}{k_0 a} - 1\right) + \sqrt{1 - (1 - \frac{D}{k_0 a})^2} - \sqrt{1 - (1 - \frac{2\pi v}{a\omega})^2} + \sqrt{1 - (1 - \frac{D}{k_0 a} - \frac{2\pi v}{a\omega})^2} + (1 - \frac{D}{k_0 a})\sin^{-1}\left(1 - \frac{D}{k_0 a}\right) - (1 - \frac{2\pi v}{a\omega})\sin^{-1}\left(1 - \frac{2\pi v}{a\omega}\right) + (1 - \frac{D}{k_0 a} - \frac{2\pi v}{a\omega})\sin^{-1}(1 - \frac{D}{k_0 a} - \frac{2\pi v}{a\omega}). \qquad 3.6$$

For $v<0.25a\omega$ the material seems to undergo a softening process, with a decrease in the static force required for plastic deformation. During each cycle the material is in fact plastically deformed before being unloaded. Residual deformation persists and accumulates in the next cycle. This causes the material to appear softer as the yield point was decreased [Astashev, and Babitsky, 2007].

It is possible to calculate the maximum decrease of the cutting force during the plastic deformation if an ideal rigid-plastic material is taken into account. In this class of materials $k_0 \to \infty$, so they are completely rigid until the deformation force reaches

a limit, after which they undergo plastic deformation with no hardening. In the case in which $v<0.25a\,\omega$ it is possible to write $v = \frac{a\omega}{\pi}(\sin\frac{\pi P}{D})^2$. To simplify even further, it is possible to write, if $P<<D$, a relation, which will provide the maximum reduction that is possible to obtain by the use of ultrasonic vibration:

$$V = a\omega\pi(\frac{P}{D})^2 = 2a\pi^2 f(\frac{P}{D})^2. \qquad 3.7$$

This is valid in the point-like, mono-dimensional case, which is elaborated in the theory.

The key difference between UAT as compared to CT is that in the former, the cutting insert has an intermittent contact with the work-piece during operations, since for optimal cutting condition is needed to have a complete separation of the cutting edge from the work-piece for every cycle. It is then possible to state a critical turning speed for Ultrasonically Assisted Turning after which there is no longer complete separation between the cutting tool and the work-piece during the cutting operations:

$$V_c = a\,\omega\, = 2\,\pi\, af_q \qquad 3.8$$

where f_q is the frequency in Hz, ω is the angular velocity in rad/sec and a is the maximum amplitude of the vibration. In order to ensure complete separation of the cutting insert from the cutting surface during each cycle of the oscillations is needed that the cutting velocity does not exceed V_c. The desired micro-impact cutting conditions are seen only with complete separation between the cutting tool and the work-piece provided that the vibrational velocity of the cutting insert is greater than the cutting speed:

$$V_c = 2\,\pi\, af_q > V = \pi n D \qquad 3.9$$

where V is the cutting speed, n the rotational speed and D is the diameter of the

work-piece. In order to increase the cutting speed during machining, it is desirable to achieve the maximum possible displacement from the concentrator. The maximum displacement achievable is however limited by the fatigue strength of the concentrator material and of the total mass of the cutting tool and tool holder. It is advisable then to increase the resistance to fatigue of the surface of the concentrator by shot peaning or similar techniques, and to use materials which offer a good fatigue resistance. The total mass of the concentrator should be also kept to a minimum to achieve maximum displacements: for these reasons nowadays a concentrator made of Ti alloy or an advanced Al alloy is preferred to the earlier steel ones.

During the cutting process, due to the interaction between the tool and the work-piece, a vibration dampening process takes place because the cutting force is always opposing the movement of the tool. The main cutting force acts primarily against the vibration displacement effectively dampening the vibration. This process is expected since the the cutting tool edge, which can be consider as behaving like an harmonic oscillator when not in contact with the work-piece, will be subject to the cutting force and friction force immediately after contact, which then pose an obstacle to its movement.

After the cutting operations begin the vibrational mode of the cutting edge starts to behave like an under-damped oscillator. In some particular conditions the dampening process is so evident (the maximum amplitude and frequency of cutting edge vibration decrease so much) that a new evaluation of V_c is required. In Figure 3-5 the amplification effect of the concentrator is described: being the mass m_2 much smaller than m_1, if total vibration energy is to be preserved, then the total displacements observed for m_2 must be larger.

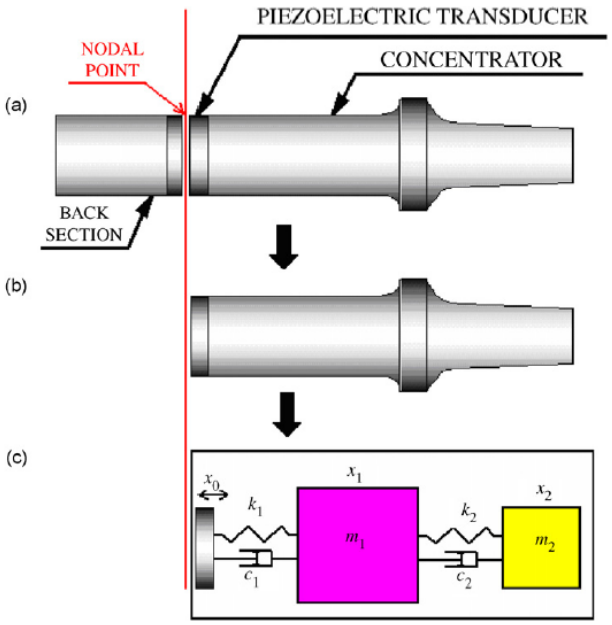

Figure 3-5: Simplifier model of transducer [Voronina *et al.*, 2008]

4 Test rig

4.1 Introduction

A hybrid CT-UAT lathe capable of performing both conventional turning and ultrasonically assisted one is currently operational at Loughborough University. The unit was developed over a time span of several years by different researchers. Various experimental tests were performed in the past to confirm the advantages of ultrasonically assisted turning in comparison to conventional one [Ahmed *et al.*, 2006; Mitrofanov *et al.*, 2005; Mitrofanov *et al.*, 2003; Mitrofanov, 2004; Mitrofanov *et al.*, 2005; Babitsky *et al.*, 2003; Babitsky *et al*., 2004, Voronina and Babitsky, 2008]. Experimental measurements of the cutting force components and surface analysis of the finished work-pieces were performed for several alloys and cutting tools to quantify the performances of the system in UAT. Different tests involving high-speed filming, thermal analysis of a chip-formation process, micro structural analysis and surface studies of machined work-pieces were performed along with numerical simulations [Mitrofanov *et al.* 2003; Mitrofanov, 2004; Mitrofanov et al, 2005] to improve the understanding of underlying machining dynamics of turning in UAT. The feasibility of introduction of an UAT head into a commercial lathe has been extensively investigated but further researches are needed to achieve a better understanding of the cutting process allowing for an industrial application in a similar fashion to commercially available ultrasonically assisted milling machines (DMG is offering a CNC UA milling machine [DMG, 2010]).

4.2UAT lathe

The lathe chosen in this study for installation of the UAT head is a widely available Harrison 300: a small-size lathe with manual controls of robust and reliable construction. Extensive modifications were required to install the ultrasonic transducer head on the lathe cross-slide retaining control on the depth of cut. In the first attempt, a customised tool holder was manufactured to replace the standard tool post, which houses the ultrasonic transducer and the dynamometer for force measurements.

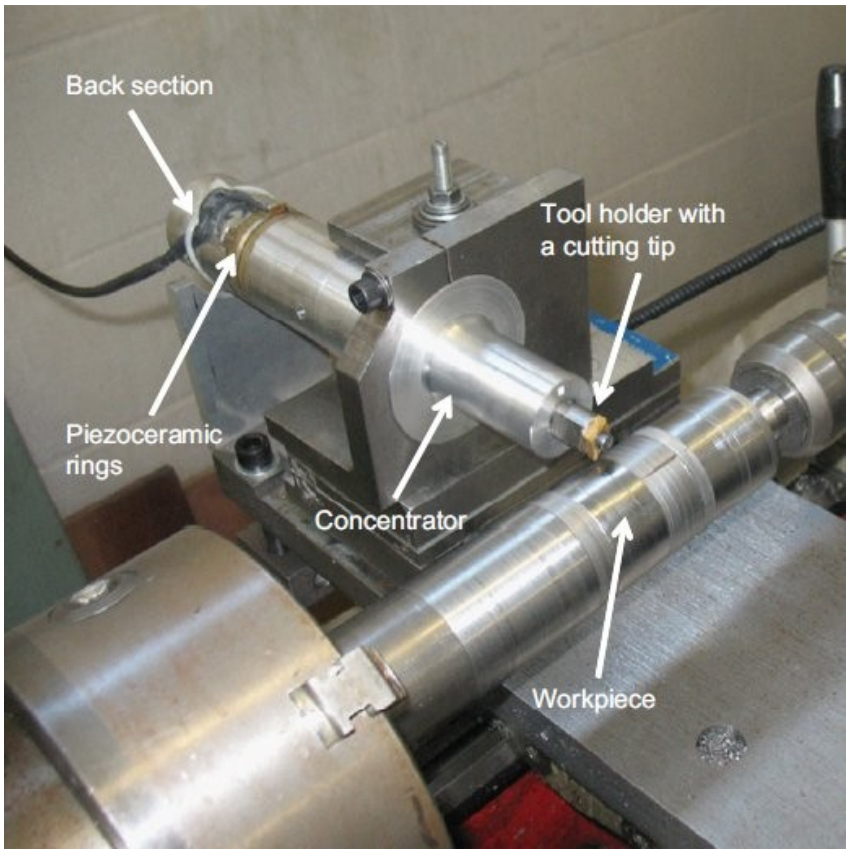

Figure 4-1: Early prototype [Voronina *et al.*, 2008]

The earlier setup [Figure 4-1] featured a simplified control of the depth of cut involving the use of interchangeable high-density plastic spacers. This setup offered the easiest way of implementing UAT on a commercial lathe. However due to its

simplicity, several shortcomings were observed. Adjustments to the depth of cut required the ultrasonic transducer to be completely disassembled from the tool post thus denying the capability of setting a variable depth of cut during operations. Moreover, the use of plastic spacers greatly affected total rigidity of the system and offered less-than-optimal precision in the depth-of-cut setting. The rotation direction of the lathe was inverted in order to allow cutting from the far end of the cross slide bringing the wiring away from the cutting zone. Still, this design was effective in the machining of Ni-based alloys and allowed for early tests of improvements to UAT as compared with CT. The first design of the tool holder was changed over the years in order to improve the control of the depth of cut as well as rigidity of the cutting assembly that is crucial for UAT.

4.3 Second prototype (Stage II)

The cutting performances of the early prototype were better in UAT than in CT however, it was obviously difficult and cumbersome to achieve a consistent depth of cut. So, given the necessity of performing tests at different depths of cut for work-pieces of different diameters and materials, a system for adjusting the depth-of-cut level more accurately was developed. Due to the dimension constraints of the UAT head it was necessary to suspend the whole cutting head and dynamometer on a cantilever system for a depth of cut adjustment.

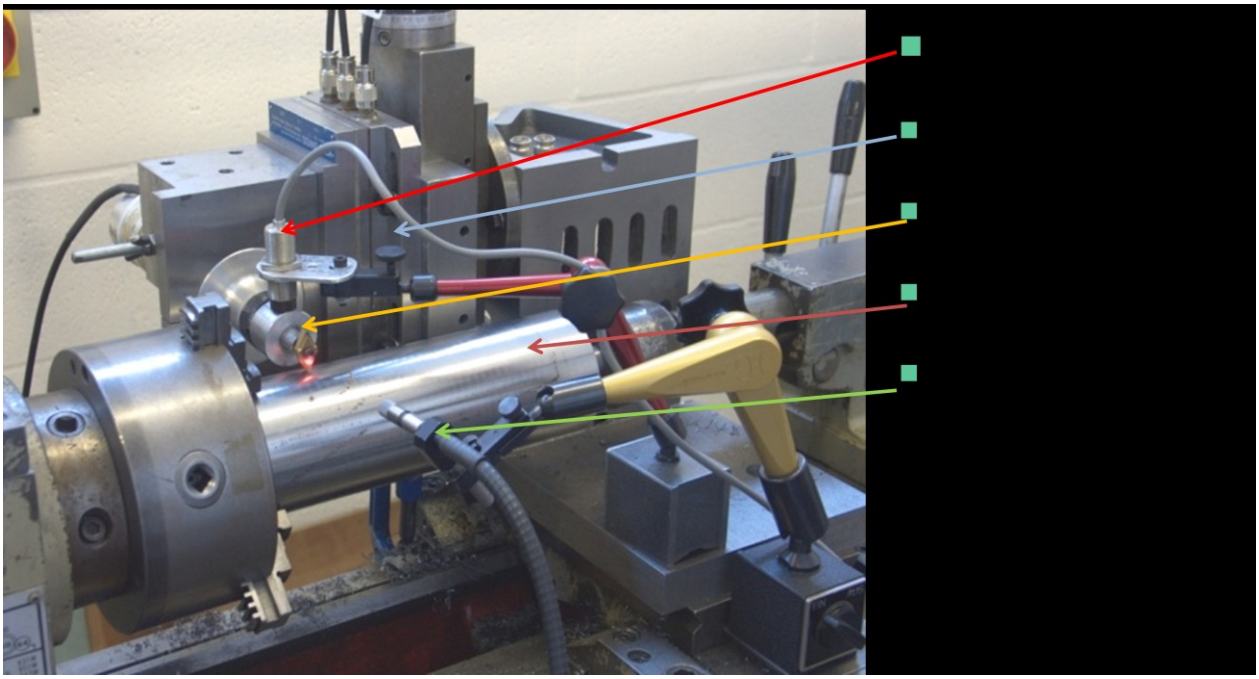

Figure 4-2: Stage II prototype

A reliable and rigid design was needed to prevent the cutting head to be subject to excessive displacements during cutting due to the additional leverage (D_c) for the cutting force introduced by the cantilever generated by the distance between the cutting tool and the fixation of the head on the cross slide [Figure 4-3]. A full-metal structure ensured that the system was no longer affected by the insufficient rigidity problems that plagued the first prototype and rendered it useless for variable depth-of-cut tests. In order to guarantee orthogonality of the cutting head with respect to the lathe cross-slide, a grade B cast iron angle plate was used as support for the micrometer [Figure 4-2]. Cast iron was selected for its good stiffness coupled with high density, ease of machining and resistance to corrosion. It was needed to keep stiffness of the cutting assembly as high as possible in order to take the most advantage of UAT cutting. The used angle plate was available with good angle accuracy (± 0.5°). For a convenient and quick adjustment of the depth of cut, a lathe micrometer was selected to be installed in the setup. It provided the necessary

sturdiness while preserving a good precision during adjustments; it is commercially available and easily replaceable in case of mechanical failure. A dynamometer was directly bolted between the cutting head and the micrometer minimizing the distance between the cutting insert and the force measurement plate, thus minimizing the distance D_c (~250 mm) [Figure 4-3].

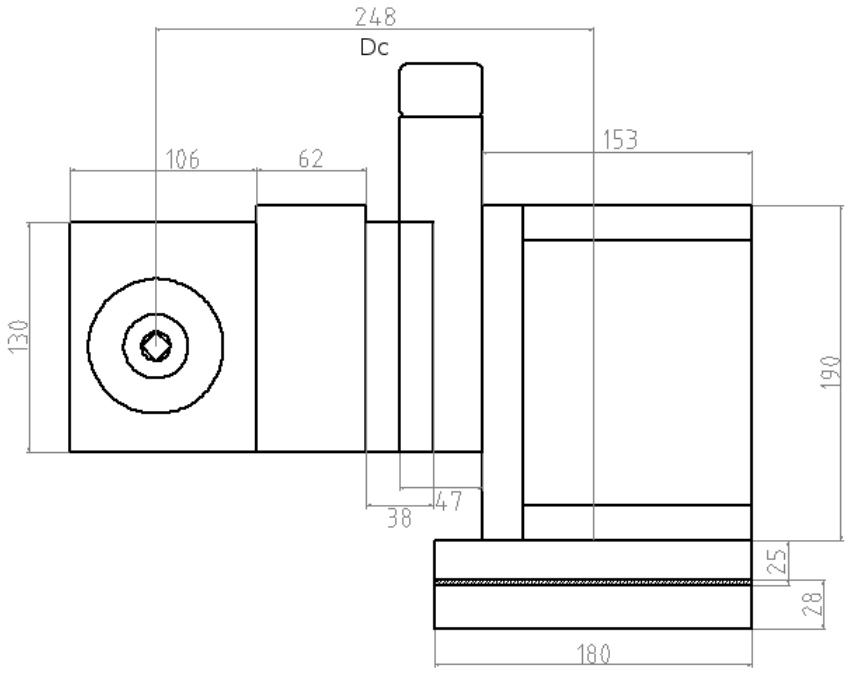

Figure 4-3: Stage II schematic

The depth of cut was continuously monitored by a non-contact eddy current sensor with a precision up to 20 μm [Figure 4-2]. It was later found out that this sensor was too sensitive to the magnetic properties of the materials measured; it needed a full calibration every time the cutting inserts were changed. It was also sensitive to electrical noise present in the laboratory to the point that it was often drifting when other machines were in use.

After several tests, that setup started to show some space for improvements: rigidity of the whole system could be further improved while minimizing the distance between the cutting head and the middle point on the cross-slide of the lathe D_c. The

lathe micrometer that was extensively used in a normal lathe before being employed in the modified cross-slide developed tolerances that were affecting the fine adjustment of the depth of cut. The whole process of setting the depth-of-cut level eventually deteriorated in a trial-and-error process. For cutting with the requested precision shown by Table 4-1 the effects of insufficient rigidity could not be disregarded anymore.

Table 4-1: Stage II prototype cutting data, V=10 m/min, f=0.1 mm/rev

set a_p [μm]	**effective [μm]**		**σ (st.dev.)[μm]**		**Difference between UAT and CT [μm]**
	CT	**UAT**	**CT**	**UAT**	
100	210	240	22	28	30
200	338	371	9.9	9.6	33
300	491	530	5.13	9.8	39

The differences in selected and observed a_p were large in both CT and UAT. During UAT, the radial component of the cutting force is reduced, higher than CT a_p were commonly observed. This effect was easy to explain as the depth-of-cut was always set during the CT operation with an higher radial component acting on the head. When UAT was switched on, this component dropped reducing the head displacement ultimately resulting in a higher a_p.

A third, revised version of the setup was then needed in order to fix these shortcomings and bring the system to cut with better precision.

4.4 Third prototype (Stage III)

The rigidity of the second design was to be further increased, and to do so a new approach was used: the distance between the cutting head and the centre line of the cross-slide had to be minimized [Figure 4-4] in order to further reduce the distance D_c.

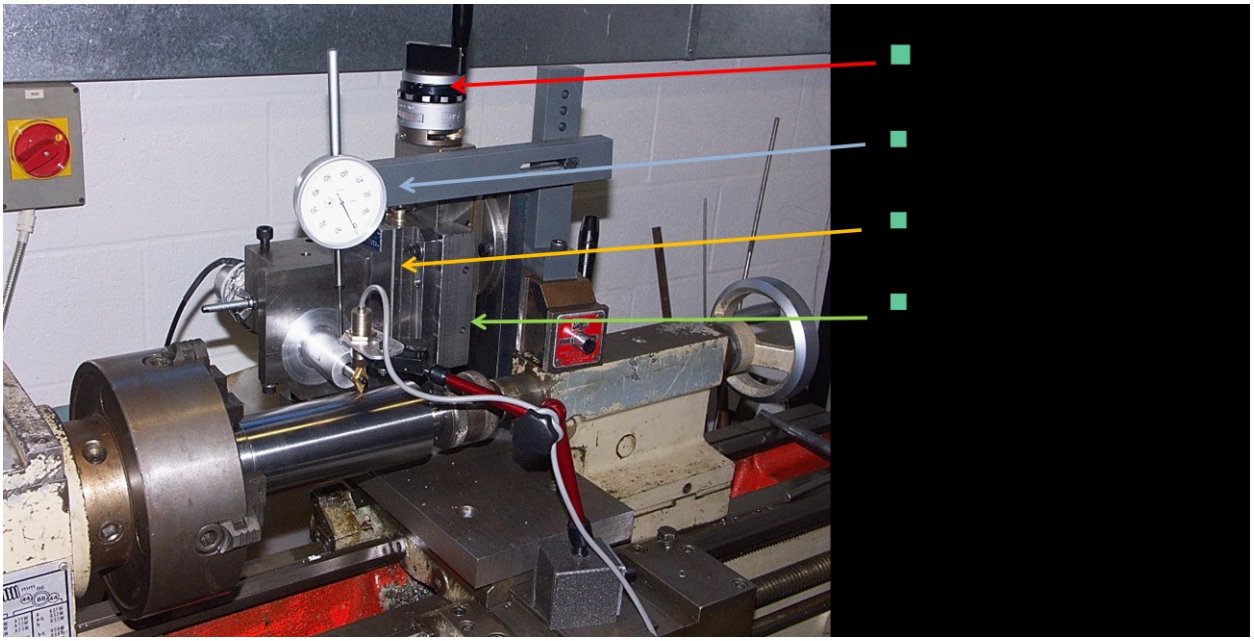

Figure 4-4: Stage III prototype

Precision-ground steel plates, 25 mm thick, were milled and bolted together to build a custom-designed holder to ensure optimal rigidity while minimizing the distance between the centre of force (the cutting tool edge) and the centre line of the lathe cross-slide thus reducing the leverage D_c.

Figure 4-5: Stage III mounting post

The lathe micrometer was then substituted with a new one ensuring smoother adjustment operations and increasing the longitudinal rigidity of the assembly [Figure 4-5].

Static stiffness of the system was improved. It is known that the machining system behaves differently when the ultrasonic vibration is used in the cutting operations. In this case the response of the whole system is influenced by the dynamic stiffness of the assembly. In UAT operation, dynamic stiffness, which is linked to the damping properties of the system at the frequency of the exciting force, is of key importance to ensure the best possible outcome. High dynamic stiffness minimizes variations in the depth of cut under the ultrasonic cutting operation, enhances the response of the system in the transient loading condition, typical for UAT, and ensures that the maximum energy is transmitted from the vibrating cutting tool to the work-piece. In order to maximize benefits, a large steel block was machined to fit precisely on the lathe micrometer serving as a base for the dynamometer. Its high mass greatly

increased the dynamic stiffness of the system ensuring the maximum effect of the ultrasonic vibration [Astashev *et al.*, 2007]. A heavier block would have further increased the dynamic stiffness but would have also increased the distance between the centre line of the cross slide and the cutting insert D_c thus worsening the leverage. Besides that, a larger block could interfere with the work-piece and increase too much the level of stresses applied to the micrometer. The chosen size was predicted to be effective without being intrusive.

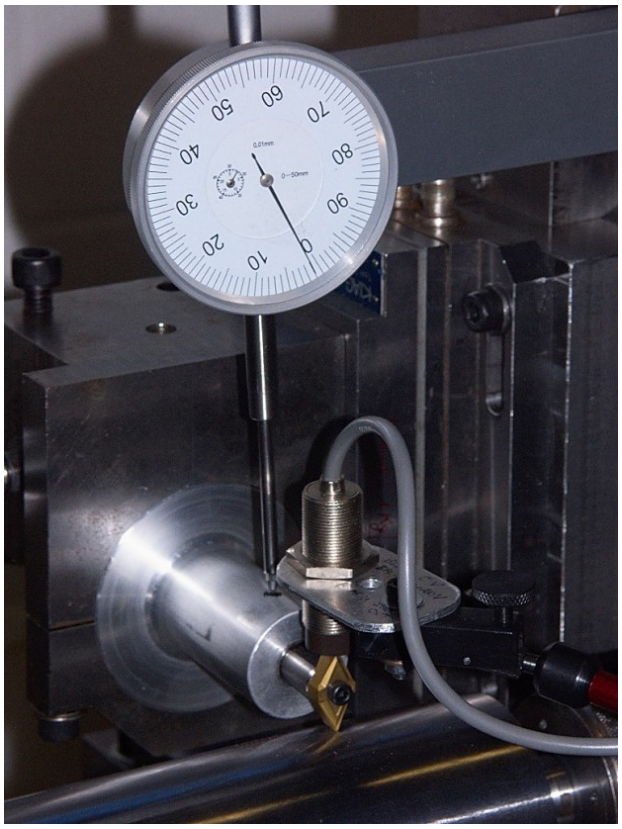

Figure 4-6: Stage III prototype close up

In order to achieve higher precision in the setting of the depth of cut, a mechanical dial gauge [Figure 4-6] with scaled in 10 μm increments was mounted on the cutting head to replace the eddy-current one which was proven to give wrong absolute readings. A long-travel model was chosen with a measuring range of 50 mm, sufficient to ensure adjustment-free operability with most work-piece diameters. The

measuring post was custom-machined from a nylon polymer block in order to ensure sufficient rigidity of the assembly and improved vibration dampening, while keeping the parasitic weight on the cross-slide as low as possible. The contact point between the tip of the dial gauge and the wave-guide was protected with reinforced neoprene rubber to prevent dangerous levels of ultrasonic vibration transmitted to the dial's inner mechanism. Due to increased stiffness of the system, the level of parasitic vibration was negligibly small. In that design the use of the eddy-current gauge was not longer considered beneficial enough to justify complexity added to the system. In order to achieve the best results, several improvements were implemented to the first design, increasing greatly reliability of the system. In particular, a custom-machined aluminium sleeve, installed between the tool and the tool holder, offered the most beneficial effect. As a result, the increased compliance between the tool and the tool holder caused the cutting force to show a reduction of 50%. All the results presented here involve the use of this component and were obtained in cutting tests of cylindrical work-pieces of Ti 15-3-3-3 alloy with diameter of 78 mm.

Table 4-2: Stage III prototype cutting data, V=10 m/min, f=0.1 mm/rev

set DOC [µm]	**effective [µm]**		**STD[µm]**		**Difference between UAT and CT [µm]**
	CT	**UAT**	**CT**	**UAT**	
50	54.5	61.5	10.6	0.7	7
100	107.3	110.3	10.2	11.8	3

200	209	232	8.5	3.5	23
300	304	321	0.8	1.4	17

It should be noted that it was considered unsafe to operate the ultrasonic vibration while the micrometric dial was in contact with the cutting head (vibration would easily displace or damage the delicate mechanism inside). All the cutting operations were started in Conventional Turning, vibration was started only after setting the desired a_p. Since in UAT the radial component of the cutting force is much smaller than in CT, the cutting head displacement was reduced and a deeper-than-expected a_p was achieved.

Additionally, in order to improve the fixture of the work-piece to the lathe, a three-jaw self-centering chuck of the lathe was replaced with a four-jaw one. That chuck allowed for a fine centring of the work-piece thus reducing the errors associated with incorrect centering of the work-piece to low levels (less than 10 μm). This setup[Figure 4-7], allowed an overall reduction of the distance D_c between the cutting edge and the cross slide by half (~119 mm) when compared to the second prototype [Figure 4-2].

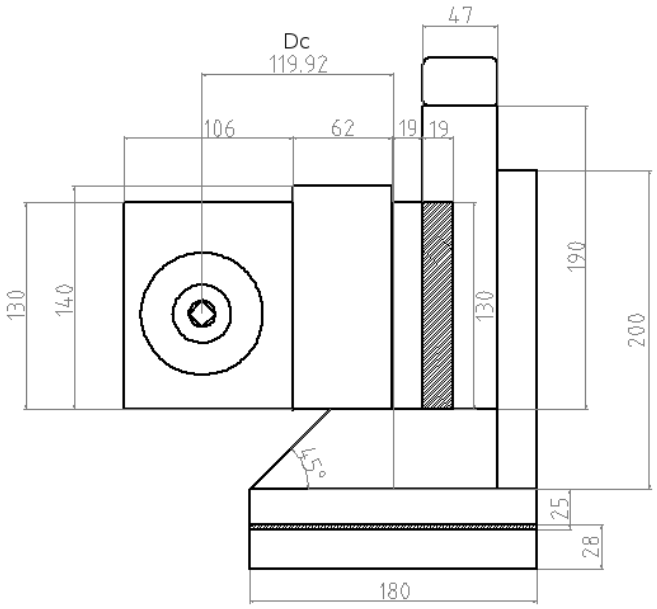

Figure 4-7: Stage III schematic

It allowed the use of a counter-centring point as a support for the work-piece from the opposite side of the lathe chuck, further enhancing rigidity and reducing the time needed for correct centring the work-piece. Increased rigidity of the cutting assembly resulted in an increased precision of the depth of cutting. Not only mechanical problems affected the Stage II prototype, other ones were obscured by its major mechanical shortcomings. In Stage III, with limited mechanical noise, these other problems moved to the front.

The ultrasonic transducer operates with a high-voltage, high-frequency signal. This signal was extremely difficult to shield out completely, and it caused considerable electrical disturbance to a highly sensitive charge amplifier, especially due to close electric contact between the ultrasonic head and the dynamometer. When this signal reached the charge amplifier, which had very high input impedance, it was amplified and disrupted significantly a weak force-measurement signal of the piezoelectric element of the dynamometer. To avoid the disturbance signal travelling to the ground through the dynamometer (which is the only element in electric contact with the

cutting head), eventually ending into the amplifier via the connection cables, a reinforced neoprene rubber insulation shield was inserted between the dynamometer and the cutting head.

That rubber element not only prevented electrical disturbances from reaching the dynamometer but also reduced the amount of ultrasonic vibration disturbing it.

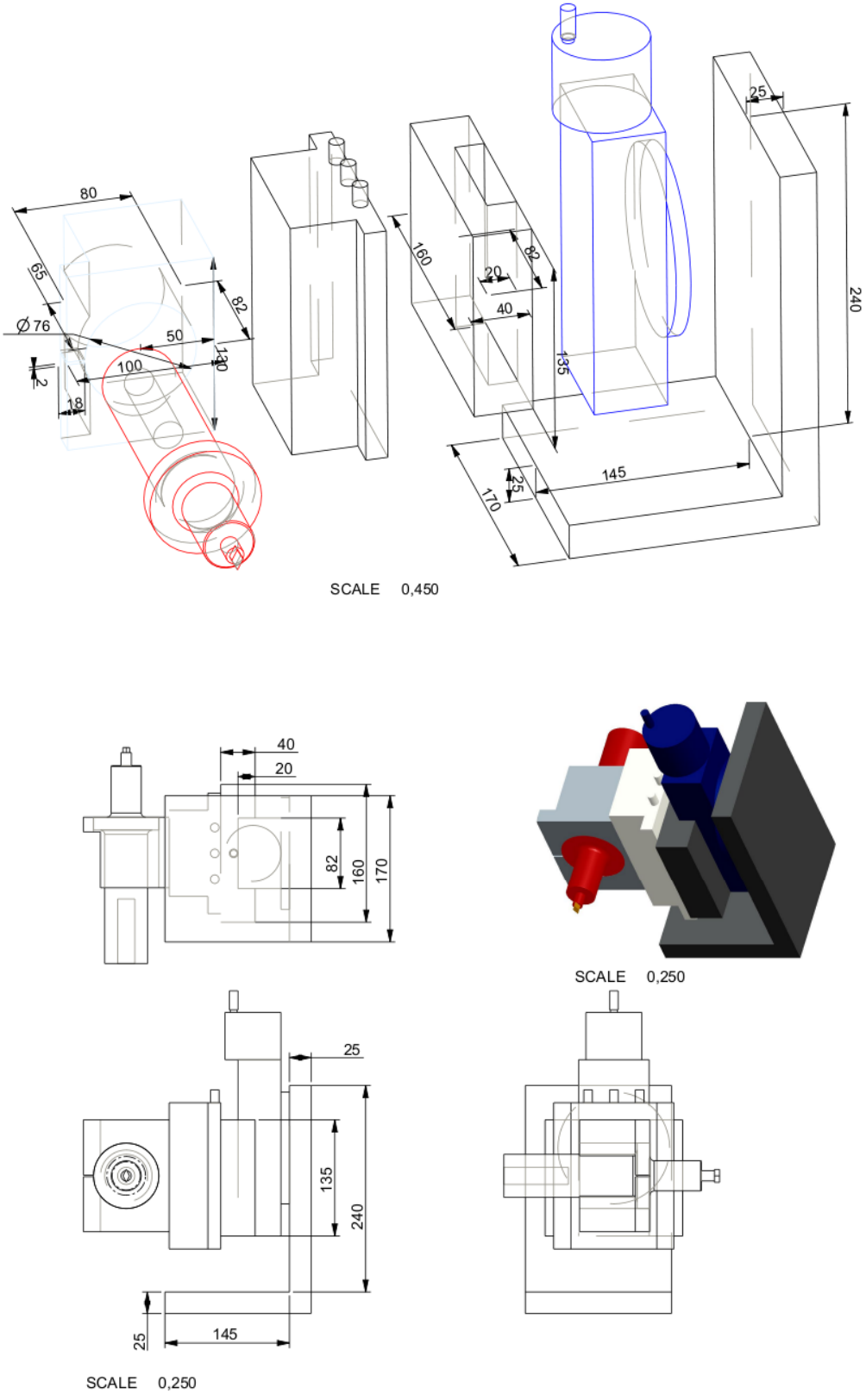

Figure 4-8: Drawing of Stage III prototype

The bolts, fixing the cutting head to the dynamometer, were completely insulated by a PTFE shield and a Kevlar groove. A low-impedance ground pole was supplied to the cutting head by means of a copper wire directly bolted on the cutting head and connected to the cross-slide to provide a preferential ground. As a result, the greatly reduced electric disturbance was below the noise level for the two major orthogonal components (tangential and radial) of the cutting force measured by the dynamometer, and appeared as an easily manageable linear drift for the third component (axial).

4.4.1 Finite element analysis (FEA)

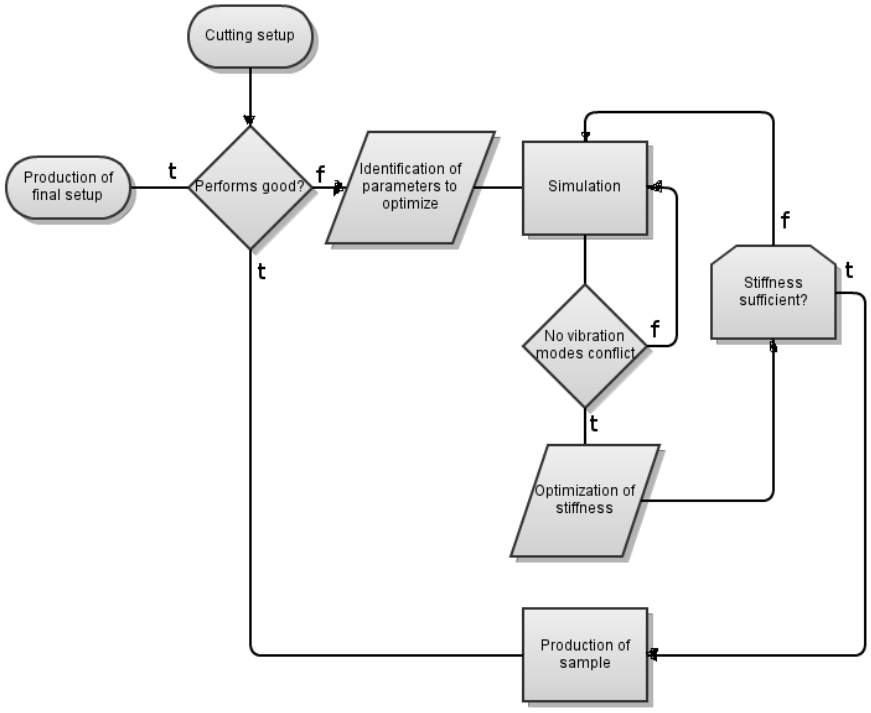

Figure 4-9: Optimization process of cutting assembly

During design of the whole cutting assembly, a care was taken to increase dynamic stiffness of the system as much as possible and to avoid driving the ultrasonic head with a frequency causing a resonance of the cutting assembly.

4.4.1.1 Introduction

A resonance in a system happens when a harmonic external driving force is applied to a system having a natural frequency equal or multiple of the driving force. In this case the resonance will cause large displacements, which might even result in the full structure to go over the elastic limit or even fail. In the simplified condition of absence of damping the harmonic driving force can be represented as:

$$F(t) = F_0 \cos \omega t, \qquad (4.3.1)$$

where, F_0 is the maximum magnitude of the force and ω is the frequency of the harmonic force in rad/sec.

If a system made of a simple mass attached to a spring in the absence of friction is considered [Figure 4-10]:

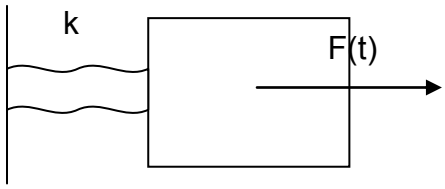

Figure 4-10:Schematic of simple mass attached to spring with coefficient k and applied harmonic force F(t)

it is possible to write the equation for the displacement x:

$$m\ddot{x}(t) + kx(t) = F_0 \cos \omega t. \qquad (4.3.2)$$

If each term of the equation is divided by the mass m, then:

$$\ddot{x}(t) + \omega_n^2 x(t) = a_0 \cos \omega t, \qquad (4.3.3)$$

where ω_n represents the natural frequency and a_0 is the acceleration of the system. Solving this equation results in the total response of the system:

$$x(t) = \frac{v_0}{\omega_n} \sin \omega_n t + (x_0 - \frac{a_0}{\omega_n^2 - \omega^2}) \cos \omega_n t + \frac{a_0}{\omega_n^2 - \omega^2} \cos \omega t, \qquad (4.3.4)$$

where v_0 is the initial speed.

For a driving frequency equal to the natural frequency, the amplitude $x(t)$ of the displacement becomes very large. This is a resonance condition, which should be avoided during the cutting operation. It must be also noted that for $\omega \to \omega_n$ the term $(\omega_n - \omega)$ becomes very small, while $(\omega_n + \omega)$ becomes comparatively large, resulting in a large variation in the amplitude known as a *beat* [Inman, 2007]. The beat condition is favourable for the system, since it is much less detrimental than the resonance condition.

In the absence of any damping the resonance condition brings ultimately large displacements that exceed any material mechanical characteristics. In the presence of damping, a viscous term does not allow for the displacement to grow infinitely but only up to a maximum limit yet negatively affecting the precision of the machining process. The ultrasonic transducer is the only element in the cutting head that is allowed to resonate; it is important that the whole system exhibits an excellent damping of vibrations and operates far from any resonance frequency.

4.4.1.2 FEA Model

For the finite element analysis the Simulia code Abaqus 6.11 Standard was used. It allowed calculating the approximate resonance frequencies and the associated resonance mode shapes of the complete cutting head. The driving frequency used in UAT, which is also the resonating frequency of the transducer complete with a cutting insert, was 17.8 kHz, this allowed reducing the input frequency range of the analysis, limited between 15 and 20 kHz, and, consequently, diminished the

computational time. The system, being continuous, in fact, exhibits infinite resonance harmonics. In order to study the response of the system to low-frequency vibration, such as these causing chatter, the first 10 modes were also computed.

The developed model used quadratic tetrahedral elements with different dimensions; the mesh was auto-generated with 26020 elements.

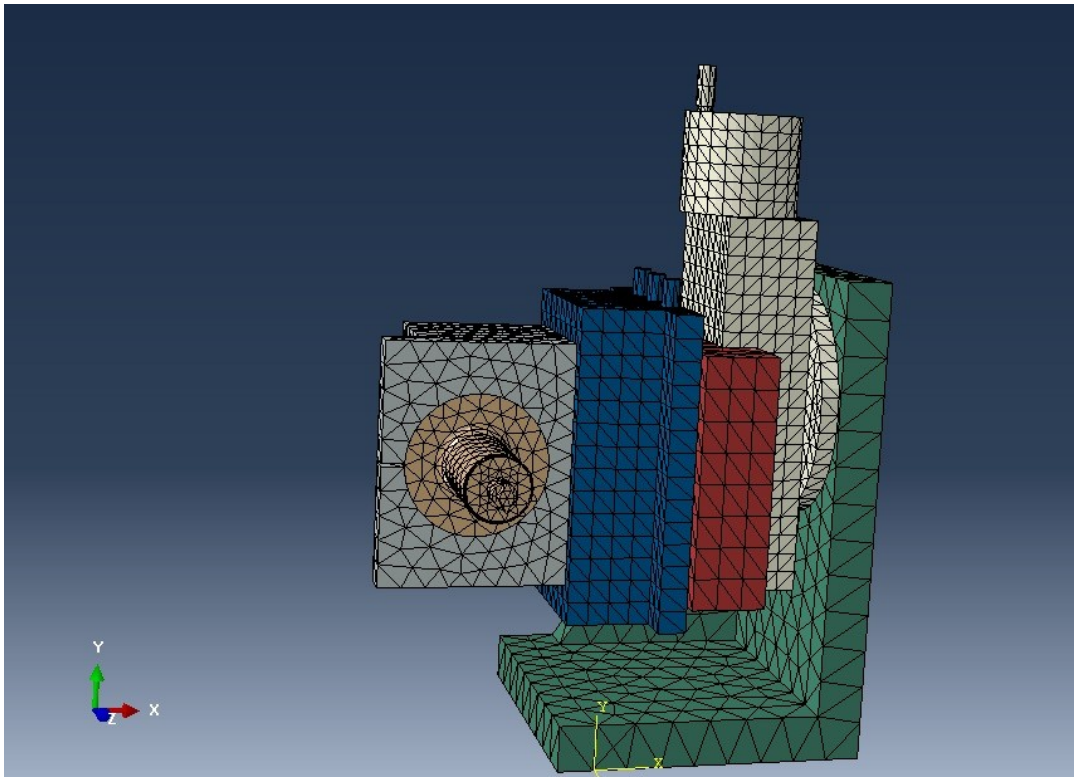

Figure 4-11: Model of cutting head with mesh

The bottom of the angle plate was restrained with all degrees of freedoms set to zero for all the analyses, to simulate it bolted to the cross-slide of the lathe.

4.4.1.3 Material properties

Most of the custom-machined parts of the cutting head were of mild steel, stainless steel was also the material of the dynamometer. The concentrator was the only

element constructed in high-fatigue-resistant aluminium. For the sake of simplicity the material properties were considered to be uniform in the steel parts ignoring the differences between mild steel and stainless steel. The materials of this simulation were considered to behave as elastic isotropic materials. All the mechanical properties [Table 4-3] were obtained from the material supplier.

Table 4-3: Material properties

Component	**Material**	**Supplier**	**Mechanical properties**	
Concentrator	High-fatigue aluminium	East Midlands alloy	Young's modulus	$7x10^4$ MPa
			Yield stress	25 MPa
			Poisson's ratio	0.25
			Density	$2.64x10^3$ kg/m^3
Angle plate	Steel	East Midlands alloy	Young's modulus	2E05 MPa
			Yield stress	160 MPa
			Poisson's ratio	0.27
			Density	$7.75x10^3$ kg/m^3
Micrometer	Steel	N/A	As above	
Steel block	Steel	East Midlands alloy	As above	

Dynamometer	Stainless Steel	N/A	As above
Transducer holder	Steel	East Midlands alloy	As above

The contact surfaces between components and between the transducer holder and the concentrator were defined as surface-to-surface interactions with mechanical properties as “rough”. The friction was assumed to be unlimited so that the parts of the assembly would not move or rotate with regard to each other during the analysis. This was necessary as all the parts of the assembly were bolted to each other not allowing relative movements during operations.

4.4.1.4 FEA analysis and results

The eigenvalues and natural frequencies in the frequency range around the resonating frequency of the transducer were obtained, all of them showing mixed vibrational modes. The effects affected predominantly only one or two of the system’s components. An extra care was taken to check that the natural frequencies of the assembly were not coinciding with the resonating frequency of the ultrasonic transducer.

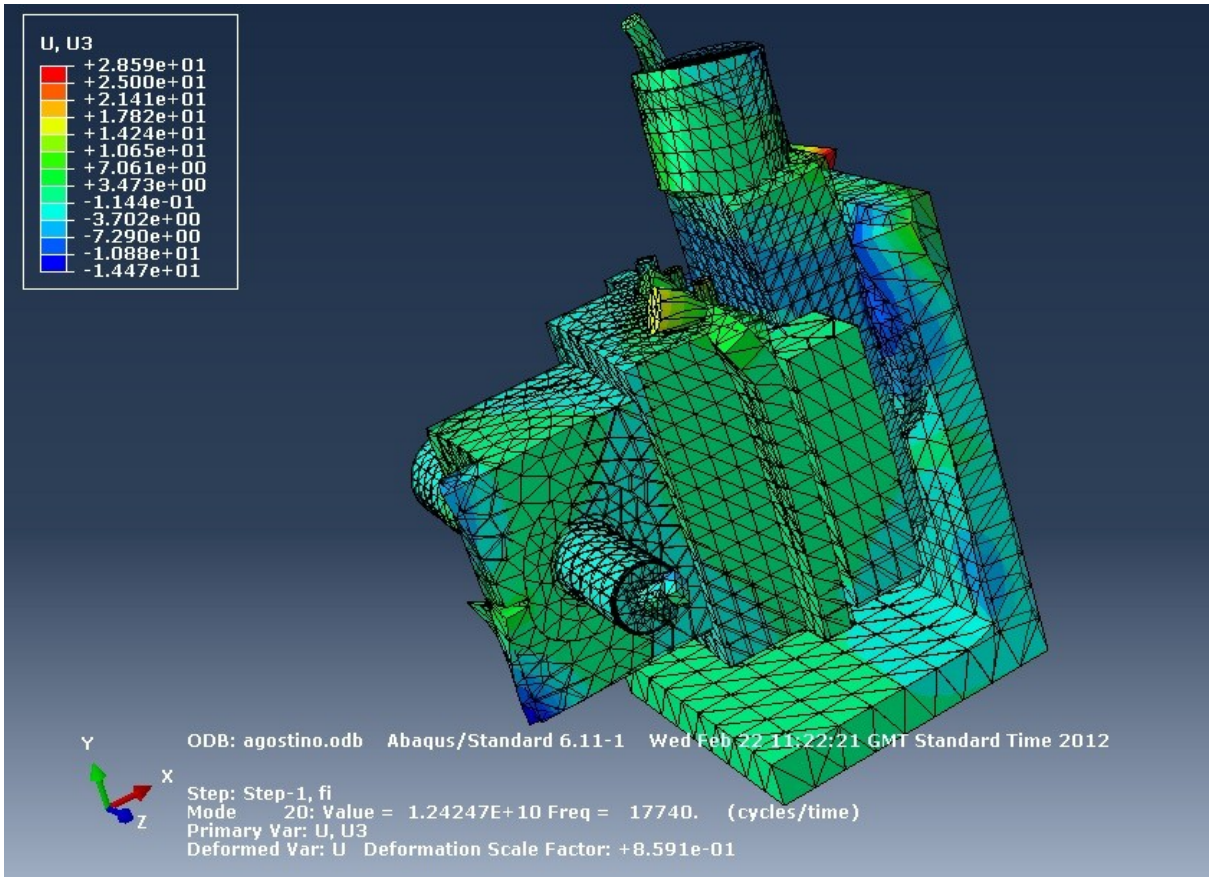

Figure 4-12: Modal shape computed for frequency slightly below resonance frequency of transducer

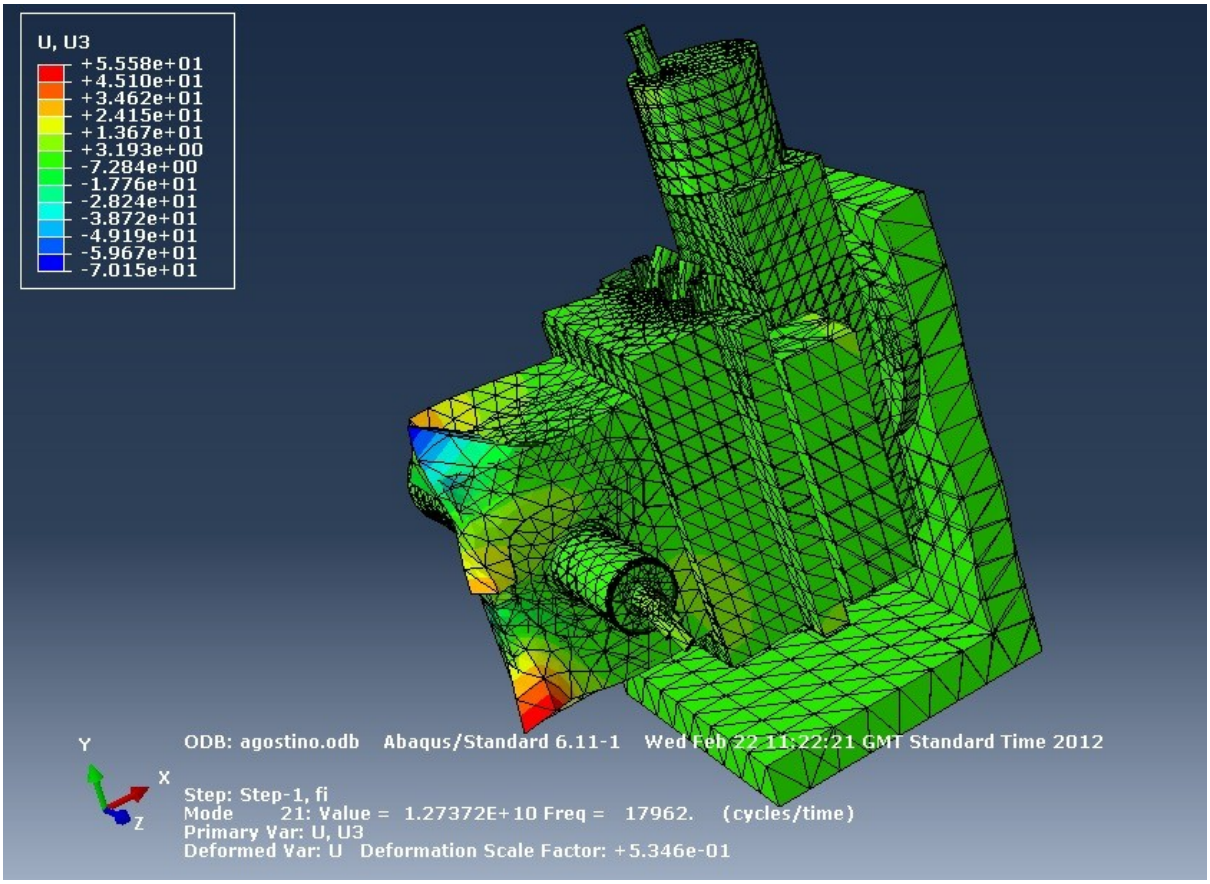

Figure 4-13: Modal shape computed for frequency slightly above resonance frequency of transducer

The colors represent the magnitude of the U3 eigenvalue (Z) direction, this orientation was selected because the transducer will effectively produce vibration along the Z direction of the model. The higher vibration amplitude appear to concentrate around zones of minor mechanical importance (around the edge of the flange), which are not directly involved in the machining process. This was observed for most of the natural frequencies around the resonating frequency [Figure 4-12][Figure 4-13] of the ultrasonic transducer with the exception of the eigenvalues correspondent to the frequency of 18111 Hz, this particular one showed heavy displacements [Figure 4-14].

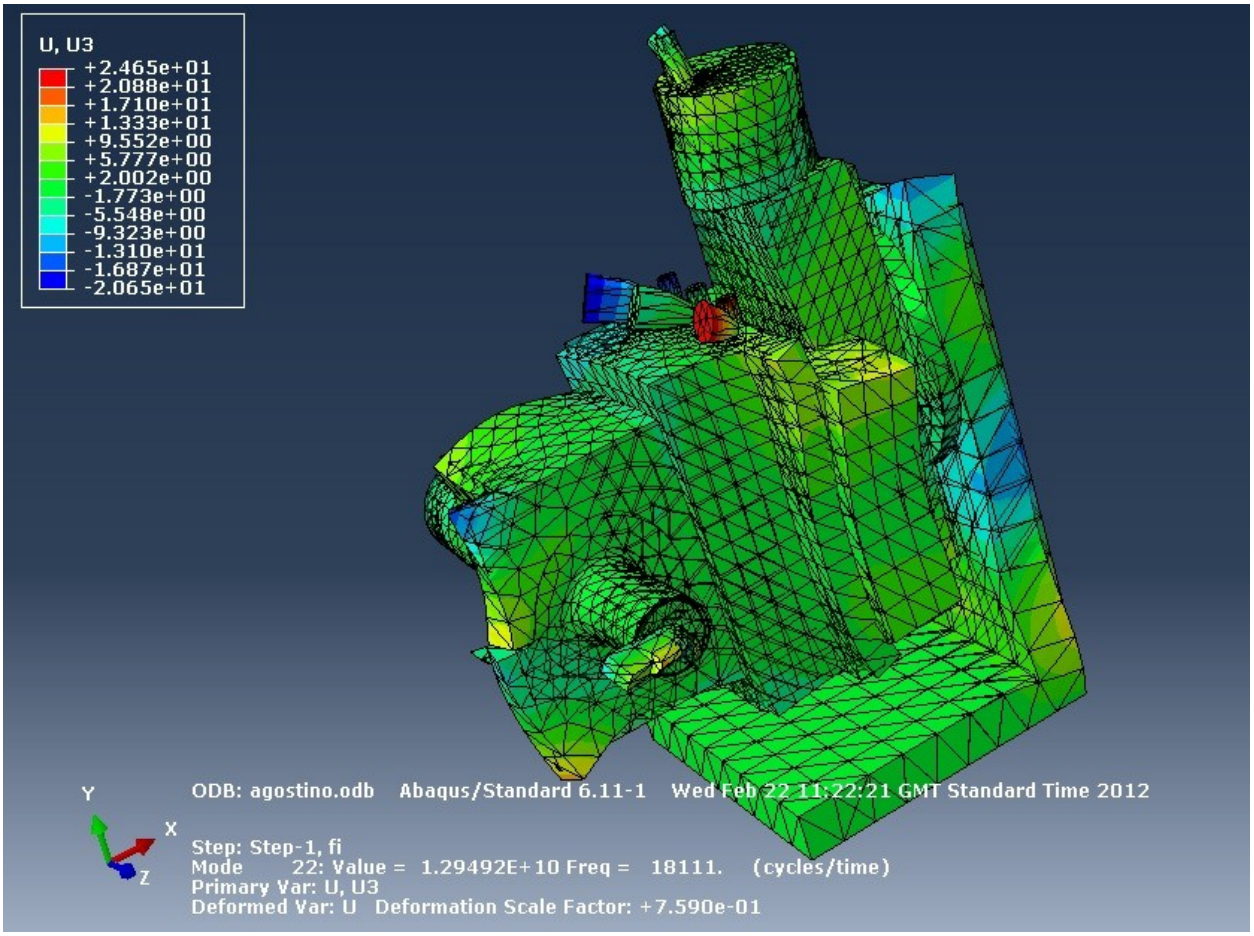

Figure 4-14: Modal shape for frequency of 18111 Hz showing large deformations of cutting assembly

Natural frequencies with mainly flexural modes of vibration of the cutting assembly were observed at 169, 298, 603 and 993 Hz (the first four modes). Largest deformations were observed in the first two modes, with the highest magnitude of the modal shape for the fourth mode [Figure 4-15]. The dominant effect observed was the flexural mode with some minor three-dimensional displacement effects.

An impact hammer test was used to calibrate the model using the resonating frequencies up to 6 kHz. Frequency response function analysis of the physical setup was valid only up to 9 kHz. Responses close or over to 9 kHz were showing reduced levels of coherence and were deemed unsafe to be used for calibration.

The low fundamental natural frequencies can be explained if the mass of the system

is considered. The steel dynamometer and the transducer holder accounts for a mass of over 10 kg, to this it must be added the weight of the transducer (less than 5 kg) and of the steel block (around 7 kg).

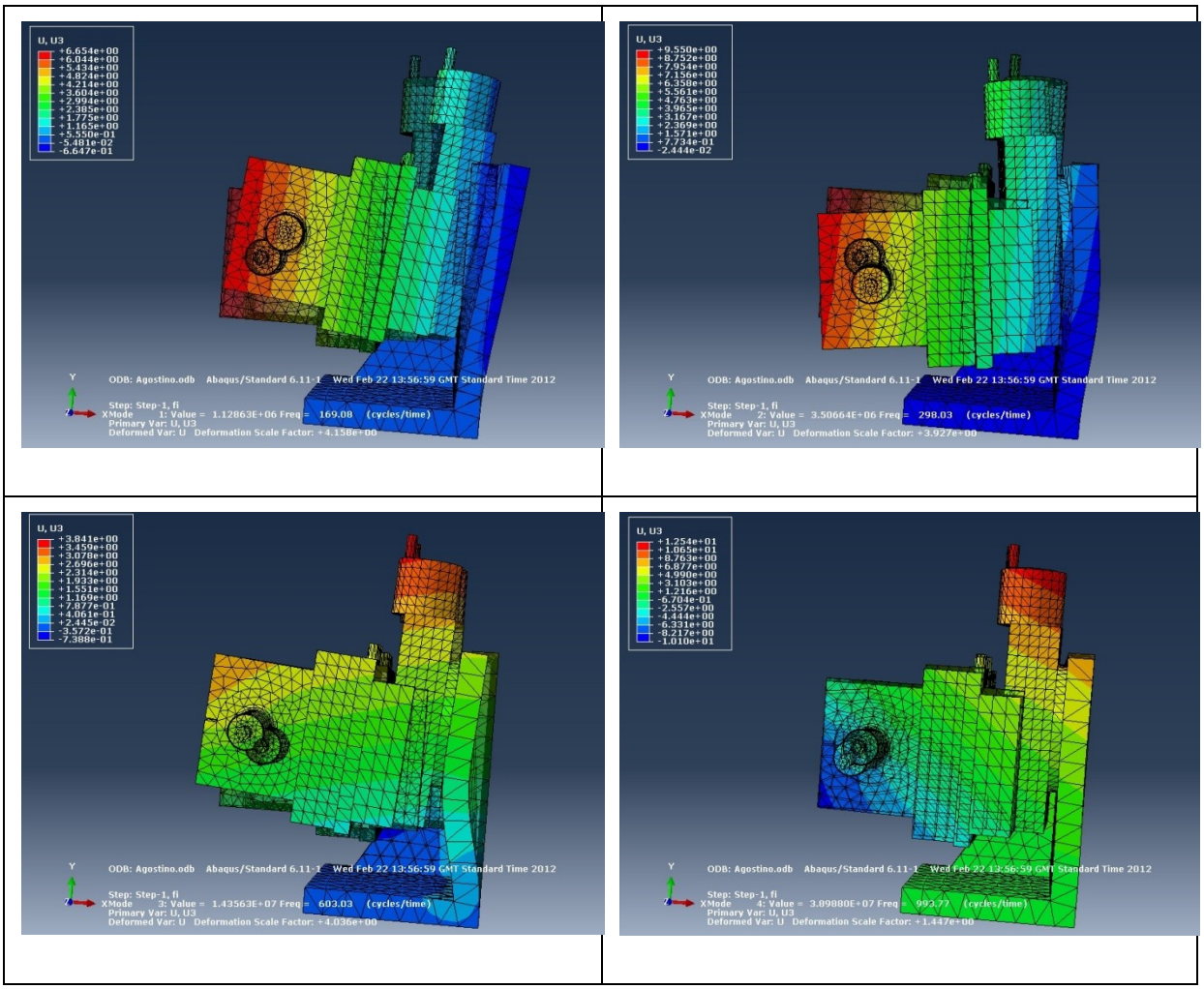

Figure 4-15: Vibrational modes for first four natural frequencies

Summary

The impact hammer test and the FEA simulations allowed to identify that the implementation of a stiffening gusset at the back of the angle plate considerably reduced the flexural vibrations of the vertical slab. This additional element was preferred in the final stage III design.

In order to avoid oscillation of the system in the first modes due to periodic forces

arousing from the machining process, such as the cutting force that a slightly offset work-piece with a rotational speed equal to any of the resonating frequencies could generate; it would be prudent to avoid them. The excellent damping properties of a lead sheet were used between the cutting head and the dynamometer; this was supposed to reduce the likelihood of exciting any of the vibrational modes.

4.4.2 Power characterization

4.4.2.1 Characteristics of transducer

Vibration stability of the transducer in UAT is a key parameter that influences greatly the quality of the finished work-piece. Resonance frequencies, a width of the resonance peak, a resonance shift under load are parameters linked directly to the transducer's shape and its material. Characterizing the resonance of the transducer in range close to the operating frequency offers more information in its behaviour under load [Puskar, 1982]. It was observed that the resonance frequency of the transducer shifted slightly to a lower frequency range under the cutting load. Besides shifting frequency; a large load on the transducer could dampen vibration to the point when the system will stop to resonate. This, however, was not observed in the experiments, even for a depth of cut of 0.5 mm.

In order to identify precisely the electric and vibrational responses of the transducer, a complete frequency sweep (in the range 17.3 to 18.3 kHz) was performed while monitoring the vibration amplitude by means of a laser-vibrometer (Picotech series 5000). It must be noted that the transducer was tested with the cutting insert mounted, to replicate as much as possible the cutting conditions. At the same time

the current and voltage applied to the transducer were monitored in real time by a custom circuit, thus allowing calculating the instantaneous power absorbed by the system. This resulted in a complete graph for the electrical/vibrational response of the transducer as a function of frequency.

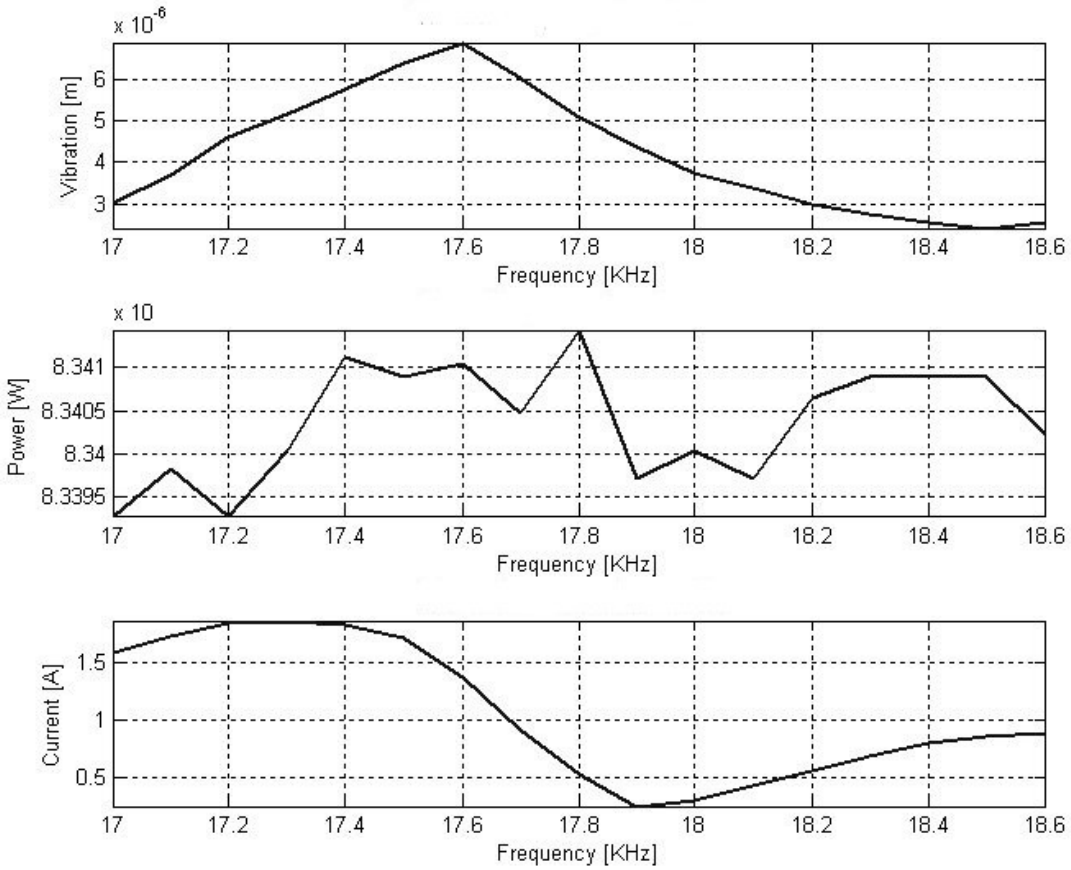

Figure 4-16: Characteristics of transducer around resonance frequency of 17.8 kHz

From these characteristics it is possible to observe how large the resonance peak of the system [Figure 4-16] is. Driving frequencies between 17.2 and 17.9 kHz could still excite sufficient vibration amplitude for proficient machining in the UAT regime. This non-critical response of the transducer is mostly desirable since it allows to machine in open loop (with no need to control the driving frequency during machining) for a large range of cutting parameters. This was proven experimentally

in the cutting-force analyses that showed an almost-flat cutting force - depth of cut graph (in the range 0.05 mm to 0.5 mm) for fixed levels of cutting speed and feed rate.

4.4.2.2 Driving system characteristics

Ultrasonic machining is a technique, which potentially brings a favourable energy balance in cutting of metals. A large cutting force reduction, a reduced need for lubricant during machining operations, a need for fewer machining passes when compared with conventional machining techniques are all characteristics which show prudently a smaller energy footprint for UAT when compared to CT. However, UAT necessitates energy to be supplied to the vibration generation system in order to perform. The quantity of energy that needs to be supplied for maintaining vibration in the system should be carefully measured in order to fully understand the benefits of UAT.

The accurate determination of the full energy footprint of the ultrasonic system requires the system to be split into its subparts. The digital signal generator is the only component that can be directly controlled by the operator; it generates a low-current driving signal of maximum 10 V peak-to-peak. Its maximum power absorption is 37 W. The driving signal is amplified by the MOSFet amplifier to a necessary level for driving the transducers. The amplifier belongs to a mono class AB (maximum theoretical efficiency of 0.78), which absorbs 47 W in standby. The power required during operations is very variable, ranging from 350 W to 143 W; interestingly, the maximum power is absorbed when the system is highly detuned thus not resonating. The output signal is then fed into the impedance transformer (ferrite core), which has a theoretical maximum efficiency of 0.9 to 0.97. The output signal is then supplied to

the piezoelectric rings that convert the electrical energy into mechanical one with a maximum efficiency of 0.95. It is hence rather easy to verify that the power measured at the transducer ($\cong 85\ \mathrm{W}$) is the sum of the input powers keeping into account the efficiencies of energy conversion:

$[37 + (143 - 47)] * 0.78 * 0.9 \cong 90\ \mathrm{W}$ [power to transducer]

The total energy footprint will thus be the sum of the power absorption of each element:

$37 + (143 - 47) \cong 135\ \mathrm{W}$ [power absorbed]

The power absorbed by the UAT system is in any case several times smaller than that absorbed by the lathe (several hundred to thousands of watts). The energy footprint requested by the UAT operations (smaller than a lathe coolant pump) is certainly lower than the power requested by a similar conventional machining session.

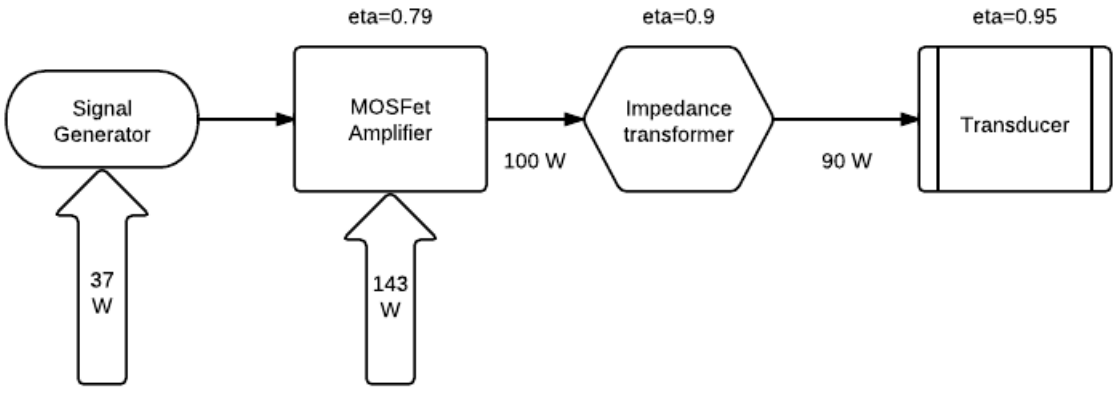

Figure 4-17: Block diagram with power footprint of vibration system.

4.4.3 Summary

The ultrasonic system was characterized in all its aspect that could influence the final results. The accurate work of minimizing the number of variables to be controlled

during machining and reducing their influence on the machining process was considered accomplished when the system started to show consistent results as regards to cutting force reduction, surface finish quality, depth of cut and vibration stability. Hence, the produced results would no longer be influenced by the surrounding conditions but only by the cutting parameters resulting in good quality data to assess the response of Ti 15-3-3-3 to UAT.

5 Experimental analyses

Early experimental cutting tests with ultrasonics were performed at Loughborough University with the first stage prototype. The obtained results already showed the benefits of the technique in terms of surface finish, cutting force reduction, reduction of chatter, and more. The first prototype was slow to set up and showed insufficient precision in setting the depth of cut. In order to improve this, a new, more easy to set-up prototype was designed. Several experiments were performed with the second prototype, showing clearly significant advantages of the second configuration in comparison to the earlier setup. Results obtained with the second prototype demonstrated notable improvements with regards to a conventional technique and are presented below.

5.1 Titanium 15V3Al3Cr3Sn

The work-piece material used in the work belongs to a group of meta-stable β-Ti alloys, showing significant precipitation-hardening characteristics. For this study, the alloy used was produced by vacuum arc re-melting. The produced 200 mm diameter bars were deformed at 850°C by rotary swaging to a final diameter of approximately 80 mm. The alloy was water-quenched from 790°C [GfE, 2011].

Table 5-1: Mechanical properties of Ti 15-3-3-3 alloy [MaMiNa, 2010b]

Work-piece material	Ti-15V-3Al-3Cr-3Sn
Work-piece diameter, *D* (mm)	80
Producer	GfE Metalle and Materialien GmbH
Heat treatment	Solution-treated and aged
Young's modulus, *E* (GPa), at room temperature	87
Density, ρ (kg/m^3)	4900
Thermal conductivity,*k* (W/Km)	8.10
Ultimate tensile strength, σ_{ul} (MPa)	1200

The resulting mechanical properties are reported in Table 5-1.

5.2 Experimental results with Stage II prototype

Several cutting tests were performed with the Stage II prototype, including the preparatory tests. During each test the cutting force components were continuously monitored by the digital acquisition system and successively analysed. Surface integrity and quality of the finished surfaces were also inspected with non-contact optical methods. The surface of the work-piece was analyzed with a Zygo interferometer capable of sub angstrom resolution, available in the metrology lab [see page 153 and following].

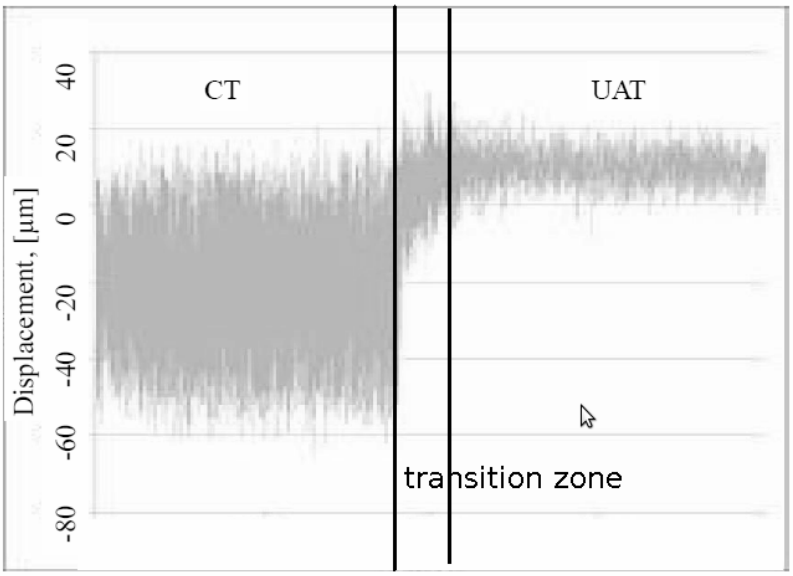

Figure 5-1: Head displacement vibration in radial direction in CT and UAT, a_p=0.1 mm, V=10 m/min, f=0.1 mm/rev [Maurotto *et al.*, 2000]

Three components of the cutting force were measured in conventional turning and ultrasonically assisted one [Table 5-2]; however, only the tangential and radial components are reported here. The axial component was found to be significantly smaller than two other components in any cutting condition; this is explained by the mutual effects of large radii of cutting tool's nose, small depth of cut and low feed rate. It should be noted that the control of the depth of cut on this prototype was still not optimal, showing difficulties in precise setting of the required a_p.

From the beginning, a qualitative reduction of the chatter in UAT was noted for every cutting speed and depth of cut as shown by the absence of chatter marks on the finished work-piece, smoother machining operations and lower mechanical noise. The reduction of chatter was also assessed by a non-contact eddy-current sensor that reported a five- to ten-fold reduction in the amplitude of chatter vibration [Figure 5-1]. A significant reduction in the variance of the recorded cutting force in UAT was also observed, suggesting that a more stable cutting process took place.

Table 5-2: Cutting force components in conventional and ultrasonically assisted turning with Stage II (average values, V=10 m/min, f=0.1 mm/rev)

	a_p **[µm]**					
Force component [N]	**100**		**200**		**300**	
	CT	**UAT**	**CT**	**UAT**	**CT**	**UAT**
Tangential	48	9	73	12.5	98	19
Radial	38.5	7.5	50	13.5	52	13.5

During the cutting tests, it was observed that the system was affected by insufficient rigidity, in fact when setting the highest a_p, successive analysis of the finished work-piece showed that it was lower than expected by up to 20%. The cutting force was actively displacing the position of the head by measurable levels. Beside that, the non-contact eddy current gauge was not sufficiently sensitive to detect subsequent positioning errors which continued to accumulate during the cutting operations. In fact, this sensor was not sensitive to slow variations in the a_p, easily failing to show errors of up to 50 µm if they accumulated slowly. This was leading to a progressive increase in the error in the cutting depth if the system was not zeroed after each cutting test. Still, with all these shortcomings, the system performed well in terms of surface finish in UAT [Table 5-3]. Interferometry surface analysis with the Zygo system [Figure 5-2] showed that UAT consistently improved the surface finish of the work-piece by measurable levels [Table 5-3].

Figure 5-2: Zygo interferometer and its control equipment

Capability of the Zygo system to produce high-quality and high-resolution numerical analyses for 3D images significantly improved the quantity of information available from each measured sample and allowed to discover the presence of micro-structures visible only on the ultrasonically machined areas [Figure 5-4].

These structures were later understood to be tiny traces of impacts of the tool during UAT, since each micro-structure was placed at the distance, at which an impacting object such as the cutting tool during UAT, would have left trace at the cutting [see page 154 and followings].

Further analyses were performed in order to explain the micro-structures observed by the interferometry analyses. Optical microscopy and Scanning Electron Microscopy were performed on the produced chips to verify the existence of impact traces which could be linked to the ones observed in the cut surface.

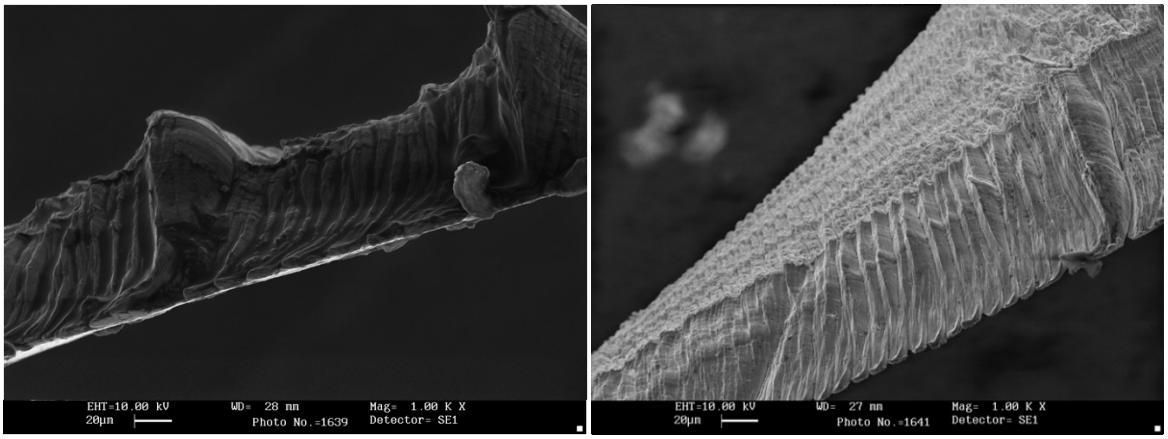

Figure 5-3: SEM image of conventionally cut chip (a) and ultrasonically cut one (b) (cross section), a_p = 0.5 mm,V = 10 mm/rev, f = 0.1 mm/rev

Several chips were collected during the machining experiments and analyzed with SEM. Similar impact traces were observed in the ultrasonically-assisted cut chips, showing at intervals of 10 µm [Figure 5-3], consistent with the traces observed during the interferometry. The SEM images of the machined chip explained traces of the micro-impacting UAT process observed on the finished work-piece; in fact, the distance between two impact traces on the chip corresponded to the travel distance of the chip in one vibratory cycle. This distance at the cutting speed of 10 m/min and vibration frequency of 17.9 kHz was averaging between 12 µm and 8 µm. It was therefore possible to relate the traces on the chips with the ones observed in the 3D images acquired with the Zygo interferometer. The quality of the finished surface in UAT was not negatively impaired by these impact traces; since the depth of these traces was in the sub-micron range, a value several orders of magnitude smaller than the peaks of the tool trails, unlikely to influence the quality of finished work-pieces directly.

The observed improvements on the surface finish are more apparent in a table comparing the peak to valley (PV), root mean square of the surface height values (σ) and surface roughness (Ra) measurements for CT and UAT cut work-piece surfaces

[Table 5-3].

Table 5-3: Parameters of surface analysis for Stage II (V = 10 m/min, f = 0.1 mm/rev)

Parameter [µm]	**PV**		**STD**		**R_a** (0.77 mm)	
a_p [µm]	**CT**	**UAT**	**CT**	**UAT**	**CT**	**UAT**
100	30	13	3.9	0.71	3.11	0.83
200	21	10	4	0.79	3.25	0.62
300	23	13	4	0.9	3.28	0.71

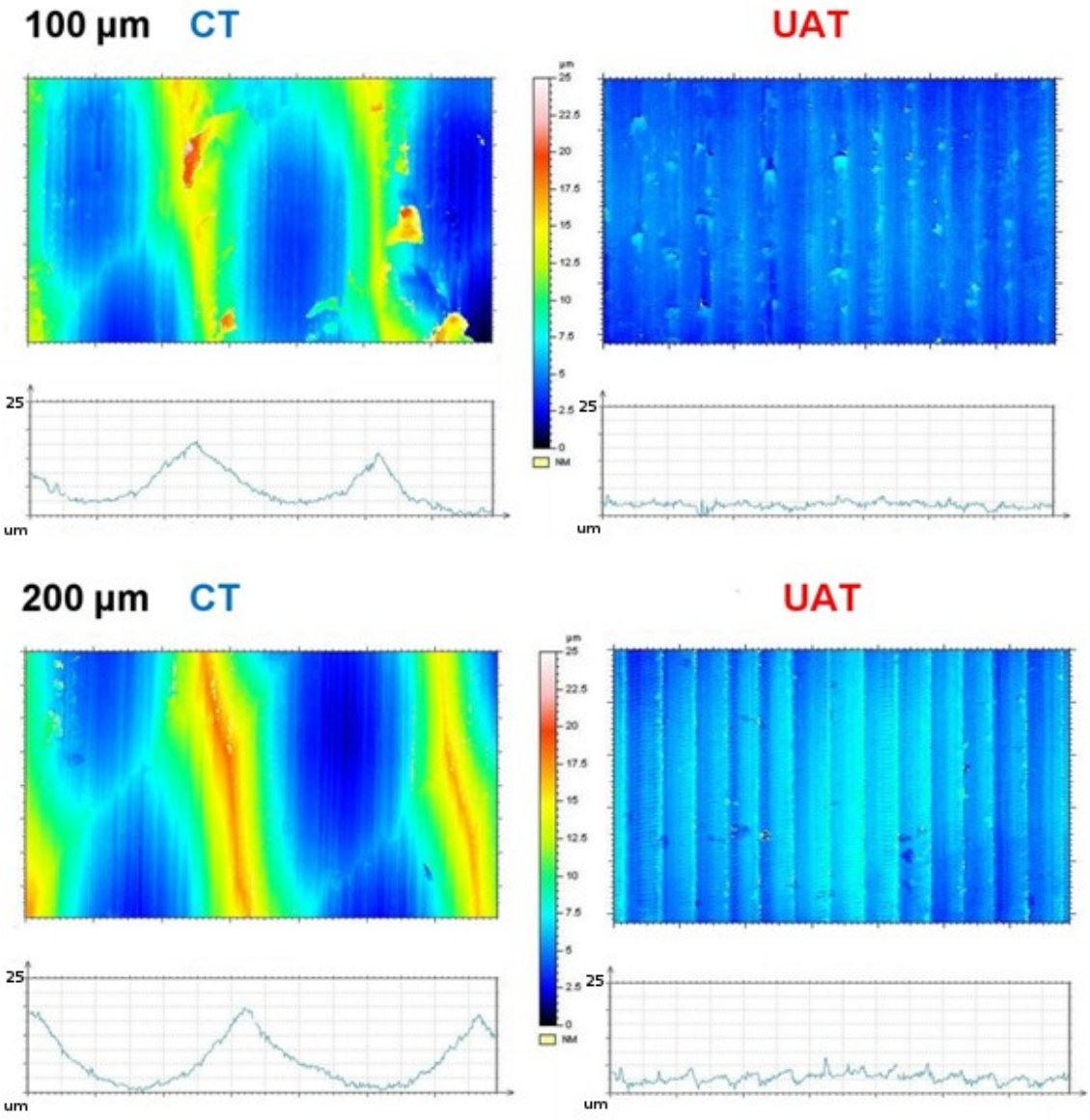

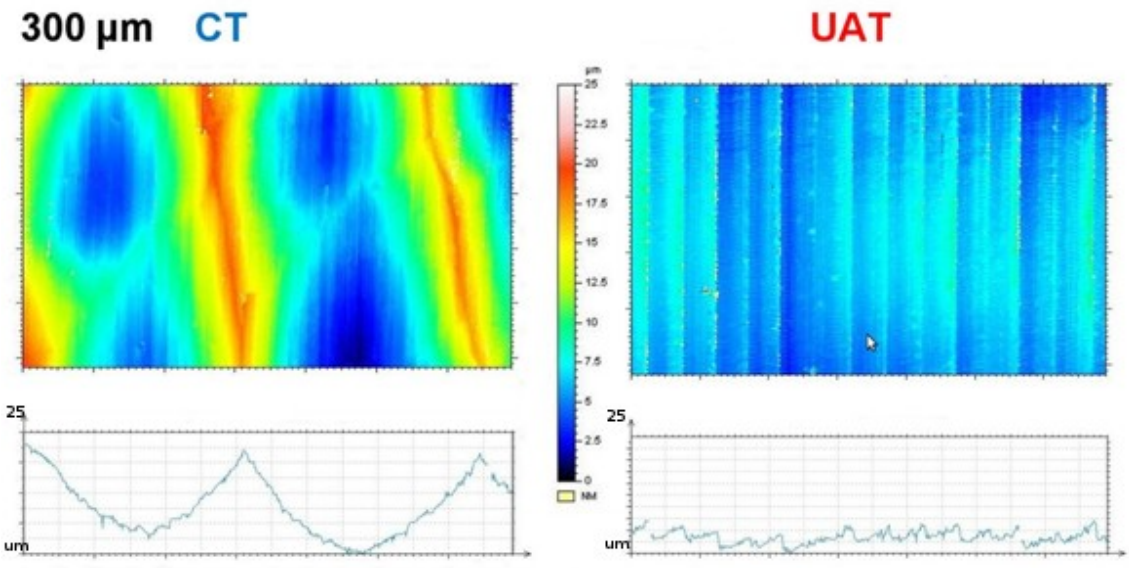

Figure 5-4: Stage II surface analysis of finished work-piece (a_p = 100, 200, 300 µm, f = 0.1 mm/rev, V = 10 m/min)

To summarize, the Stage II prototype addressed some of the shortcomings of the previous prototype (fixed a_p, insufficient rigidity, non-continuous adjustment of a_p) and allowed for a more consistent repeatability of the test results.

Figure 5-5: Kistler dynamometer 9257 [Kistler, 2011]

The average cutting force was consistently reduced [Table 5-2] as well as its standard deviation; at the same time, surface quality underwent similar improvements with a global reduction of roughness of UAT-machined surfaces [Table 5-3]. Despite that, the new shortcomings, which became apparent during the

tests, required to be addressed.

5.3 Stage III UAT system

The third revision of the system was developed taking into account all the experience gained in designing and operating the second one. Large shortcomings in the previous setup were identified and were, when possible, minimized in this revision.

5.3.1 Force sensors

Cutting force reduction was the most immediate effect of UAT. Just by switching the ultrasonic vibration on during the cutting operations resulted in a large reduction in the cutting force. In order to investigate this, the cutting head was suspended on a force plate.

The force plate is a larger force-sensitive element than a tool dynamometer; this device should satisfy a number of requirements such as high sensitivity, rigidity and accuracy. In particular, it should be rigid enough not to affect static rigidity of the assembly. In the CT setups, the tool dynamometers are generally installed right behind the cutting insert. This was not possible in the prototype since every additional mass would directly impact the frequency and amplitude of vibration. While technology advancement allowed miniaturizing force-sensitive elements, these miniaturized dynamometers are considerably delicate and expensive. Probably, these are not capable of withstanding the ultrasonic vibration directly and impact negatively on the maximum amplitude of the vibration. For these reasons a traditional and sturdier force plate was preferred for the third prototype. The force-

sensitive element in all the prototypes was a Kistler force plate (dynamometer), model 9257A [Figure 5-5]. This dyamometer is capable of measuring forces with a frequency up to 2.3 kHz (fnx) so it was not sensitive to the micro-impacts of the ultrasonic system, thus giving out an average measure of the impact force. It should be noted, however, that the natural frequency of the dynamometer mounted in the assembly would be considerably lower than this value due to the added mass. This force-plate came in an impact-resistant package, built fully in stainless steel, which also made it corrosion-resistant. It was well protected against the penetration of cutting fluids or water, even at a moderate pressure by an IP67 grade welded/epoxy seal. While all the experiments were performed in dry cutting conditions, cutting fluids were sometime used for accelerating the cooling of the used tools to allow safe handling, thus rendering a possibility of splash or spray wetting very likely. Excellent precision of 1% of the scale and its reliability rendered it a rather valuable tool to be employed during the tests.

Table 5-4: Kistler dynamometer specifications [Kistler, 2011]

Measuring range [kN]	Fx,Fy,Fz	±5
Sensitivity [pC/N]	Fx,Fy,Fz	-7.5,-7.5,-3.7
Natural frequency [kHz]	Fnx,Fny	2.3,3.5
Operating temperature range [°C]		0-70
Length [mm]		170
Width [mm]		100
Height [mm]		60
Mass [kg]		7.3

It was reasonable to believe that the effective natural frequency of the dynamometer and cutting head was well below its nominal maximum, due to a large mass of the

cutting head being bolted to it; hence the maximum acquisition frequency would be considerably lower than what specified in the manufacturer details. So, the force measured by the dynamometer was not the instantaneous force but an average over a large number of vibratory cycles.

The force-sensitive element (piezoelectric crystal) inside the dynamometer provided an extremely small measurement signal (a few pico-Coulombs); this charge had to be amplified to measurable levels.

Figure 5-6: Kistler 5001 charge amplifier [Kistler, 2011]

This was accomplished by a charge amplifier [Figure 5-6], which converted the charge accumulated on the sensitive element faces into a higher signal; it also provided the necessary feedback return signal to the dynamometer. In fact, measuring the charge on the dynamometer effectively destroys information, and it was needed to replenish the same charge before the next measurement cycle. The maximum frequency of charge amplifier accounts for 200 kHz, a value several times higher than the maximum frequency of the dynamometer. Measurements were acquired in bursts, which were the ultimate reason why it was not possible to measure the instantaneous cutting force during the vibratory cycle, but the value averaged over a large number of cycles. Three charge amplifiers (for three force

components) are Kistler rack mount units model 5001 [Figure 5-6].

The amplified signal, coming from the charge amplifier, was then fed into a Picoscope 4424, an advanced 4 channels digital oscilloscope (analogue-to-digital converter) then elaborated and recorded by the computer.

Table 5-5:Specificcations of Picoscope 4424 [Polytech, 2011]

Real-time sample rate	Up to 80 MS/s
Analogue bandwidth	20 MHz
Sample buffer memory	32 Mb
Digital resolution	12-16 bit
Accuracy of conversion	1%

The software of the Picoscope took charge of visualization and recording of force components in a familiar digital oscilloscope pattern. It allowed easy management of the recorded file and provided a useful buffer to store waveforms. It allowed saving the measurements in various file formats, among them comma- or tab-separated file for easy import into a more powerful post-processing program.

Before bolting the dynamometer to the setup it was necessary to calibrate it. Due to a long exposure to moisture, the measurements were showing a drift in the signal, which was negatively affecting the results. In order to remove the excess moisture from the dynamometer and its cables, they were heated to 60°C in vacuum for two hours, and then allowed to cool off and stand in the vacuum chamber with desiccant for several days. This allowed moisture to diffuse out of the instrument seals and get trapped by the desiccant. The instrument was then statically calibrated along the three axes using calibrated weights in order to find the relation between the force

and the measured voltage. To allow this to be performed with good accuracy, an angle plate was used to mount the dynamometer and 1 kg calibrated weights were used in increments up to a total of 6 kg. The gain of the charge amplifier was then adjusted so that for each kg of applied weight the change in the output signal was 100 mV; this process was periodically repeated to verify appropriate system calibration.

5.3.2 Signal generator and power circuit

An ultrasonic transducer needs a driving system capable of providing the necessary signal for its operation. The current driving system is the results of many years of developments using a modular approach (each part of the system was developed separately and independently from the others) [Mitrofanov, 2004]. For the sake of simplicity and reliability the same approach was maintained in this study. The current system was separated into the signal generator and the power circuit, which comprised the amplifier and the matchbox.

In the course of several field tests it was observed that the highest amplitude of vibration was obtained by a square-wave driving signal at the resonance frequency of the ultrasonic head. A sine-wave drive signal performed slightly worse, offering a smaller amplitude in maximum displacement with and amplitude lower by approximately 10%. However, as known from the Fourier analysis of the signal, square waves present a large harmonic spectrum. The square-wave driving signal was observed to reduce the stability of the system rendering the tuning more critical and sensitive to the load variations observed during the cutting operation. Thus, a more conventional sinusoidal signal was selected to drive the transducer, resulting in a higher stability during the machining operations. The driving frequency needs to

match the resonance frequency of the transducer head. Unfortunately, the resonance frequency of the head depends ultimately on the weight of the cutting tool used. A more stable fixed generator was thus ruled out since it lacked the necessary capability of performing frequency adjustments in order to be able to tune easily the driver frequency for the resonance one (which also changes during the different load conditions experienced during cutting). For this reason a modern frequency- and phase-lock digital signal generator was used to generate a balanced sine wave signal to be used as a driver [see Table 5-5].

Table 5-6: Instek signal generator SFG-2104

Frequency range	0.1-4 MHz
Resolution	0.1 Hz
Stability	±20 ppm
Accuracy	±20 ppm
Flatness	≤±0.3 dB
Sine Harmonic Distortion	-55 dBc
Advanced processing	Sweep, amplitude and frequency modulation

The generated signal, which due to the limitation of the signal generator could only reach 10 V peak-to-peak, was insufficient to drive directly the piezoelectric elements of the transducer.

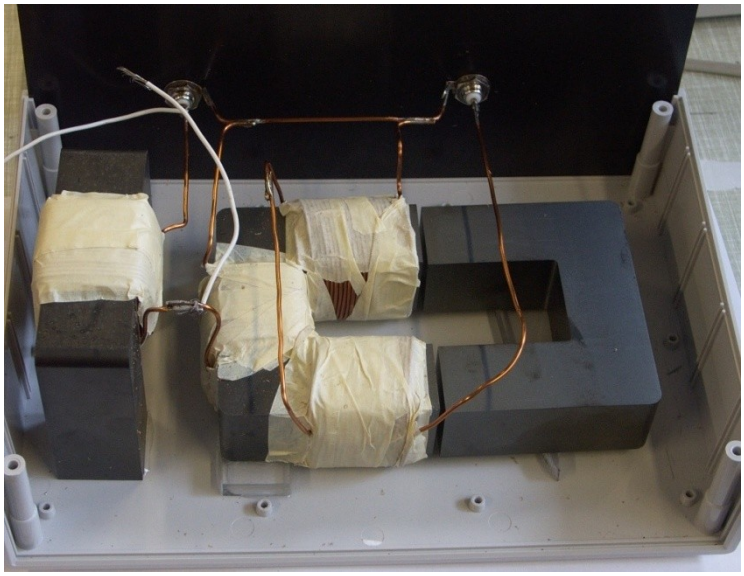

Figure 5-7: Matchbox

The piezo elements required a driving voltage of at least 500 V peak-to-peak. The total power generated by the signal generator was also below 10 W; this combination of low output voltage and low output power didn't allow for a direct driving of the transducer. The signal needed to be amplified. An amplifier was selected to provide a signal amplified to required amplitude. A custom-built MosFet mono amplifier was selected to amplify the driving signal with the required characteristics. This amplifier was designed to offer a large reserve in power in order to be able to drive efficiently the transducer even for the highest transient of the cutting load (such as the beginning of a cut); at the same time the MosFet construction offered excellent reliability and low distortion of the driving signal. Low power consumption during operation at maximum power and a low standby power use were desired characteristics, which helped in the selection of device.

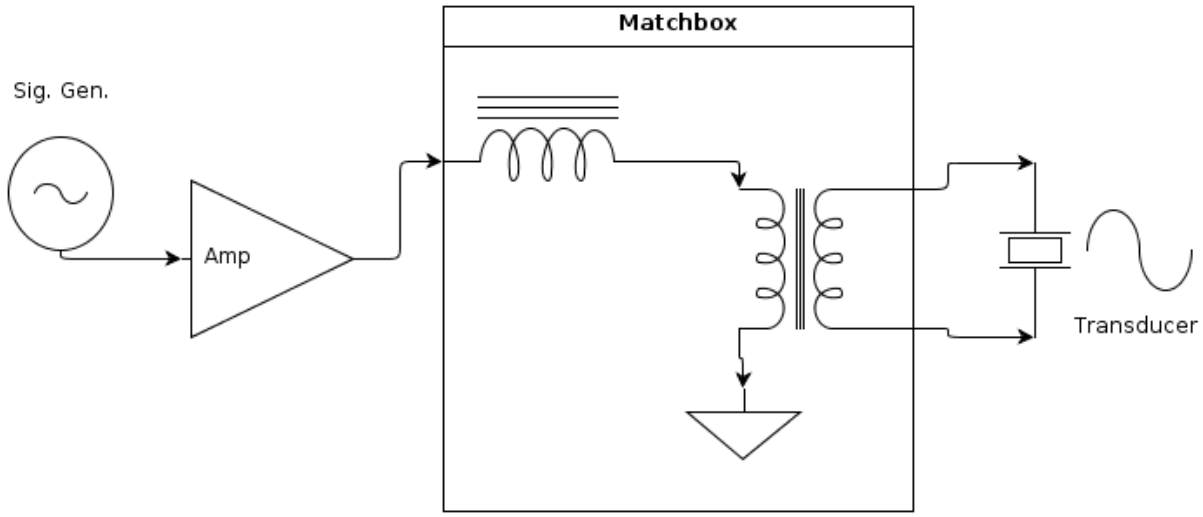

Figure 5-8: Block diagram of connections in power circuit

Due to the characteristics of the amplifier, which was originally designed to work as an audio amplifier with a frequency up to 100 kHz, it didn't couple well with a pure capacitive load as the transducer; this amplifier was designed to perform best to drive inductive-resistive loads as the ones offered by speakers. A large impedance mismatch between the load and the amplifier would cause excessive stress to the amplifier and generate large distortions to the signal (phase rotations, reflections, beats, form distortions, etc.). In order to couple efficiently the transducer and the amplifier, an impedance transformer [Figure 5-7] was built and experimentally tuned for the best energy transfer between them [Figure 5-8].

The impedance transformer consists of several coils of copper wire wounded on large C-shaped ferrite cores. The transformer not only adapt the pure capacitive load of the transducer to the impedance of the amplifier, it also increases the output voltage to over 700 V, necessary for driving the piezoelectric rings, and electrically de-couples the circuits of the transducer and the amplifier thus increasing safety (danger is also virtually nullified by the balanced configuration used to drive the transducer). The resonance frequency was accurately monitored by a laser

vibrometer, which measured parameters of ultrasonic vibration on a position close to the cutting edge monitoring the vibration amplitude to ensure proper tuning.

6 Force measurements

When monitoring the cutting force with the Picoscope, cutting force reduction represents the most important and immediately visible effect of ultrasonic machining. Consistent and noticeable reduction of the average cutting force components in excess of 65% was observed in all the experiments. Stage III prototype guaranteed the necessary stability to perform extensive turning tests monitoring the cutting force components in both CT and UAT with good repeatability of the results.

6.1 Cutting parameters

Machining parameters [Table 6-1] were chosen carefully to match the industrial machining parameters used in the medium-finish of titanium alloys which generally use cutting speed below 50 m/min as recommended by cutting tool manufacturers [SECO, 2011]. Depths of cut between 0.05 mm and 0.5 mm were chosen to match commonly used a_p in the machining of these alloys [Sandvik Coromant, 2009]. In order to investigate the response of the material to ultrasonic vibration in the most challenging conditions it was decided to perform only dry cutting. In dry cutting no coolant or lubrication is used during the machine operations. Dry machining is of interest since it addresses current needs for environmentally friendly manufacturing as an appropriate alternative to conventional machining with flood cutting-fluid supply [Weinert *et al.*, 2004]. [Mativenga & Rajemi, 2011] noted that dry machining compared favourably traditional one in reducing the energy footprint of machined products, since a significant portion of the total machining power could be spent alone on pumping high pressure coolants. Elimination of lubricants and coolants

presents some additional challenges in machining of difficult-to-cut materials [An *et al.,* 2011]. Well-known negative effects, in addition to rapid tool wear, are generation of high cutting forces, poor surface finish and, ultimately, poor dimensional accuracy of a finished component [Machai & Biermann, 2011]. As a result, several finishing steps need to be incorporated into a manufacturing process in order to obtain the desired component quality, increasing the overall machining cost. Thus, dry machining represents a very attractive technique when coupled with a technique able to reduce cutting forces, improve the surface finish and reduce the extent of chatter in the machining of Ti alloys.

Table 6-1: Cutting parameters

Cutting speed, V (m/min)	10 - 70
Feed, f (mm/rev)	0.1
Depth of cut, a_p(μm)	50-500
Vibration frequency, f (kHz)	17.9
Tangential vibration amplitude, a (μm)	10
Coolant	None

Each experimental run ranged from 30 to 500 seconds, with a prevalence of shorter test runs. Over time it became apparent that a standard test was needed to ensure proper repeatability of the measurements, this was addressed by the design of checklists and protocols which are reported in the appendixes. Most turning test lasted approximately 40 seconds. Within the first 10 seconds the depth of cut was set to the desired magnitude (this was ensured with the use of a micrometric dial gauge that tracked the displacement of the cutting head within an accuracy of ±10 μm along with the lathe micrometer). Such a technique based on two independent settings and measuring methods for the depth of cut eliminates errors, which the

lathe micrometer is susceptible to, especially in the sub-millimetre length scale due to inherent system compliance. This was followed by CT for 15 seconds. Next, the ultrasonic cutting head was switched on (with the machining continuing) for approximately 15 seconds before being switched off to recover CT cutting conditions [Figure 6-1]. Between the two cutting processes there was a period of transient cutting conditions, which lasted for approximately 2 seconds; that was subsequently eliminated from the data analysis. Between experimental runs, the cutting tool was disengaged and allowed to cool to room temperature. This was done to ensure repeatability of experimental conditions for subsequent experimental runs. Ideally, a new tool should be used for each experimental run in order to circumvent the effect of tool wear on the machining process. For higher depth of cuts this was the case; however, for smaller depth of cuts tool wear was observed to be minimal and as such the cutting tool was replaced after 3 experimental runs without any detrimental consequences to the observed experimental characteristics.

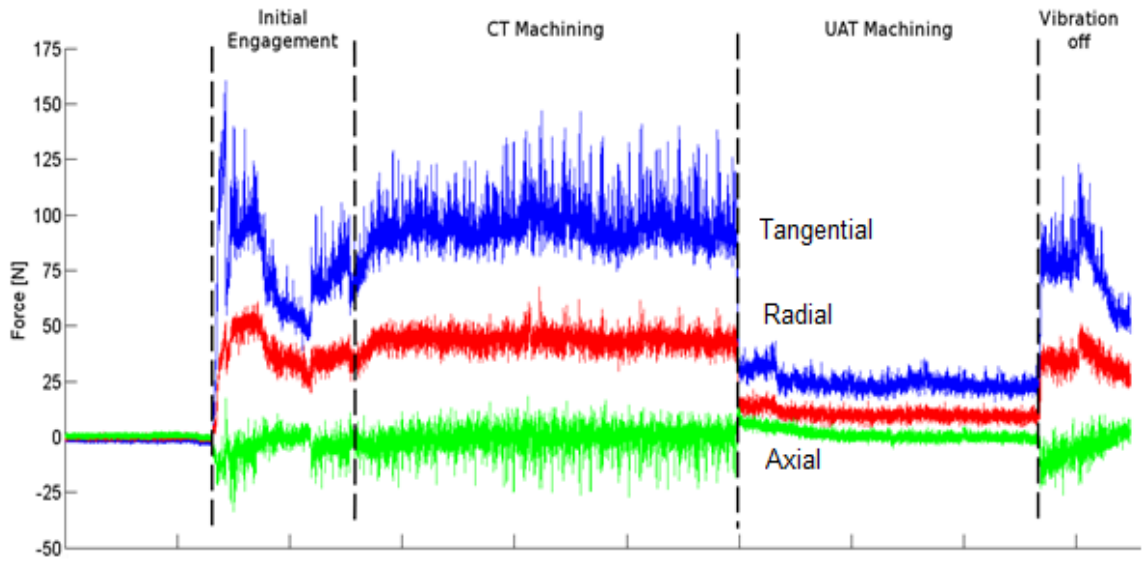

Figure 6-1: Evolution of force components signals during single run, a_p=0.2 mm, V=10 m/min, f=0.1 mm/rev

The original lathe featured several values of RPM controlled by a mechanical gear

system. If precise control on the cutting speed was to be used, being unable to adjust the rotational speed required the use of work-pieces of precise diameters.

Figure 6-2: Lathe Inverter ACS150 by ABB

The process of producing stepped test samples was deemed inefficient and expensive in terms of sample requirements. In order achieve a complete control over the cutting speed a lathe inverter was installed [Figure 6-2].

Table 6-2: Technical data of the ACS150 Lathe Inverter by ABB

Input power	380-480 VAC-3 phase
Frequency	0-500 Hz
Frequency resolution	0.01 Hz
Switching frequency	4/8/12 kHz
Analog input connection	0-10V, 0-20 mA
Accuracy	1%
Efficiency	95-98%

The device, ACS150 by ABB, allowed for seamless adjustment of the cutting speed and offers soft start-up and shutting-off [Table 6-2] of the lathe chuck.

6.2 Low-speed cutting force measurements

Cutting force reduction was the most significant and noticeable effect that was

observed when ultrasonic vibration is superimposed on the cutting insert. Several experimental tests (over 250 to date) have confirmed the consistent reduction of the cutting force in the machining of Ti 15-3-3-3 at different a_p [Table 6-3]. The measured cutting force components at various depths of cut a_p is presented in Figure 6-3. The diagram represents average values obtained from multiple machining runs; the error bars indicate the standard deviation of the measured forces and the standard deviation of the measured a_p.

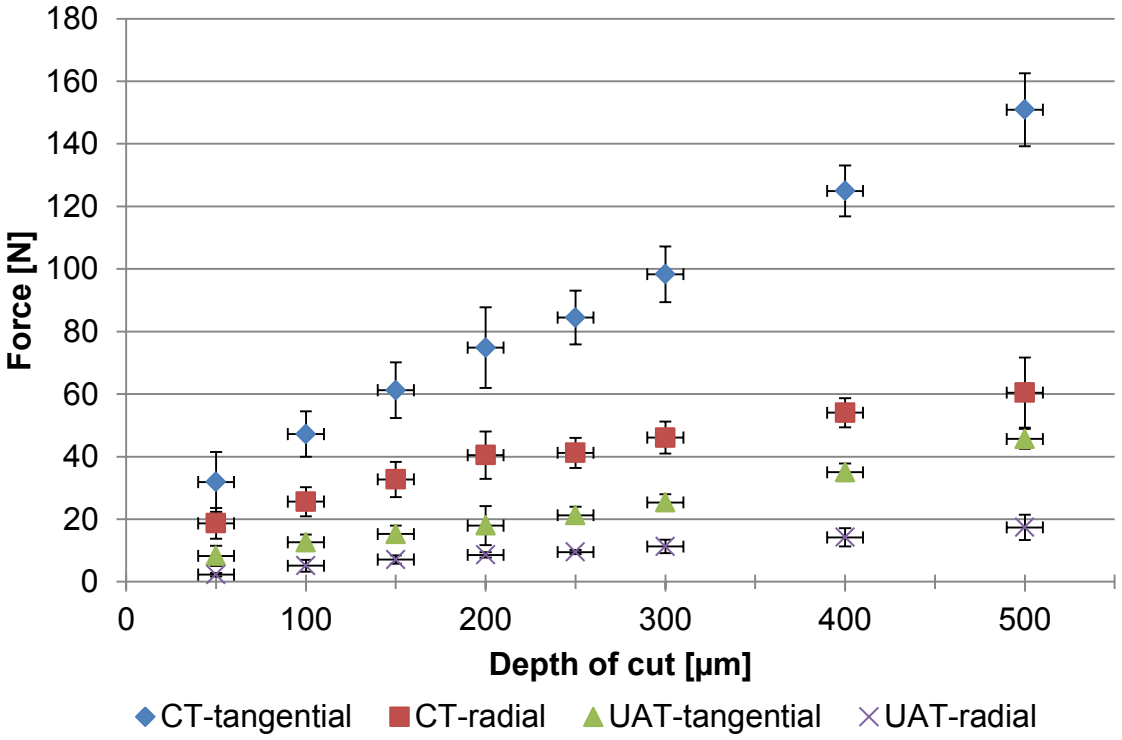

Figure 6-3: Cutting forces for CT and UAT at various depths of cut, V=10 m/min, f=0.1 mm/rev

Tangential and radial components of the cutting force in UAT increased almost linearly with increasing depths of cut [Figure 6-3]. The same was observed in CT. Large reductions in the tangential and radial components of the cutting force were expected when ultrasonic vibration was applied along the cutting speed direction (Tangential). At the cutting speed of 10 m/min complete separation between the

cutting tool and the work-piece was expected for each cycle.

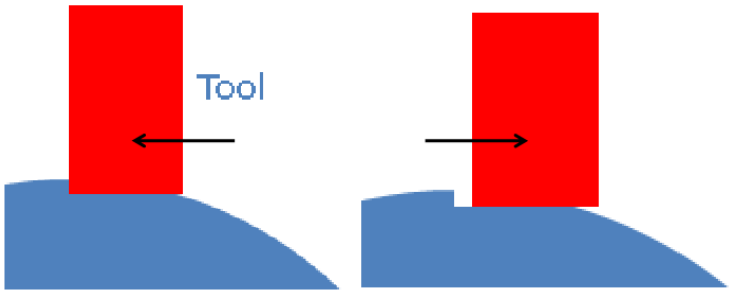

Figure 6-4: Movement of the tool during the cutting process

Similarly, the curvature of the work-piece allowed for a reduction of the pressure between tool and work-piece in the radial direction.

Table 6-3: Cutting forces for CT and UAT with standard deviations, V= 10 m/min, f=0.1 mm/rev

a_p [µm]	CT [N] Tangential	CT [N] Radial	UAT [N] Tangential	UAT [N] Radial
50	31.9±9.6	18.7±4.9	8.3±3.2	2.3±0.6
100	47.2±7.3	25.6±4.6	12.6±2.4	5.1±1.9
150	61.2±8.9	32.7±5.6	15.2±2.7	7.1±1.4
200	74.8±12.9	40.5±7.6	18.0±6.2	8.6±0.9
250	84.5±8.6	41.2±4.8	21.3±2.8	9.5±0.7
300	98.3±8.9	46.1±5.1	25.4±2.7	11.2±2.1
400	124.9±8.2	54.0±4.6	35.0±2.8	14.2±2.9
500	150.9±11.7	60.5±11.2	45.6±3.2	17.4±4.1

It was noticeable that the tangential component of the cutting force while machining in UAT for an a_p=0.5 mm was lower than the same component in CT for an a_p=0.1 mm showing a great potential for high performance cutting with the UAT system. If the percentage reduction between the components in CT and UAT was plotted in a graphical form, it was possible to see how the system responds for increasing depths

of cut [Figure 6-5].

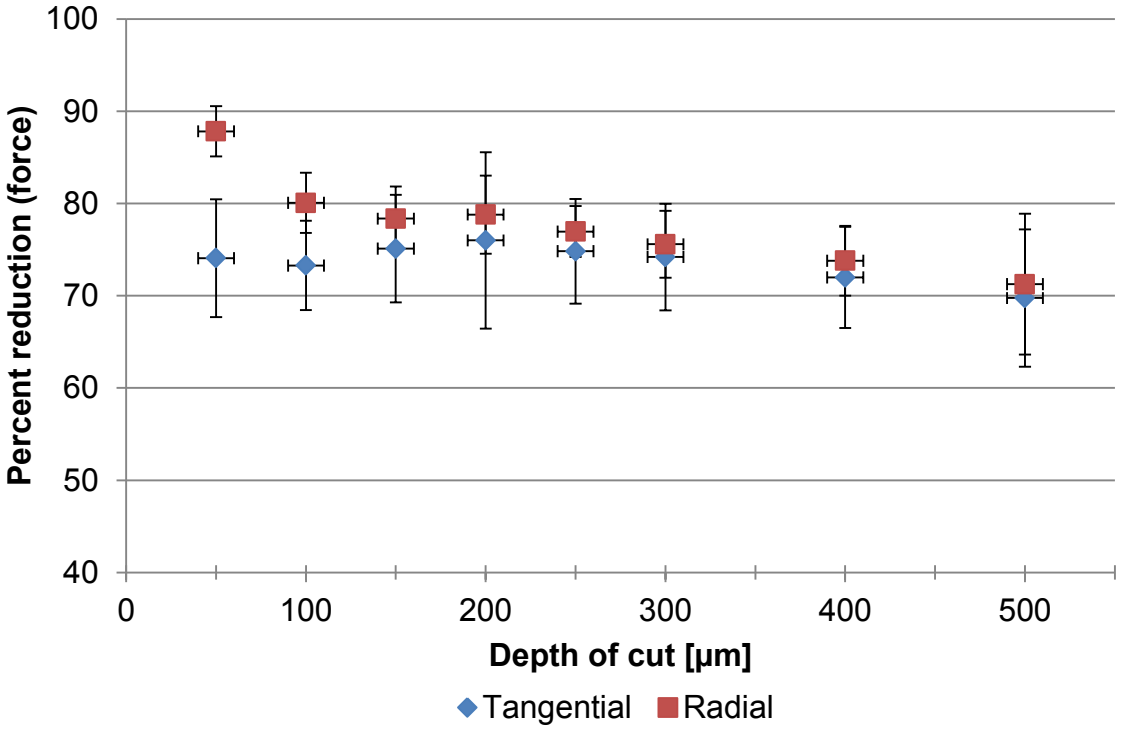

Figure 6-5: Reduction of tangential and radial components in UAT, V=10 m/min, f=0.1 mm/rev

The system exhibited a flat response in the range of a_p studied even at the highest values showing a resistance to the damping processes which could affect the amplitude of the vibration. It was reasonable to foresee that the ultrasonic vibration could significantly reduce the cutting force even at higher a_p. One of the shortcomings of the system at these cutting parameters was the low MRR due to the low cutting speed, increasing the cutting depth consequently increased the MRR while maintaining the same cutting speed so reducing the impact of the low cutting speed in the machining of this alloy.

The observed considerable force reduction (70-80%) was considered beneficial in the machining of less stiff components that are more prone to deflections during the machining operations (such as turbine disks). It should be noted that most of the

finishing operations in these components are still conventionally performed by grinding, a time and resource expensive process. The ability to cut with minimal cutting force would greatly reduce the displacements of the parts thus increasing the precision and effectively rendering the highly expensive finishing operations not necessary. Reduction of the cutting force could also reduce the residual stresses in the finished work-piece; this point will be investigated in a following chapter.

One common problem in machining this alloy at low speed and high a_p especially in large components with limited stiffness, was the facility of starting self sustained vibrations during the machining process, this phenomena is also known as chatter, and it could severely impair the surface quality and dimensional accuracy of the finished work-piece imposing also unnecessary stresses on the cutting tool. In Figure 6-3 and in Table 6-3 it was shown how the standard deviation of the tangential and radial components of the cutting forces decrease in UAT. This large reduction worked by effectively lessening the likelihood of starting self-sustained vibrations during the cutting of the work-piece. This process was already observed in the Stage II prototype [see 5.2] where a large reduction of the displacement vibrations of the cutting head was measured by the eddy current proximity sensor.

It should be noted that the current trend in machining is to increase the cutting speed as much as possible in order to increase the material removal rate MRR, having larger MRR reduces the time needed for machining thus reducing the machining costs. In this light, it was beneficial to investigate the propensity of the technique to machine not only at higher a_p but also at higher cutting speeds. In order to avoid the large number of test needed to perform with the necessary statistical significance measurements at all the depth of cuts for all the cutting speeds of interest, a statistical inference technique was used to validate the results of a limited number of

tests as representative of the behaviour of the alloy in UAT.

6.3Variable-speed cutting force measurements

A depth of cut a_p=0.2 mm was selected to be representative of the finishing operations which were of interest in this work. Cutting speeds of 10, 20...70 m/min were chosen since they were in the industrial range of cutting speed used in the machining of this alloy (30-60 m/min). It was expected that the system would became progressively less effective in UAT for a cutting speed V approaching the critical velocity as stated in Chapter 3 . This was verified in the cutting speed interval taken into account.

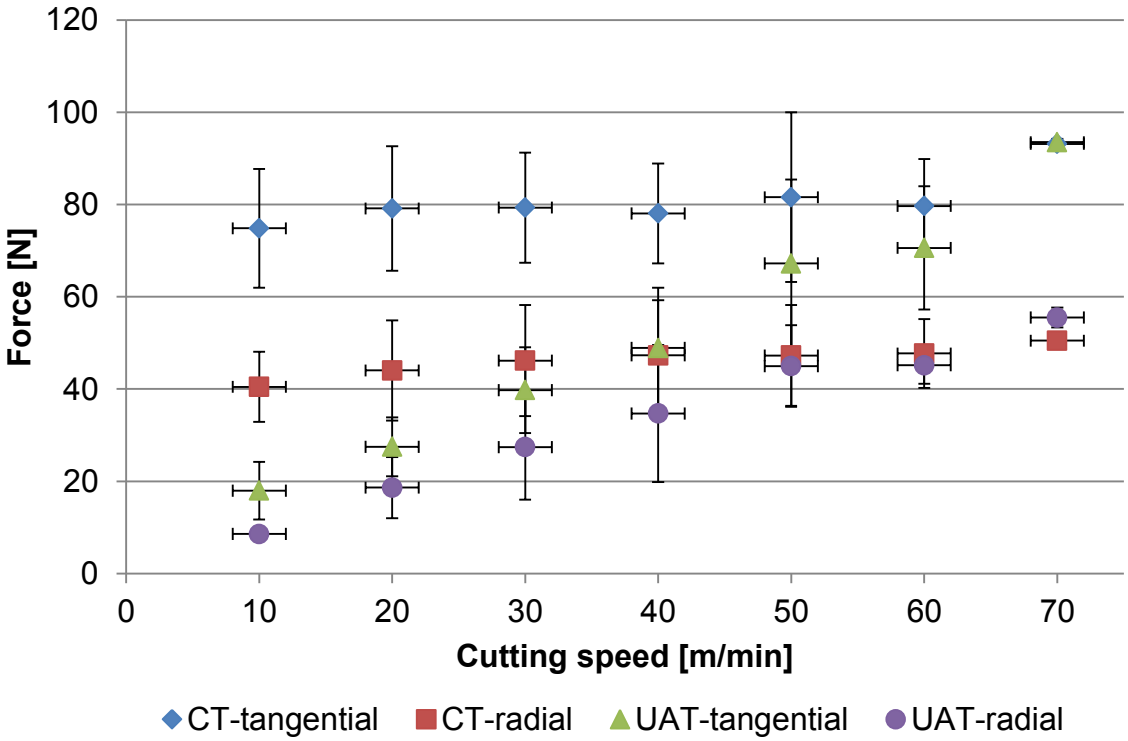

Figure 6-6: Cutting forces for CT and UAT for a_p=0.2 mm at different cutting speeds, f=0.1 mm/rev

In Figure 6-6 was shown how the tangential and radial cutting force components for conventional machining showed little increase for increasing cutting speed. This was

expected since cutting force should increase very slowly in this limited interval of cutting speed studied for this material [Hoffmeister, 2010].

When comparing the conventional components with the behaviour of the UAT ones a very different pattern was observed. The UAT components increased more rapidly becoming equal to the CT ones at a cutting speed of 70 m/min. This cannot be completely explained by the mono-dimensional theory of UAT [Astashev & Babitsky, 1998]. In this theory the vibratory movement of the tool is considered to occur purely in one direction. According to this theory, the critical velocity of the system was approximately $V_c=2\pi af\approx60$ m/min, hence no reduction should have been observed in the UAT cutting forces when compared with the CT ones for tests performed at a cutting speed above 60 m/min. However, it was understood that the hypothesis of generating purely mono-dimensional vibration was unrealistic in a real system. In fact, the minute differences in the position of the elements rendered inevitable that a certain level of misalignment of the centres of mass was achieved. This transformed the ideal mono-dimensional vibratory regime into a much more complex tri-dimensional one that cannot be solved analytically due to the complexity of the mathematics needed. Unfortunately, so far, there were no successful attempts to describe analitically bi-dimensionally vibrating systems, not to mention the more complex real system vibrating in 3+ modes. Having a complex vibratory mode effectively increased the range of cutting speeds in which the system was effective, rendering able to show some effects at a cutting speed well above the critical velocity. The presence of at least a tri-dimensional vibratory regime has been verified with the laser vibrometer showing that the vibrations not in tangential direction accounts for between 5 and 15% (relative) of the total displacement amplitude (these measurements appeared to vary with every tool change due to the minute variation

in the positions of the barycentre for each tool).

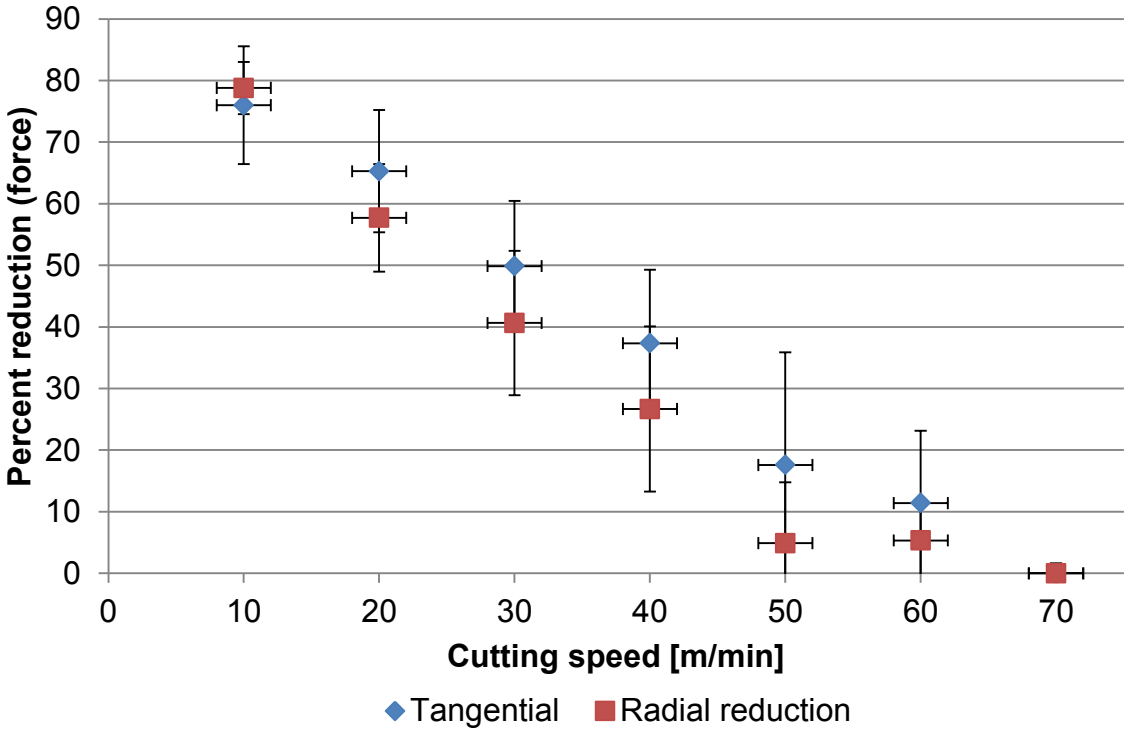

Figure 6-7: Percent reduction of tangential and radial components at variable cutting speeds for a_p=0.2 mm, f=0.1 mm/rev

The observed reduction of the cutting force was more easily visible if the percentage of cutting force reduction is used instead and is plotted for the CT and UAT components. In Figure 6-7 it was shown how the efficiency of the UAT system in reducing the cutting force components progressively vanished approaching a cutting speed of 70 m/min. At 70 m/min the observed reduction vanished rendering the UAT process undistinguishable from the CT one. It was noticeable however at cutting speeds representative of the cutting speed currently recommended by the tool manufacturer (30 to 60 m/min) the UAT system exhibited reductions of between 50 and 10%. These reductions were significant in a less-than-optimal (higher speed and no coolant) situation and prove that the technique was suitable in the machining of this Ti-alloy effectively improving the MRRs at the same cutting speed when

compared with CT.

6.4 Impulsive force measurements

In order to characterize accurately each cutting cycle a new force sensor was to be developed since the Kistler dynamometer did not respond quickly enough (max theoretical frequency below 2.6 kHz) to follow the evolution of the cutting force in the UAT cycle. At the frequency of the ultrasonic vibration (17.8 kHz) each cycle lasts for approximately 56 μs, it was therefore needed to develop a new sensor with a fast response able to track the evolution of the cutting force in the impact. While this absolute value was not relevant for the performances of UAT it was important if used to validate the simulations which predicted a maximum cutting force slightly higher than the force in CT [Ahmed *et al.* 2006]

Most force measuring instruments make use of the piezoelectric effect, hence it was decided to try and develop a sensor based on this effect to measure the peak cutting force.

A piezoelectric ring of 10 mm diameter with a central hole of 5 mm and a thickness of 2 mm was supplied by Steminc to be used as a force sensitive element [Figure 6-8].

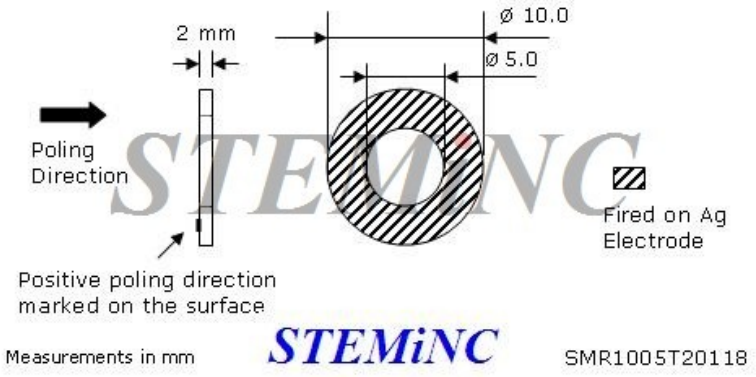

Figure 6-8: Dimensions of piezoceramic ring

Its resonating frequency of 154 kHz was sufficiently high to allow 9 measuring points for each cycle thus allowing for characterization of the peak cutting force in a cycle.

Different mounting options were evaluated till the final decision was to mount the ring between the cutting tool and the tool-holder. This would allow for the necessary pre-loading of the ring to be performed by the tool fixing screw. First tests indicated the piezoelectric sensor to generate potential differences of over 100 V, far beyond the maximum input voltage of the Picoscope. For this reason, a shunt resistance of 100 Ω was inserted between its poles to reduce the maximum generated voltage and the other mechanical effects caused by the separation of charges.

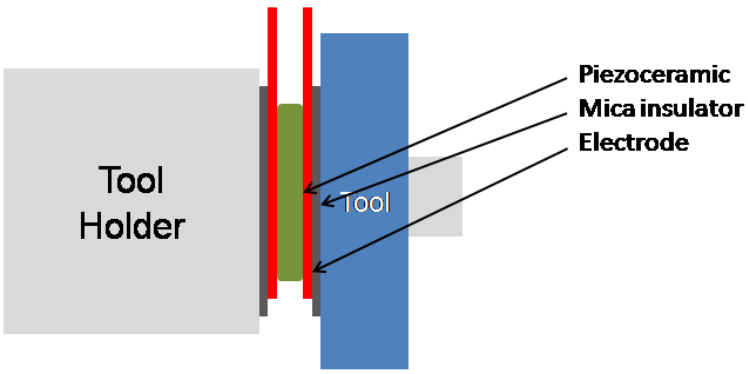

Figure 6-9: Schematics of peak force sensor

One of the major problems to solve in this configuration was the conductivity of the

tool and the screw used to fix it. During the machining operations, it became evident that proper insulation was needed to prevent the produced charges being shorted. The fixing screw was insulated using a Teflon pipe, and a Teflon groove was used to insulate its head from the cutting tool. Nevertheless the system was still acquiring more noise than signal in this configuration; therefore it was decided to completely insulate the piezoceramic ring by two very thin mica insulators. Their excellent dielectric rigidity (over 2 kV in optimal conditions) and resistance to heat were desirable perks which were outweighing their fragility. In this configuration the sensitive element was sandwiched between the tool and tool holder and electrically insulated, an optimal condition to measure the peak force [Figure 6-9].

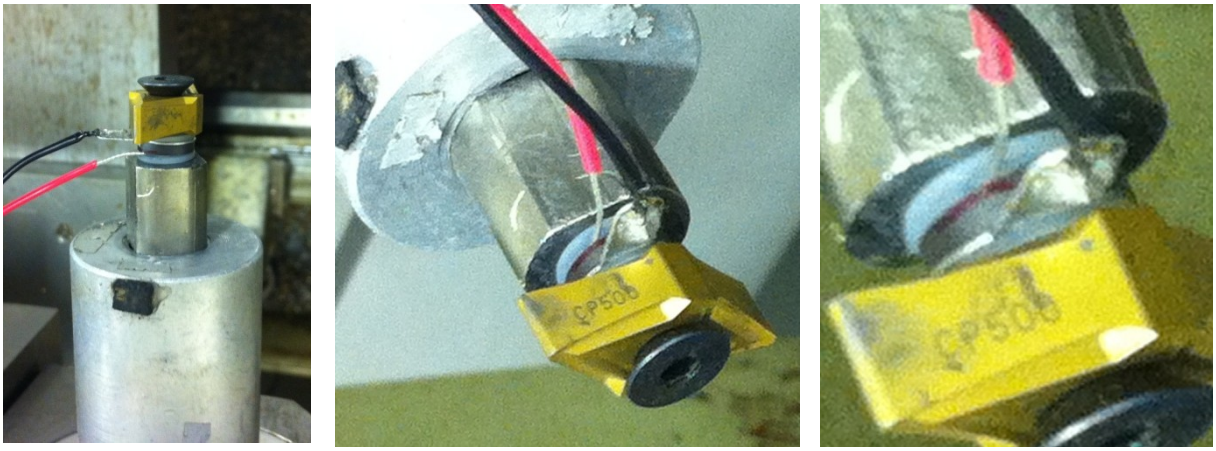

Figure 6-10: Peak force sensor, first prototype with Teflon insulators; mounted on the cutting head [see Figure 6-9]

The force signal was measured at the shunt resistor, this configuration allowed to maintain the signal range between -200 and +200 mV thus avoiding to overload the Picoscope. This configuration while satisfactory from the electrical point of view was showing several mechanical shortcomings. First of all, the piezo-ring was fragile and it was frequently damaged while tightening the fixing screw to preload it, this would cause the ring to crumble when ultrasonic were turned on rendering the test invalid.

During operations, a depth of cut larger than 0.2 mm was hardly achievable, since the additional space between the tool and the tool-holder the fixing screw was to bear additional loading, if the a_p was larger than a certain level, the load and the leverage were sufficient to cause the assembly to bend and crumble the sensitive element. The electrical noise generated by the transducer high voltage driving signal was severely disturbing the peak force signal, causing distortions and phase rotations, ultimately this was the hardest problem to solve. Mechanical shortcomings were addressed by a larger fixing screw (M5 instead of M4) and by reducing as much as possible the thickness of the electrodes, applying a large load by the fixing screw was also helpful. Ultimately, while the preliminary results looked promising [Figure 6-11], it was decided to abandon the development of the impulsive sensor since peak force measurements were mostly of interest for validating simulations which were not the core interest of this work.

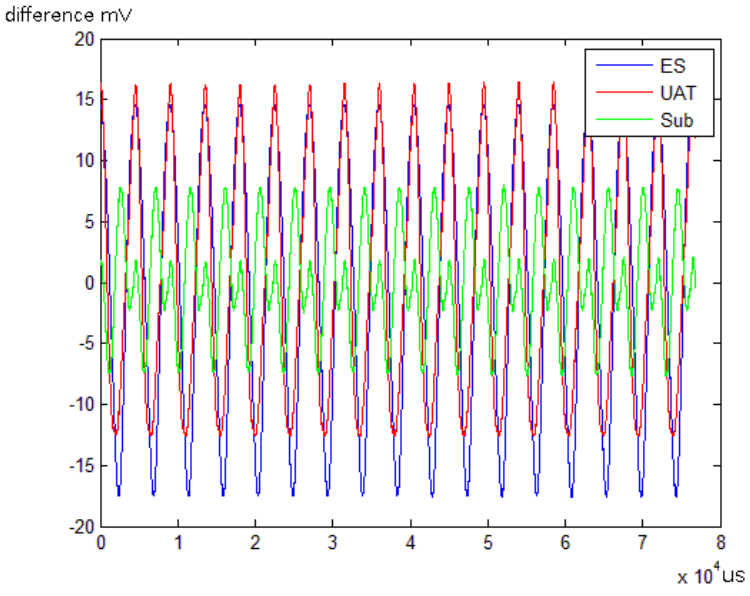

Figure 6-11: Peak force signal during UAT cutting (UAT in red) and with tool disengaged (ES in blue), in green the difference of signals (Sub in green)

6.5 Summary

Force reduction effects (70 to 80%) have been observed while machining Titanium 15-3-3-3 alloy in UAT. The system exhibited an almost flat response in the force reduction at increasing a_p up to a depth of cut of 0.5 mm. Minimal dampening effects were observed at the highest a_p it is therefore prudent to say that it is expected the system to be effective at higher cutting depth (tests at a_p=1 mm showed minimal reduction in efficiency). Heat built up effects on the cutting insert became important for $a_p \geq 0.4$ mm due to the lack of coolant impairing the ability of the system to machine higher depth of cuts for the standard test time. Some tests were performed with the use of water as a coolant (unfortunately this was not acceptable since they produced heavy rusting on the machining surfaces), while they showed improvement in tool life their analysis is beyond the scope of this work which concentrates on dry tests.

The effects of ultrasonic vibration remain noticeable at higher cutting speeds reaching the high end of the range recommended by the tool manufacturer (60 m/min). At these cutting speed the system still showed approximately 10% cutting force reduction in UAT when compared to similar cutting conditions in CT. Chatter was virtually eliminated during the machining operation in UAT with the standard deviation of the UAT component showing two to three-fold reductions at 10 m/min. Similarly, machining noise was also noticed to lessen and become more regular [see Figure 5-1]. The whole machining process appeared to become more stable: setting the depth of cut required minimal efforts and no adjustments, the machine appeared as it was cutting effortlessly a difficult to machine alloy. These effects exceeded the initial expectations especially in a hard to cut alloy such as Ti 15-3-3-3. The

observed cutting force reduction dwarfed the ones obtained by commercial employer of the technique such as DMG which was claiming 17% force reduction for its milling system [Mori Seiki, 2012]. While the two systems cannot directly be compared for the inherent differences in the processes the large advantage of the Stage III prototype should not be overlooked [Anon, 2001].

Previous experimental studies [Mitrofanov *et al.*, 2005] and simulations [Muhammad *et al.*, 2012] showed that the temperature in the chip and therefore in the process zone would be higher for UAT when compared to CT at the same a_p. Ti grain structure and phases could be influenced by high temperatures. It was therefore deemed necessary to investigate the temperature at which the alloy was exposed during the machining operations especially at the highest a_p.

7 Thermal analysis

Titanium alloys are considered difficult to machine materials due to their poor thermal conductivity causing high temperatures in the process zone in particular at the immediate interface between tool and work-piece. Their high strength generates high cutting forces which translate into friction generated heat at the tool-chip interface [Hope, 1977]. Beside this, their high chemical reactivity with many cutting tool coatings is worsened by elevated temperatures ultimately bringing to premature tool failure [Ugarte *et al.*, 2012]. In UAT the average cutting forces are smaller than in CT, but the dry cutting conditions worsen the thermal management during the cutting. The absence of lubricant and coolant and with the poor thermal conductivity of the alloy it is understood that the heat generation during the machining operations gain great importance [Klocke & Eisenblätter, 1997].

Measuring the temperature in the process zone is a challenging task. Direct measurement requires invasive methods to be implemented such as thermocouple embedded into tools [Ahmed, 2008], right next to the tool [Ren *et al.*, 2004], into work-pieces [O'Sullivan & Cotterell, 2001], or technological challenging solutions such as thin-film thermocouples [Basti *et al.*, 2007] and tool-work-piece EMF measurement techniques [Grzesik & Nieslony, 2000]. The mechanically challenging conditions which characterize the tool work-piece interface in UAT discourage the use of tools with thermocouples embedded due to the short-contact length which renders difficult to embed successfully a thermocouple in a region so close to the edge. While they offer accurate point measurements it is not possible to drill an hole in the tool while maintaining the structural integrity necessary to machine in UAT)

Difficulties in machining the Ti 15-3-3-3 alloy and its poor thermal conductivity [see 5.1] furthermore render difficult obtaining a successful measurement from embedding the thermocouple into the work-piece material. The alloy was provided into solid ingots, it was therefore challenging to drill the thin holes needed to embed the thermocouples. The presence of the large high-frequency high-voltage interferences from the transducer head could render difficult to obtain a clean signal for temperature evaluation with the EMF method rendering again this technique probably difficult to implement successfully. Thin-film techniques would offer a good chance of direct measurement given that the modified tool would retain long enough the active film to obtain valuable data. The vibrational challenging conditions of the cutting tool could be associated with a short life of the active layer.

Indirect methods such as thermal imagery have become nowadays the standard in the measurement of the temperatures in such a fast process as cutting. It should be noted however, the process zone is not optically accessible since both the work-piece and tool are opaque to infrared light. The zone in which most of the heat is generated is positioned deep inside the work-piece at the interface between the tool edge and the cutting material [Muraka *et al.*, 1979; Muhammad *et al.*, 2012], it is therefore impossible to obtain a direct measurement of the cutting zone temperature using thermal imagery methods unless by resorting to special procedures [Davies *et al.*, 2005]. The most attractive features of this technique were its simplicity of implementation and its insensitivity to electrical disturbances which were always present when the UAT system was switched on. These alone were deemed sufficient for choosing real-time thermal imaging as the technique of choice for measuring the difference in temperature between CT and UAT.

7.1 Thermal imaging equipment

The experiments were performed using a Flir SC3000 thermal camera featuring a Stirling-cooled quantum well infrared photodetector. This excellent detector features a sensitivity of 10 mK at 30 °C and can measure in the range -20 +2000 °C. The detector is sensitive to infrared radiation of wavelength between 7 and 9 μm and offers an accuracy of ±2 °C above 150 °C. It was available in short loan from the EPSRC instrument pool complete with its macro lenses and control PC: The acquired images have a resolution of 320x240 pixels at the used range of 14 bits radiometric IR digital image and were elaborated using the FLIR proprietary software provided with the camera.

To prevent any damage to the delicate germanium lenses it was decided to avoid the use of macro lens, which required the lenses to be positioned very close to the measuring zone. The produced chip, especially at high speed cutting, could easily scratch or damage the lens surface, while normal lenses allowed to be positioned at a larger distance thus reducing the chances of damage.

Before the camera was used to monitor the cutting temperatures it was calibrated for the emissivity of the alloy. The emissivity parameter describes the attitude of a body to emit infrared radiation from its surface; it is the ratio of the energy radiated by the body to the energy radiated by a black body at the same temperature. The angle on which the camera sees the body also plays a role in the emissivity, in this case however, due to the viewing angle being less than 50°, it is possible to assume its influence marginal. It is therefore an important parameter to calculate to obtain sufficiently precise measurements of the temperature of the body. It should be noted that the nearest object to the process zone, which was easily visible from the camera

position, was the chip in formation. For this reasons calibration was performed for the alloy and not for the material of the tool.

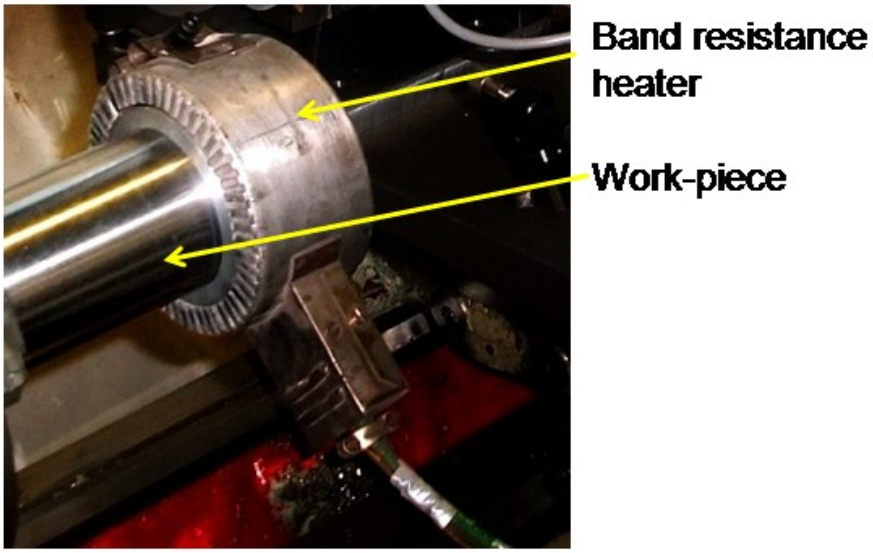

Figure 7-1: Band resistance heater and work-piece

The alloy ingot was heated up with a band resistance heater to a temperature of 200 °C and the camera was then calibrated on it. The low calibration temperature was required due to the long time needed for the calibration operations, a long permanence of the sample to temperatures higher than 300 °C would in fact cause grain growth, ultimately modifying the mechanical characteristics of the alloy. Other calibration points, such as ambient temperature, humidity and distance of the sample from the camera were measured and used as an input to the FLIR software which calculated the emissivity. Three points were used to calculate the emissivity: ambient temperature, 100 °C and 200 °C. The resulting emissivity was very close to the one provided by FLIR into the metal database: 0.32. This emissivity was therefore used in all the experimental tests to calculate the temperatures of the alloy.

Figure 7-2: SC3000 camera mounted on cross slide

The camera was mounted on the cross-slide of the late on a custom designed bracket [Figure 7-2]; this was to avoid having to continuously focus the process zone as the cutting continued. The depth of field of the camera was in fact quite small, hence the decision of having it mounted on the cross slide, avoiding any relative movement between the camera and the cutting tool. Precise positioning was achieved by a fine threaded screw mechanism and vibration dampening was obtained by rubber blocks and cast iron parts. The results were deemed to be more than satisfactory since even in UAT no blurring (due to the vibrations) was noticeable in the acquired images.

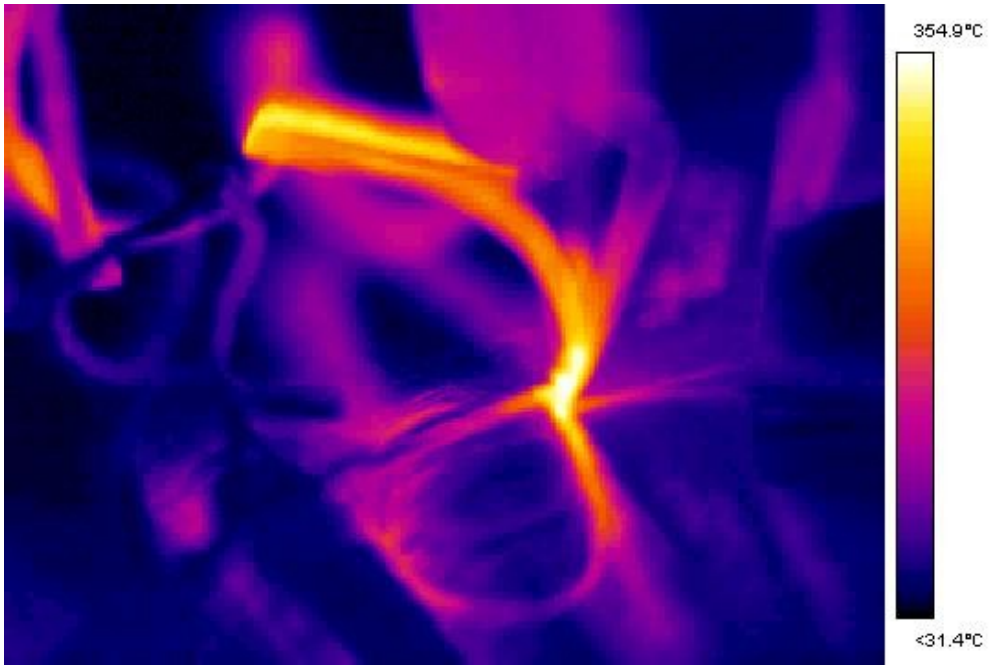

Figure 7-3: Thermal image of UAT cutting process, a_p=0.2 mm, V=10 m/min, f=0.1 mm/rev

7.2 Thermal measurements

The camera was mounted on the bracket and focused on the contact point between the tool and the work-piece. If the normal lenses were used the area in focus was sufficient large to hold the tool and a good portion of the chip. The lathe was then started and the tool lowered till contact to the work-piece. Even with an a_p=0.05 mm the temperature generated was sufficient to show a clear colour difference spot in the camera. It was then easy to accurate refocus the camera to keep the high temperature spot in focus. The camera software offered several temperature ranges to be selected, when changing the temperature range, a servomechanism inside the camera switched filter lenses slightly changing the focus, it was therefore important to refocus the image each time the range was changed. The software provided with the camera (ThermaCAM Researcher 2) converted the difference in temperature between the ambient temperature and the measured one to a difference in colors or

grey tones, several palettes were available in the software to allow the best contrast in the image. For this case the palette named “iron” was selected since it offered a clear image which did not require to be printed in colours to be viewed with highest temperature in white. This was deemed intuitive since hot parts usually tend to acquire a lighter colour with increased temperatures. In our case, the software colours in white the temperatures which were outside the maximum temperature measurable. It was therefore easy to identify when it was needed to switch to a higher thermal range during the machining operations. Generally for $a_p \leq 0.2$ mm an intermediate range was used, for deeper depth of cuts the highest range was needed.

Once the calibration was satisfactory the machining operations were started, the camera was acquiring both the tool and the work-piece, and the software was used to calculate the maximum visualized temperature which was also visualized in the scale of the image [Figure 7-3]. Incidentally, the emissivity of the tool was very close to the one of the work-piece (calibration was also performed on tools), this allowed visualizing in the same picture what temperatures were reached by the tool during the cutting operations.

In all the cases, the temperature taken into account was the one of the chip, at the nearest visible point to the process zone. The tool was, most of the times, covered by the chip and it was not possible to measure its temperature in the zone near the cutting edge but only at a zone several millimetres far from it. Temperatures of the work-piece and of the cutting tool were acquired before machining and considered equal to the ambient temperature.

If ultrasonic vibration did not have any effect on the tool temperature while vibrating

the tool in air it could be assumed there were minimal relative movements between tool and tool-holder. This could be used to verify that the correct torque was used when fixing the insert to the tool holder. In the case the torque was insufficient, the friction generated during the relative movement between the tool and the tool holder was sufficient to increase the observed tool temperature by several degrees. This provided a useful check before the machining operations, it was not uncommon, in fact, that an insufficient fixing torque would cause the tool to became loose during the machining operations in UAT ultimately causing the failure of the test.

Data acquisition was started immediately before setting the a_p thus engaging the tool, since the operation was performed manually and gradually, the measured temperatures underwent a transient before reaching the operation value. The duration of this transient was varying between 5 and 15s, accordingly to how fast was the operator in engaging the tool [Figure 7-4]. The transient values were later removed from the comparative graphics to avoid confusion and the graphs were post-processed to alloy side-to-side plotting of the CT and UAT temperatures for each depth of cut.

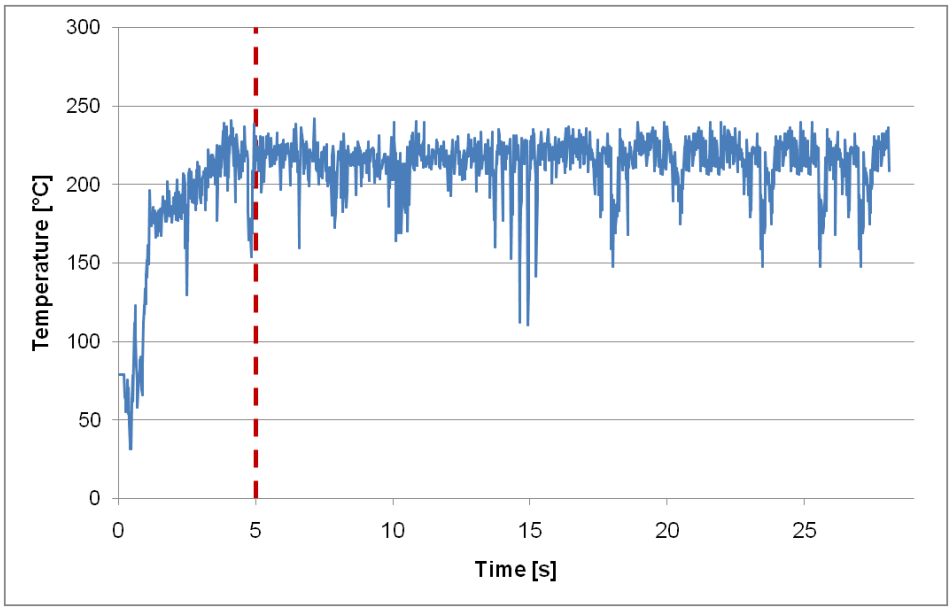

Figure 7-4: Temperature plot for a_p=0.1 mm in CT, dashed line denote end of transient, V=10 m/min, f=0.1 mm/rev

Thermal imaging acquisition was performed for five different a_p: from 0.1 mm to 0.5 mm using a clear area of the work-piece in several steps. After each experiment the tool edge was replaced with a new one and allowed to cool to be touched without feeling too hot. Due to the large mass of the work-piece its temperature was usually not changing during the tests, small temperature changes were noticed only at the deepest a_p, in these cases it was allowed to cool before continuing the experiments.

Comparative thermal analysis

Simulation results in titanium [Muhammad *et al.*, 2011a; 2011b] showed that the temperature in the cutting zone for UAT should be somewhat higher than in CT. That was reasonable since the material undergoes a higher strain rate in UAT, beside that; the additional energy added by the ultrasonic vibration was likely to be converted into thermal excitation. Higher temperatures were therefore expected in UAT machining of Ti alloy.

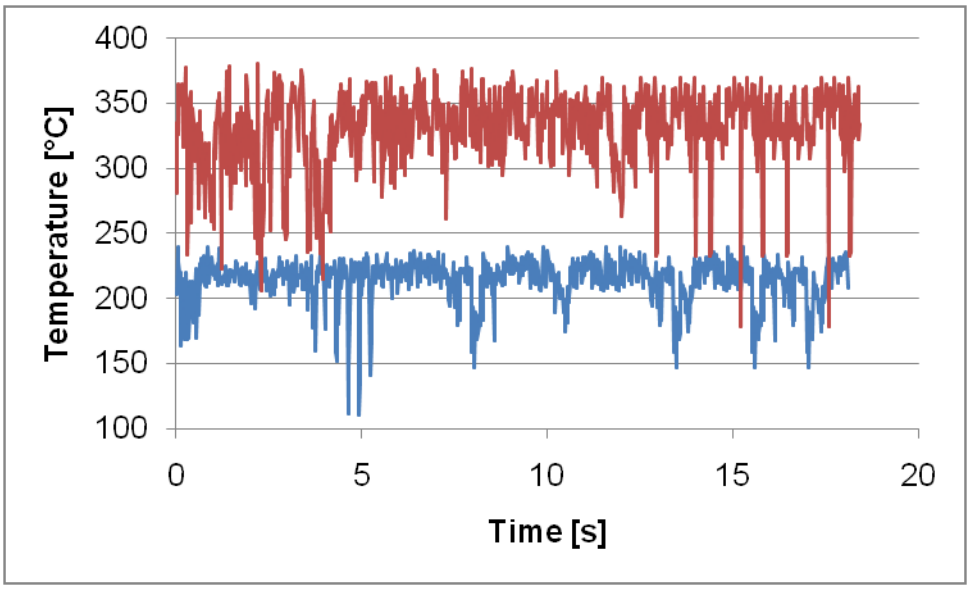

Figure 7-5: Comparison of chip maximum temperatures for a_p=0.1 mm in CT (blue) and UAT (red), V=10 m/min, f=0.1 mm/rev

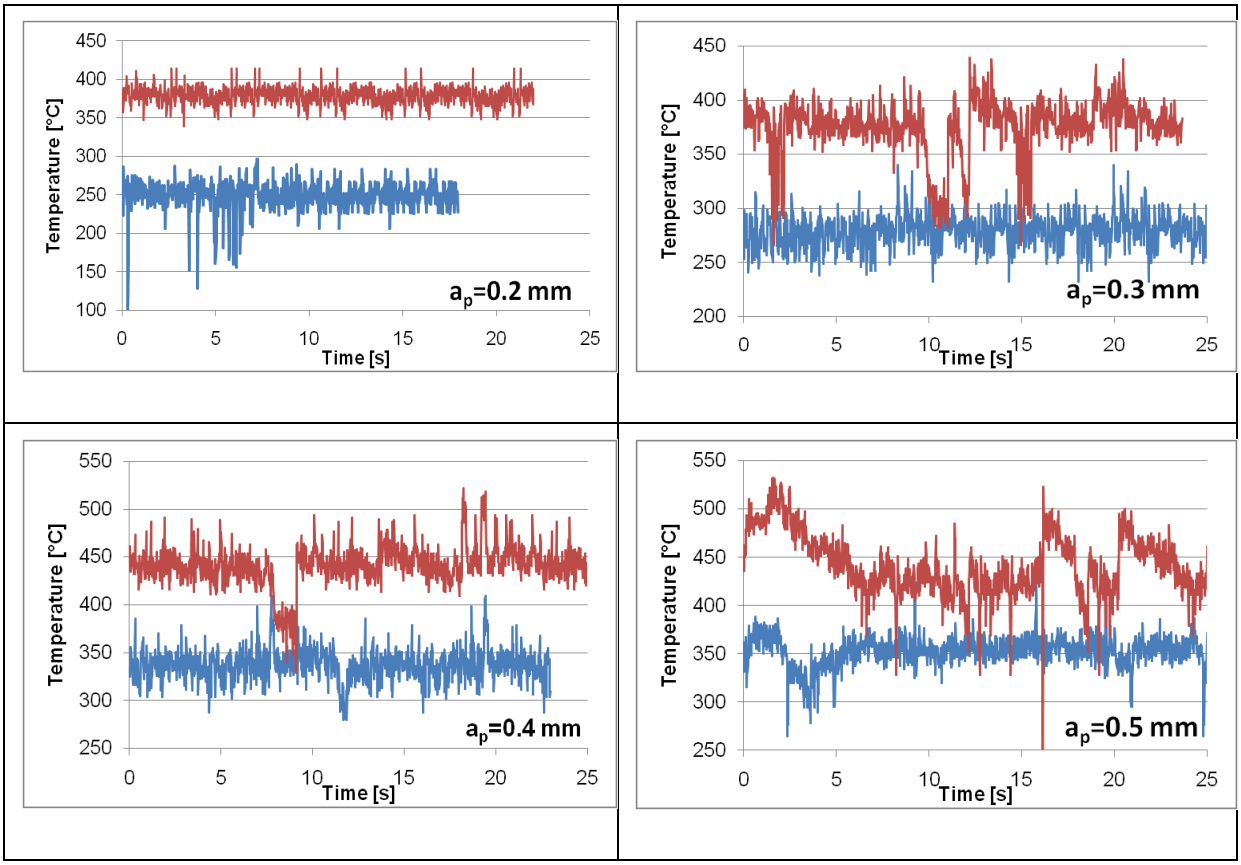

Figure 7-6: Comparison of chip maximum temperatures for a_p=0.2-0.5 mm in CT (blue) and UAT (red), V=10 m/min, f=0.1 mm/rev

Previous experiments in Nickel based alloys [Babistky *et al.*, 2004; Mitrofanov *et al.*, 2005] showed limited increased temperatures in UAT, however since most of the

effects of ultrasonic vibration are strongly material dependent it was not possible to predict how much temperature difference would be observed in the comparing between CT and UAT at the same a_p.

Not surprisingly, the strong material dependence of UAT was also shown in this Ti alloy, maximum temperatures of the chip were significantly different for CT and UAT as opposed to the results obtained in the Ni based alloy [Mitrofanov *et al.*, 2005].

The highest temperature difference was for an a_p=0.1 and 0.2 mm, with a difference between the averages of over 100 °C [Figure 7-5 and Figure 7-6]. It should be noted that at these depth of cuts the thickness of the chip was low, with this low mass it was easier to increase its temperature because of the additional energy introduced by the ultrasonic vibration.

Temperature differences vary with a_p, they peak at the lowest depth of cuts and became progressively closer at high a_p. Ultrasonic machining chip temperatures appear higher than the conventional turning, this could be explained by the additional energy which is introduced into the system by the ultrasonic vibration, additionally, the contact time between the chip and the tool is reduced while machining in UAT, allowing less heat to be transferred by conduction to the work-piece and virtually increasing the temperature of the chip. Large nose radius rendered also the cutting process prone to ploughing effects which could have influenced the temperature gradients. For higher depth of cuts, this effect was reduced, hence they were considered more reliable in offering an insight of the temperature reached in the process zone. Simulation results [Muhammad *et al.*, 2012] predicted temperature for UAT in excess of approximately 70 °C when compared to the temperature reached in CT, while this results deals with the temperature reached in the process zone, it

was easy to understand that this differences would be carried out to the chip and ultimately measured by the camera. The temperature differences were small compared to the design operation temperature of the cutting inserts, and they were also far from the melting point of the alloy.

However, β-Ti alloys, when exposed to oxygen rich atmosphere at high temperature are known to undergo oxygen diffusion. Oxygen is a strong α-stabilizer in these alloys, and attempts have been made to reduce the oxygen content in the cast alloy [Su *et al.*, 2009]. During the cutting process, the lack of coolant and lubricant facilitated the exposure of the alloy to the atmospheric oxygen; this process was even favoured by the intermittent contact between the tool and the work-piece of the UAT machining process. The cutting process was brief, and the temperature reached by the chip were not in excess of 500 °C, which is considered the lower limit for transformation of β-titanium into α structures, however it was not possible to exclude completely effects in the process zone, which would ultimately became the newly formed surface of the work-piece. Additional investigations were therefore deemed necessary to investigate in detail the effect of the machining technique on the surface of the work-piece [see 8.2, page 158 and higher].

8 Surface quality

The high sensitivity of Ti to notches, in fact, requires surface finishes of great quality. By reducing the surface defects and imperfection, the number of sites from where a crack could form is therefore also reduced. Most of the cost associated with the machining of Titanium alloys comes from the large number of subsequent finishing processes needed to achieve a correct size and finish of the work-piece. Tool traces, chip welding and surface smears are all unwanted results observed when machining high strength titanium alloys. Machining processes generate a texture on the surface of the work-piece which could ultimately influence its useful life and tribological characteristics. Mission critical application request also a high reliability and long life of the component, machining of high strength Titanium alloys generally result in high tensile residual stresses in the sub-surface layers of the work-piece. These residual stresses are detrimental for component life hastening the progression of hairline cracks. Ideally, compressive near surface residual stresses are desirable.

Machining processes have the objective to ensure that the produced surface is within the certain dimensional range from a reference. Ultrasonically assisted grinding was used to improve the surface and dimensional quality of the work-pieces when compared to traditional broaching or blind hole drilling. Later, ultrasonically assisted machining with solid tool was used to improve the quality of surfaces in difficult-to-machine materials, such as glasses, ceramics and hard alloys. 1D ultrasonic machining (vibrations are only in one direction) is known to improve the surface quality when machining brittle materials by rendering the machining process more similar to the machining of a ductile material. 2D ultrasonic machining was

used to improve the surface finish of optical parts and greatly reduce the cutting forces, however only low material removal rate were used.

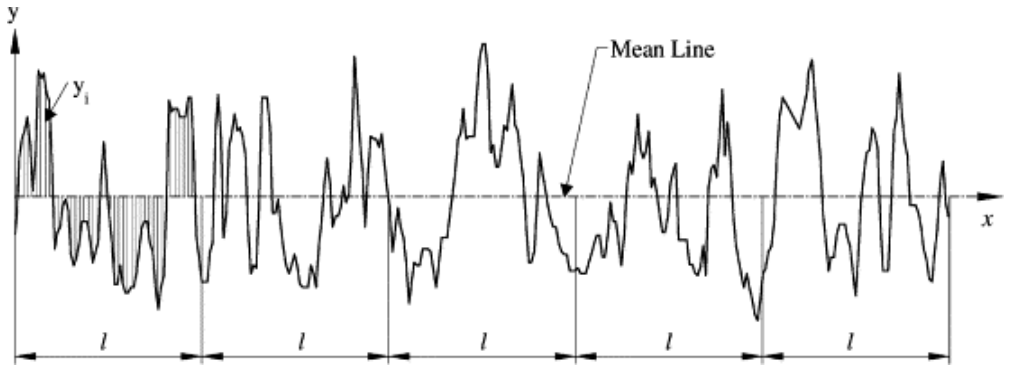

Figure 8-1: Definition of Ra

8.1 Parameters and instruments

A large number of surface texture parameters are available from the literature, most of them with statistical significance, but a limited number is used a lot more than others. 1D parameters, such as Ra, Rz, Rq were the most used in assessing the surface of a machined work-piece due to the widespread use of contact instruments, also called stylus profilers. Ra represents the arithmetic average of filtered roughness deviations in relation to a centreline along an evaluation length [Figure 8-1]. Being an average, doesn't give direct information about excessive peaks or valleys in the measured area [Gadelmawla *et al.,* 2002].

$$\mathrm{Ra} = \frac{1}{\mathrm{L}}\int_0^{\mathrm{L}} |\mathrm{y(x)}|\mathrm{dx} \qquad 6.1$$

where L is the measurement length and $y(x)$ the position of the profile in respect to the centreline.

Rz is also called ten-point height because it represents the difference in height between the average of the 5 highest (p_i) and 5 lowest points (v_i) in the measured

profile [Figure 8-2]. It is obviously more sensitive to large peak and valley than Ra.

$$Rz = \frac{1}{n}\left(\sum_{i=1}^{n} p_i - \sum_{i=1}^{n} v_i\right) \qquad 6.2$$

Rq, also known as RMS, uses statistical methods to define the roughness of the surface, it represents the standard deviation of the distribution of surface heights. It is a parameter that gives higher weight to large deviations from the centreline, thus resulting more sensitive than Ra where large irregularities are present.

$$Rq = \sqrt{\frac{1}{L}\int_0^L [y(x)]^2 dx} \qquad 6.3$$

Other more specialized parameters (R_{10}, S_{pd}, etc.) give information about the maximum deviations of peaks and valleys, about their density, or different averages.

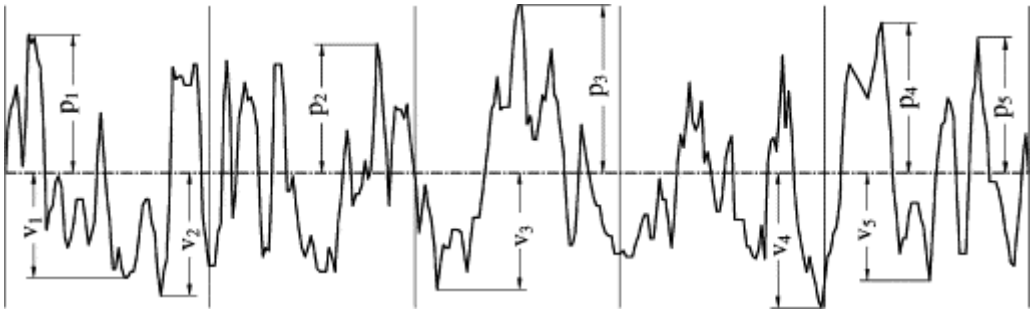

Figure 8-2: Definition of Rz

Not only the deviations from the centreline are of interest when checking the surface quality, the sharpness of the peaks or their prevalence in respect to valley are also assessed because they greatly influence performances of the surface in different uses. Skewness (Rsk) and kurtosis (Rku) are two statistical parameters that measure the prevalence and shape of peaks on the surface. Rsk parameter measures the symmetry of the profile around the centreline, so that profiles with more peaks than valleys have a positive skewness [Figure 8-3]. It is a parameter useful when comparing surfaces with the same Ra.

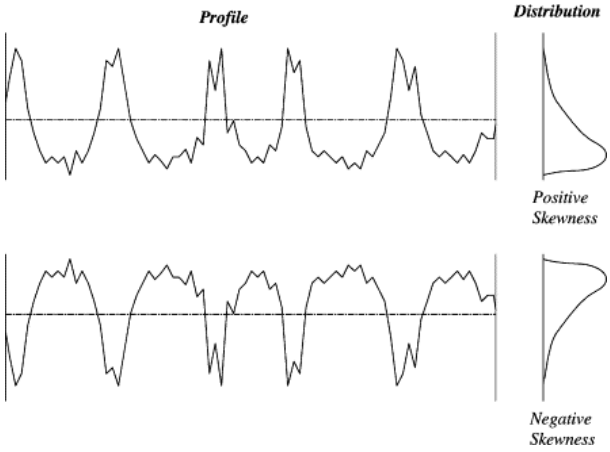

Figure 8-3: Skewness of surface profile

Rku parameter measures the sharpness of peak and valleys so that a surface with thin peak and valleys is showing a kurtosis ≥3 [Figure 8-4] (a surface with equally spaced peak and valleys has a kurtosis of 3). This parameter is also useful to characterize the tribological properties of a machined surface. It might also be used to distinguish between two surfaces with the same Ra.

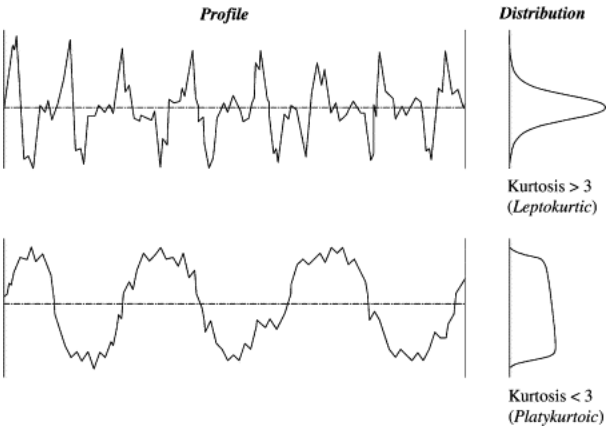

Figure 8-4: Kurtosis of surface profile

With the technological advancements in surface analysis new and improved machines became available, in particular non-contact optical ones. These machines gain the ability fo measure 2D surface parameters over a standard area. These texture parameters are gaining more and more importance nowadays because they allow for a better evaluation of the surface quality of the machined work-piece. These

topographical measurements parameter give more information on the roughness of the surface than the traditional 1D ones. They are generally linked to their 1D counterpart, so that Ra (roughness) is linked to Sa (area roughness) and maintain similar significance [Gadelmawla *et al.,* 2002]. The complete characterization of the surface topography of the finished work-piece is essential in assessing machining quality; insights into the fatigue strength of the machined component could also be gained [Korzynski *et al.*, 2011].

8.1.1 Laser interferometry

The Zygo newview 5000 is a non-contact instrument that uses white light interferometry to acquire the topography of the measuring surface. With the software MetroPro produced by Lambda Photometrics it allows the acquisition of high resolution 3D contour plots to characterize the surface structure of the test area. The instruments allows for a very accurate measurements of surface contour in a fraction of the time needed by a contact instrument.

Table 8-1: Zygo NewView 5000 specs

Objectives	5, 10, 50X
Vertical resolution	0.1-20 nm
Lateral resolution	0.64-2.6 μm
Vertical scan rate	≤10 μm/s
Max roughness	100 μm

The excellent vertical resolution of the instrument allows obtaining high resolution characterization and analysis of the measured surface. The measured 3D plots were then elaborated in TalyMap Platinum software to obtain the needed measurements.

8.1.2 Surface analysis

In order to avoid introducing errors in measuring the surface quality care was taken to handle the test work-piece carefully after the machining operations and to perform the analysis immediately after the cutting experiment. The freshly cut surfaces were marked with a permanent marker and three large areas selected at 120° between each other. Each of these areas was further divided into three smaller parts, and in each two of a series of 18 measurements would be taken. The resulting surface parameters represent the average of the series of tests. The work-piece sample to be tested was held in place on the Zygo measurement plate by metal blocks and not fixed into it to prevent any possible damage to the surface.

This procedure was selected to minimize the effects of local damages or imperfections over the overall surface analysis. In this section, results obtained for a_p=0.2 mm and V=10 m/min are presented. The results are representative of all other depths of cut studied.

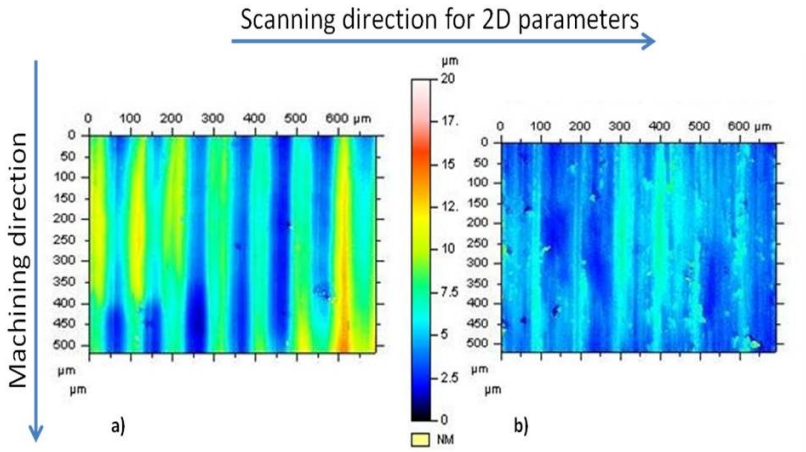

Figure 8-5: Surface plot for a_p=0.2 mm in CT a) and UAT b), V=10 m/min, f=0.1 mm/rev

Figure 8-5 shows two measured surfaces, in figure Figure 8-5a it is possible to see the machining traces with deep valleys and peaks, it is also possible to distinguish a slightly oblique pattern caused by the machining chatter. In figure Figure 8-5b, during UAT machining, the deep valley and high peaks that characterize the CT machined surface are absent. The oblique patterns caused by the chatter are also not present. The UAT machined surface appears flatter than its CT counterpart. Several key 1D and 2D parameters are used to characterize the surface [Leach & Haitjema, 2010]. Full range measurements for this and the other depth of cuts (0.1…0.5 mm) are provided in the appendix.

Table 8-2: 1D roughness parameter (a_p=0.2 mm, V=10 m/min, f=0.1 mm/rev)

[µm]	**Ra**	**Rz**	**Rq**	**Rsk**	**Rku**
CT	1.73±1.33	7.46±0.97	1.97±0.33	0.11±0.23	1.93±0.5
UAT	0.89±0.25	5.97±2.1	1.17±0.35	0.72±0.54	3.92±1.6

The surface measurements of Table 8-2 show a consistent improvement for the UAT machined surface when compared with CT. 2D surface parameter show similar pattern:

Table 8-3: 2D roughness parameters (a_p=0.2 mm, V=10 m/min, f=0.1 mm/rev)

[µm]	**Sa**	**Sz**	**Sq**	**Ssk**	**Sku**
CT	2.14±0.27	16.3±2.3	2.58±0.35	0.08±0.18	2.41±0.4
UAT	1.2±0.28	19.4±7.3	1.55±0.34	0.83±1.08	9.45±13

In Table 8-3 is shown how the roughness parameter Sq reduces consistently when measuring the UAT machined surface.

In order to validate the efficacy of the technique in the range of a_p taken into account is useful to visualize how the average value of the roughness Ra changes for higher a_p. In [Figure 8-6] is clearly visible how the roughness of the UAT machined surface is always smaller than the CT one in the whole range of cutting parameters taken into account.

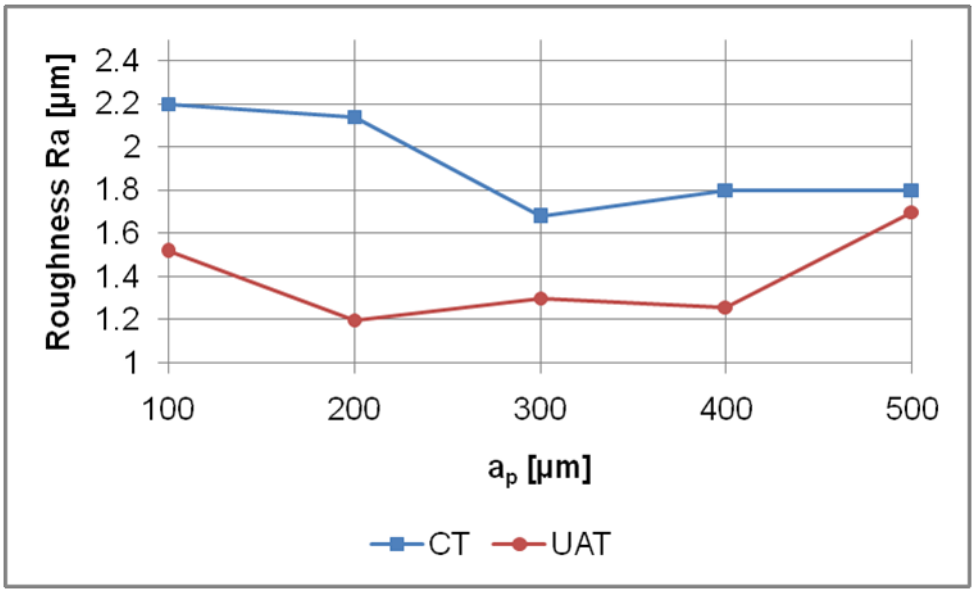

Figure 8-6: Roughness Ra for varying a_p, V=10 mm/rev, f=0.1 mm/rev

In turning operations the generated surface finish is directly influenced by the combination of tool nose radius and machining feed. It is possible to calculate the roughness generated by the machining process:

$$R_a = \frac{f^2}{8 \times r_n} \times 10^3 \qquad 8.1$$

where f is the feed and r_n the tool nose radius. In this case, given the feed of 0.1 mm/rev and the tool nose radius of 0.8 mm, the roughness generated by the cutting process would be R_a=1.57 µm [Armarego and Brown, 1969]. This formula doesn't keep into account of machining defects such as chip welding and built-up edge welding on the surface. These defects, in particular chip welding, are commonly

observed in the machining of Ti alloys. However, UAT surface roughness [Figure 8-6] was observed to be even lower than the expected value, acting as an indicator of the process improvement.

It is evident that the UAT machining conditions are completely different than the CT one, the complete separation between the tool and the work-piece is likely leave a trace on the surface. These traces were found in some favourable cases since they were approaching the limit of detection of the Zygo instrument. Distinct periodicity of the micro-impact traces is observed in the UAT machined surface [Figure 8-7], as it was observed in other researches [Gao *et al.*, 2002] [Figure 2-13].

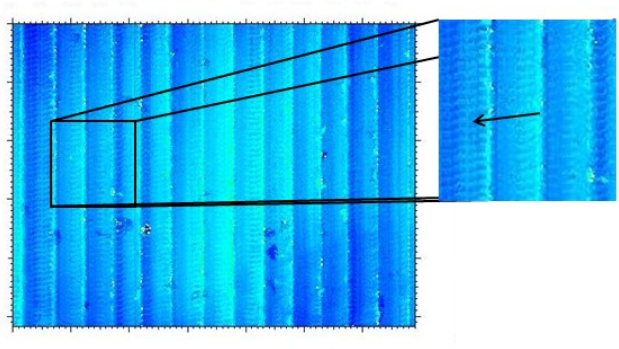

Figure 8-7: Micro-impact traces for a_p=0.2 mm, V=10 m/min, f=0.1 mm/rev

They appear as a regular series of peaks, each one spaced approximately 10 μm from the others, along the direction of machining. These peaks appear to have a thickness below 2 μm and they raise approximately 4-10 nm from the centreline. Optically they give the machining traces a textured appearance and are most visible for an a_p of 0.2-0.3 mm.

They do not seem to significantly affect the calculated surface roughness; however they greatly influence the density of peak parameter Spd. This parameter is defined as the number of peaks per unit of area measured. This texture parameter could influence the sliding behaviour properties of the machined surface.

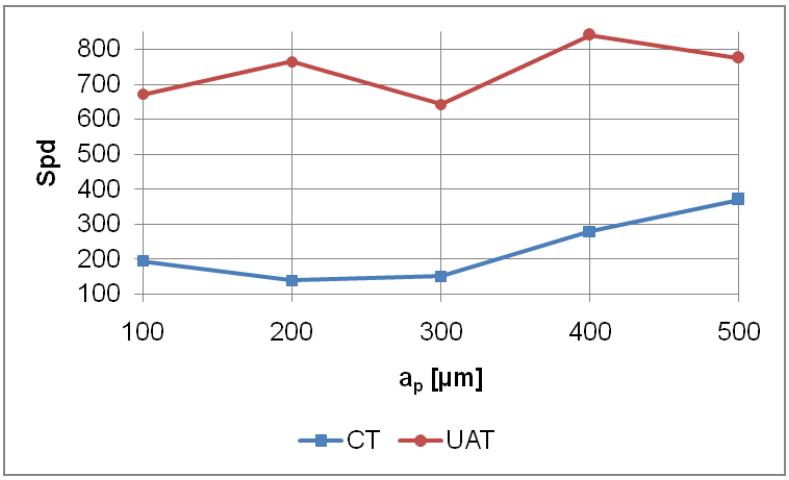

Figure 8-8: Spd for CT and UAT machined surfaces, V=10 m/min, f=0.1 mm/rev

8.2 Evaluation of surface hardness

Ultrasonically assisted machining chips show higher temperatures than conventionally cut one. It is possible to suppose higher temperatures are reached in the cutting zone. Numerical models of UAT predict higher temperatures in the process zone when compared to CT for the same machining conditions [Mitrofanov *et al.*, 2003]. Higher a_p also lead to higher cutting forces and temperatures in the process zone during machining as demonstrated in the numerical studies conducted by Muhammad *et al.*, 2011a; 2011b. Titanium alloy grain structure is stable up to 300 °C, between 300 and 500 °C could undergo grain growth and the transition to α-Ti becomes possible. This well known process, namely α-casing, is generally responsible for strong surface effects in Titanium alloys. The exposure of high temperature freshly cut surface to oxygen could lead to the formation of a hard and brittle layer of α-needle structures, this layer is prone to the formation of micro-cracks, thus greatly reducing the fatigue resistance of the finished work-piece.

Surface integrity in Ti alloys is of great importance because is critical in applications in which the components are generally employed. Two different tests have been

performed on work-pieces' CT and UAT machined surfaces in order to assess the effect of the technique on the material structure in the superficial and sub-surface layers. It is reasonable to predict that grain growth or α-casing layer, if present, would be confined to the immediate surface of the work-piece. This area is subject to the highest thermal excursions and exposed to oxygen. Because the α-casing layer is harder than the normal β-Ti, it could be possible to investigate its presence indirectly by micro-indentation of the surface in search of variation of hardness. However, the increased hardness is not a direct proof of α-casing presence; it could be caused by other factors. It was therefore decided to investigate also directly, by embedding, polishing, etching the work-piece and observing it under microscope.

Micro Materials NTX^3

The micro-indentation tests, even if the test itself is a non-destructive one, required the work-piece to be sectioned in order to accommodate it into the machine slide [Figure 8-10]. The work-piece was sectioned using an automated metal saw, at low cutting speed and feed, and with pressure fed coolant and lubricant. The work-piece was sliced into small chunks which could be directly loaded into the machine. A sample test specimen was glued with cyanoacrylic adhesive to a sample holder which was fixed with screws to the machine slide. Areas of measurements were selected far from the cut edges in order not to introduce errors.

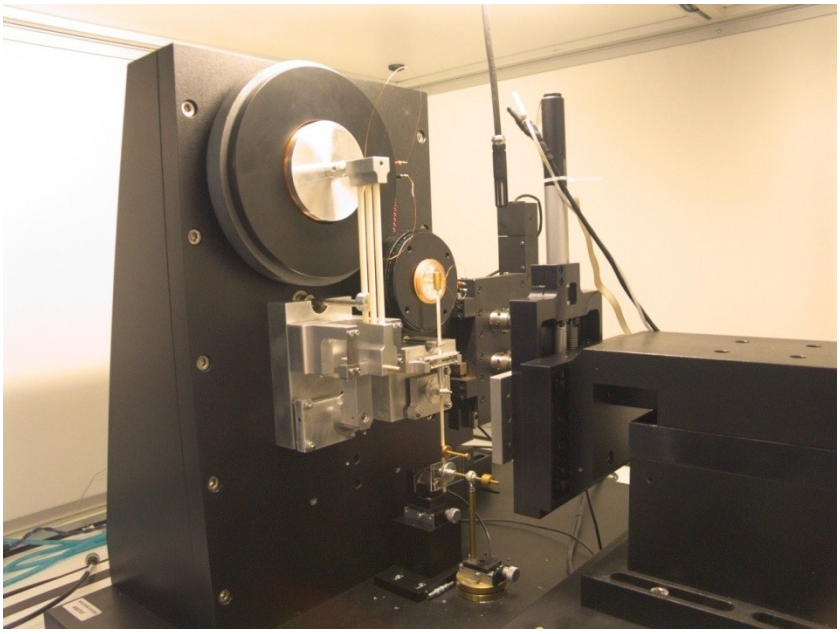

Figure 8-9: NanoTest NTX^3

The NanoTest NTX^3 from Micro Materials [Figure 8-9] was used for the micro-indentation tests, its excellent sensitivity and versatility [Table 8-4] allowed to perform fully automated tests on several areas of the machined surface.

Table 8-4: NTX^3 NanoTest specifications

Maximum Load	20 N
Load Resolution	≤100 nN
Force noise floor	100 nN
Maximum displacement resolution	0.05 nm
Thermal drift	≤0.004 nm/s
Maximum displacement	80 µm

Obtaining reliable measurements with minimal area effects was considered of great importance. Therefore, each indentation test consisted of several indentation points nearby each other; the pattern used was a parallelogram shaped cluster of 9 measurements arranged in 3 columns spaced 200 µm between each other and misaligned 100 µm. This pattern was used to lower the chances of obtaining single

grain indentations since Ti 15-3-3-3 exhibits large grain sizes (≥100 μm) A standard, diamond tip Vickers indenter, was used for all the tests.

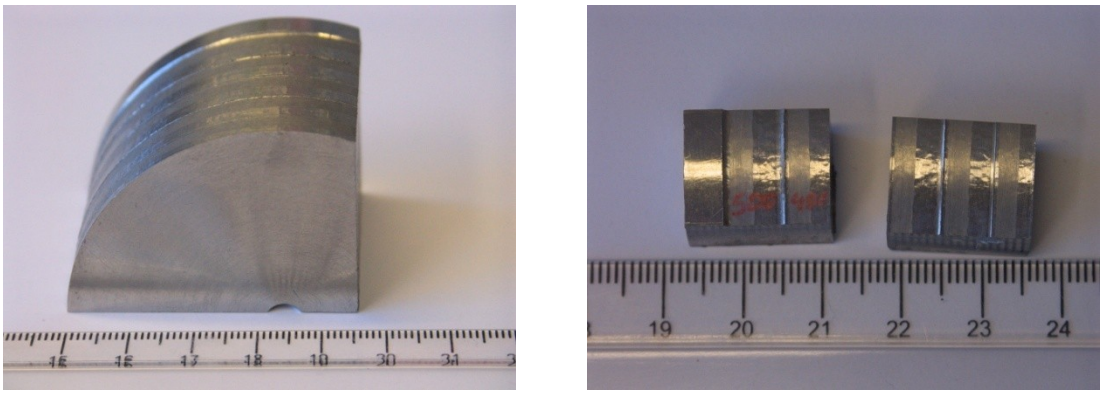

Figure 8-10: Indentation sample preparation

Tests were performed with a fixed maximum load of 2 N, achieving penetration of the indenter below 7 μm. This shallow depth was chosen for two reasons: it allowed to use the machine well below its maximum load of 20 N and concentrated the investigation in the immediate surface, which was considered of interest in this study. Contribution of the results obtained from indentation would also come from strain hardening and residual stresses. While these stresses were considered of interest, they were not investigated by indentation due to the low accuracy and specificity of this technique.

Before performing the indentation on the machined surface a sample was prepared by carefully wet grinding its surface to avoid introducing any changes. The bulk properties of the alloy were then investigated to be used as a benchmark against the valued obtained from the machined surface.

Table 8-5: Indentation measured bulk properties of Ti 15-3-3-3

Max depth [μm]	Plastic depth [μm]	Hardness [GPa]	Moduls [GPa]	Plastic work [μJ]
5.7±0.14	5.2±0.14	3.05±0.17	97.4±3.5	3.6±0.1

These properties are similar to these provided by the manufacturer, a sign that the

technique used to measure was good. A higher a_p generates higher cutting forces and ultimately brings higher temperatures into the process zone, it was therefore expected that the higher cutting depth samples show larger differences from the control bulk properties.

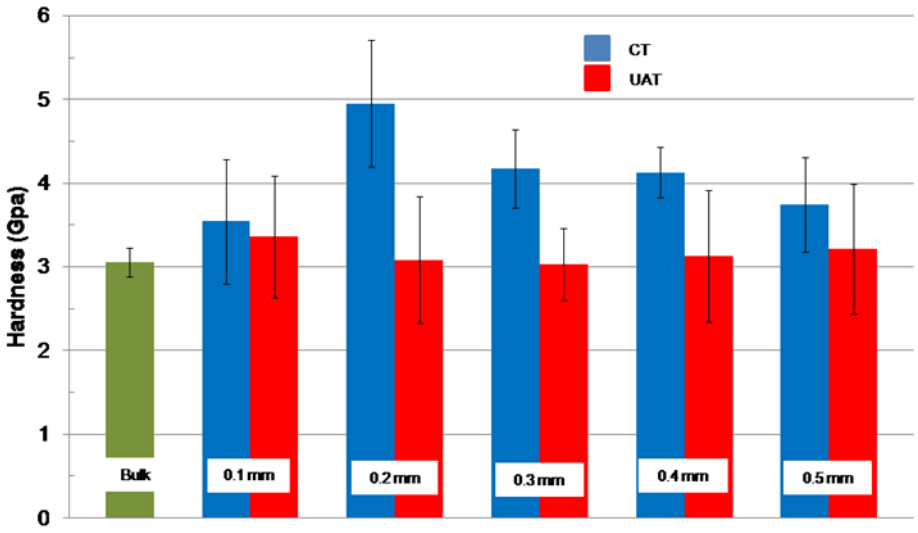

Figure 8-11: Surface hardness for CT and UAT machined surfaces at different a_p, V=10 m/min, f=0.1 mm/rev

When taking in consideration the hardness of the surface, one of the parameters that could potentially identify changes in the material structure, it was observed that the CT and UAT surfaces behaved very differently. The surface hardness of the CT machined work-pieces appears to be higher than the bulk hardness of the unprocessed material, probably because the work hardening of the alloy. The maximum effect was observed for a_p=0.2 mm. This could be explained as an indirect effect caused by the ploughing cutting of the tool at these a_p caused by the scope of this study. This effect was however not replicated in the UAT tests [Figure 8-11]. From the surface indentation tests it was observed that the UAT surface hardness was differing very little from the bulk one. This interesting finding was not expected since the strain rate to which the material was subjected during UAT was higher than

in CT. The intermittent contact between tool and work-piece would require the deformation rate to be higher during the impacts as the effective cutting time is a fraction of the total time. Therefore, a higher surface hardness in the UAT surfaces was to be expected if strain hardening was the cause of the increased hardness. Other causes could be metallurgical with grain or phase changes, especially in the formation of α-Ti or residual stress. The reduce hardness of the UAT work-piece when compared with the CT one, could be explained by smaller residual deformations, a sign of reduced residual stress in the deformed layer.

The indentation experiments performed consisted only of shallow indentations on a surface of roughness comparable to the depth of indentation. The process was therefore prone to errors. To rule out possible effects of roughness of the hardness a deeper indentation was performed on the a_p=0.5 mm cut sample reaching a depth of approximately 15 μm with a force of 10 N and Vickers micro-indenter. The sample was chosen since the high a_p would maximize the thermal and deformation effects. The results were again showing UAT hardness 12% lower than the CT one, however the statistical significance of these values appeared to be small.

The ultrasonically machined surfaces show hardness comparable to those of the virgin material. This more predictable behaviour could be beneficial to the industry since the bulk hardness of the material is preserved. The investigation however did not completely rule out the presence of changes in the material which could have been below the error limits of the technique. For this reason a direct observation of the material surface was performed.

9 Metallographic tests

Ti 15-3-3-3 alloy is a difficult to prepare and etch material. Its high surface hardness, high modulus, and tendency to smear require careful preparation of the metallographic samples. In order to avoid subjecting the work-piece sample to further thermal stresses it was attempted at first to perform cold embedding with epoxy resins. These resins when mixed with the hardener undergo setting with an exothermal reaction; the chemical heat generation increases the temperature up to 60-70 °C. The selected resin was Buehler Epoxicure, which was available in the materials lab, set in soft silicon moulds. The resin did not show to have good edge retention so during the polishing, edge effects were unacceptably high. The same resin was also used mixed with conductive Ni particles for early SEM analyses. A resin with lower shrinkage and better edge retention was needed; It was therefore necessary to switch to hot mounting.

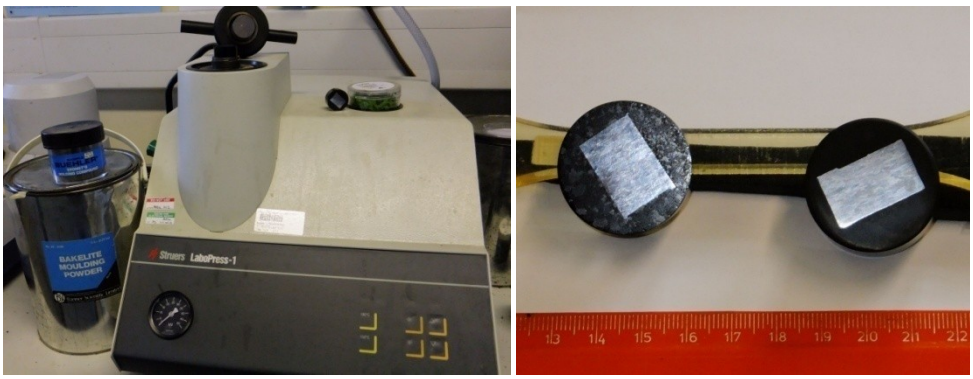

Figure 9-1: Embedding hot press and etched samples

The resin of choice initial was Buehler Bakelite. This resin offered higher performances than the cold set Epoxicure granting better edge retention and lower shrinkage. The samples were embedded on a Struers mounting press, with a

mounting pressure of 20 kN at 180 °C. The mounted samples were difficult to polish correctly, requiring long polishing time with high pressure, and showed defective edge retention that prevented a successful examination. A layered embedding was then tried, with a layer of very hard, low shrinkage resin on top of a clear support one. The two resins selected were Buehler Epomet G, top grade embedding resin and Buehler Transoptic as a support resin. The Transoptic resin offered the advantage of being transparent, therefore rendering easier to visually check the grinding process.

The mounted samples were manually polished on silicon carbide wet grinding paper with increasing grit sizes up to 4000. Polishing was also manual in three steps, first on Buehler Texmet 1500 with 6 μm diamond paste, then Buehler Microcloth with 1 μm diamond paste and finally Buehler Chemomet with 20 nm colloidal silica. Required polishing times were rather long (over 20' on Chemomet) due to the toughness of the material. Samples were then washed and etched in 10'' steps with Kroll solution (HCL+HF+H_2O) until the grain structure became evident to the naked eye due to the grain structure of Ti 15-3-3-3 composed by large grains (≥0.1 mm) [Rokicki *et al.,* 2010].

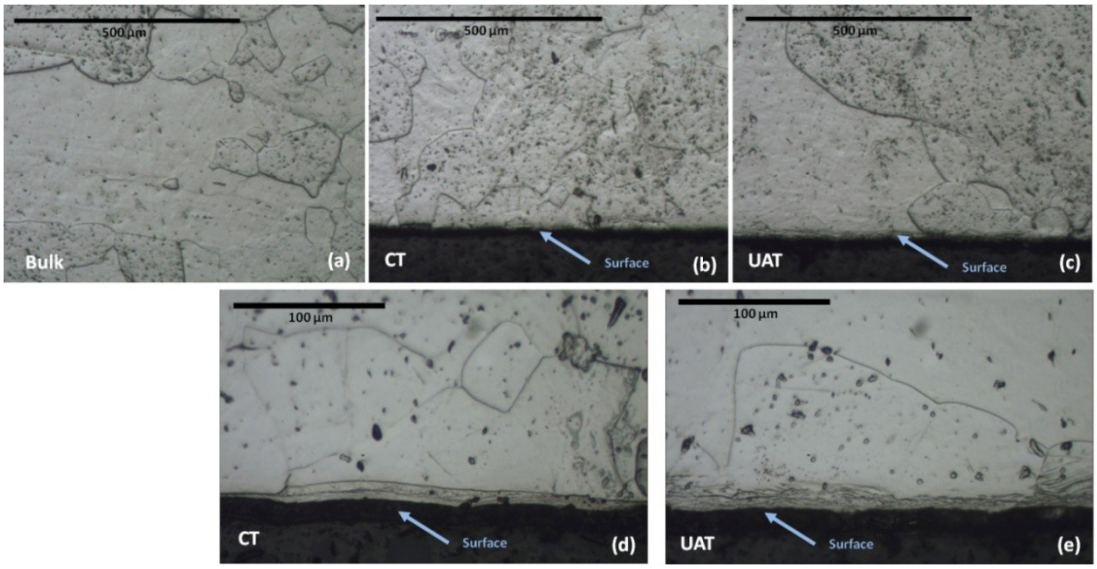

Figure 9-2: Etched cross sections of work-pieces: (a) virgin-state bulk sample; (b, d) machined with CT; (c, e) machined with UAT. Note different scales, a_p=0.5 mm, V=10 mm/rev, f=0.1 mm/rev

The etched samples were analysed using an optical microscope; the grain structure of the alloy was large so the grain structure is clearly visible even without SEM analyses due to good contrast obtained. Figure 9-2 refers to a cross-section of a_p=0.5 mm however analyses were performed for a_p=0.1-0.5 mm. A higher a_p inevitably leads to higher cutting forces and temperatures in the process zone during machining as demonstrated in the numerical studies conducted by Muhammad *et al.*, 2011a, 2011b. Also, numerical models of UAT predict somewhat higher temperatures of the process zone when compared to CT for the same machining conditions [Mitrofanov *et al.*, 2003]. Thus, analysis of the sub-surface layers obtained with UAT becomes crucial at such high depths of cut. The image doesn't show any needle like structure that is typical of α-Ti and the sub-surface layers grain structure of CT and UAT machined work-piece appears to be somewhat similar to that of the virgin material [Figure 9-2]. Some polishing artefacts are still present near the machined surface due to the shrinkage of the mounting resin and the difference in polishing rates. From the optical metallographic analysis it is not possible to verify

the presence of any grain structure different than the classical grains of this alloy. This result, when associated with the absence of significant hardness changes could probably rule out the possibility of α-casing formation in the ultrasonic machining of Ti 15-3-3-3.

It was possible to notice that a thin area (5-10 μm) in correspondence of the edge appeared with a different shine at the optical microscope. Due to the limitations of depth of field it was not possible to investigate further this area optically. It was therefore decided to prepare a new sample with a different polishing technique, and analyse it with the field emission gun scanning electron microscope (FEGSEM). This device offers significant signal-to-noise ratio when compared with conventional scanning electron microscopes, and when used with back-scattering electron detector should be able to provide a better chance of clearly distinguish α- and β-Titanium without resorting to the time intensive electron back-scatter diffraction which would require large amount of time to process the area of interest.

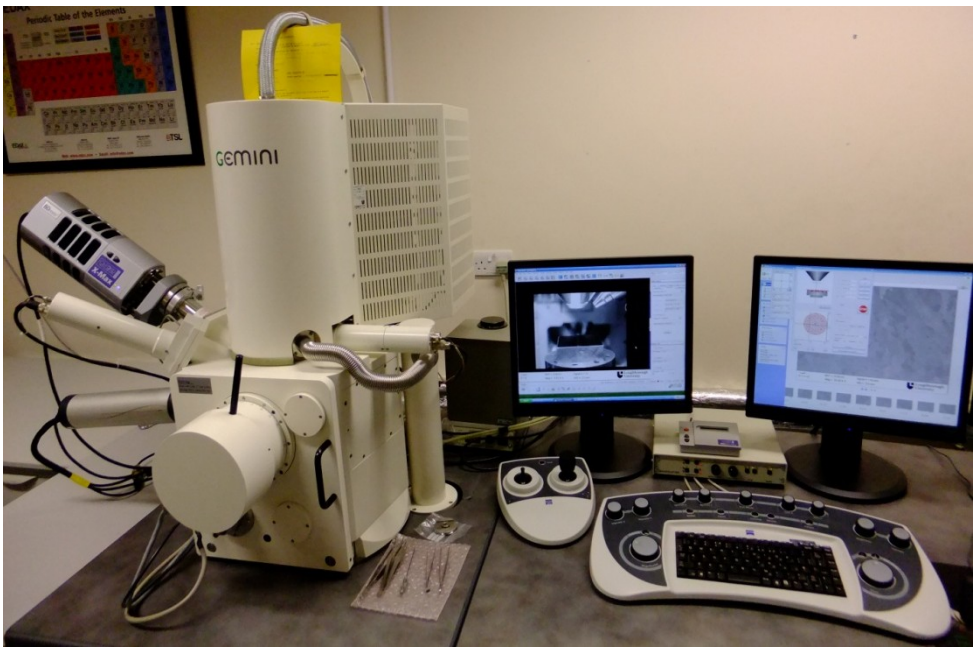

Figure 9-3: Carl Zeiss electronic microscope

Sample preparation for FEGSEM requires a high surface quality to be obtained, Ti 15-3-3-3 because of its high ductility, was difficult to polish to the required grade. To ease the polishing process, the area of interest was identified and the sample was mounted so that a minimal part of the sample was exposed. This was done to reduce the chance of debris being generated during the polishing and travelling around the surface damaging it with traces. Polishing was also performed with longer permanence of the sample on the finer polishing grits. Sample was wetted with 10% solution H_2O_2 to speed up and improve the polishing process. Final polishing were done on Chemomet with 20 nm colloidal silica suspended in 20% H_2O_2 solution for an extended time with an automatic grinder and final steps were done manually for greater control. Polishing was stopped as soon as the sample appeared sufficiently clear of traces to be analysed on FEGSEM to reduce the chances of debris smearing on the surface.

The embedding resin was non conductive, it was therefore necessary to render the sample conductive to allow the analysis at the FEGSEM to be performed. To avoid possible, even if highly improbable, reaction between a carbon vacuum coating and the alloy, it was decided to coat the sample with an Au-Pd film. In this technique a target of Au-Pd was bombarded with argon atoms at very low pressure, the consequent sputtered metal was deposited on the sample in the form of nanometer sized islands. The thin layer of conductive metal rendered the non-conductive embedded sample conductive enough to prevent charge accumulation effects and shielded it from damage by direct electron beam exposure. In the absence of this conductive layer the high energy beam of electrons would rapidly charge up the specimen to the point that no observation would be possible. Sputter coating by Au-Pd doesn’t apply a uniform coating to the sample; therefore it is not suitable when

observation of details below 30-50 nm is required. In this case, given the size of the grains of the alloy, it was considered a reasonable trade-off between ease of preparation and obtained results.

Figure 9-4: EMTECH Au-Pd sputter coater coating sample

After coating the sample it was loaded into the Carl Zeiss Leo 1530 VP [Figure 9-3] electronic microscope. This instrument features variable pressure chamber for analysing samples without the need for coating and a high speed evacuation pump, however coating the sample was preferred to allow better resolution and ease of operation. The maximum resolution of the instrument was 2 nm in optimal conditions; at the highest magnification it was possible to clearly identify the spatter islands of Au-Pd. The instrument featured also an electron backscatter capability which was required to investigate the possible changes of phase of the alloy.

The coated sample was introduced into the target chamber and evacuation was started, the accelerating voltage was set to 10 kV and the sample was quickly scanned to verify the absence of charge build-up.

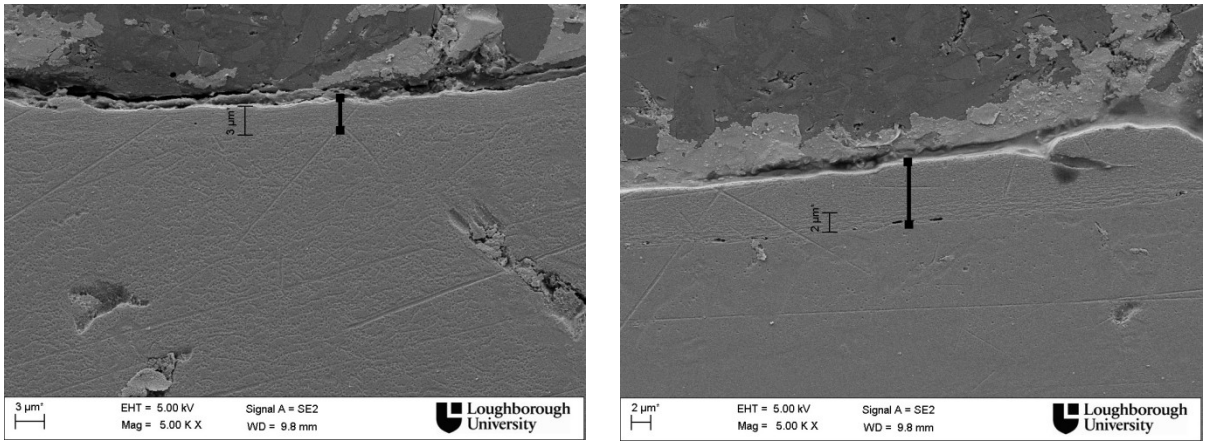

Figure 9-5: SEM images of gold-coated etched sample (a_p=0.5 mm): left CT, right UAT, V=10 m/min, f=0.1 mm/rev

Both the samples showed a layer that etched differently, this could be for a number of reasons including α-Ti formation [Figure 9-5]. Ti 15-3-3-3 formed α-structures when annealed at temperatures as low as 450 °C for one hour time, and dense precipitates when annealed at 600 °C. In the primary shear zone temperatures in excess of 900 °C could be observed, it was therefore needed to investigate if the short exposure to high temperatures which the material underwent while being machined could cause the formation of α-Ti especially after the surface hardness tests reported anomalous hardness in the CT machined work-piece [Dodonov *et al.*, 2009].

Hence, it was decided to perform a backscatter analysis of the samples. Ti alloys, when exposed to high temperatures in presence of oxygen tend to absorb it and displace the strong β-stabilizer Vanadium. If this was the case, being the atomic weights of O and Va very different, the backscatter analysis would show the areas clearly. The backscatter effect, is in fact heavily dependent on the average atomic weight of the examined area, the microscope would show in different tones of gray areas at different average atomic mass.

In order to prepare the sample for the backscatter analysis, it was decided to remove the sample from the resin and embed it in conductive aluminium filled resin, thus removing the need for gold coating it and allowing performing the etching without the need to remove the coating. The sample was prepared with a similar technique but polished at slow speed revolutions with an automatic machine for 25 minutes on Chemomet with 30% H_2O_2, 20 nm colloidal silica and 10 N polishing force.

The resulting samples showed better surface quality than the one embedded in Epomet G and did not require having the electrically conductive coating.

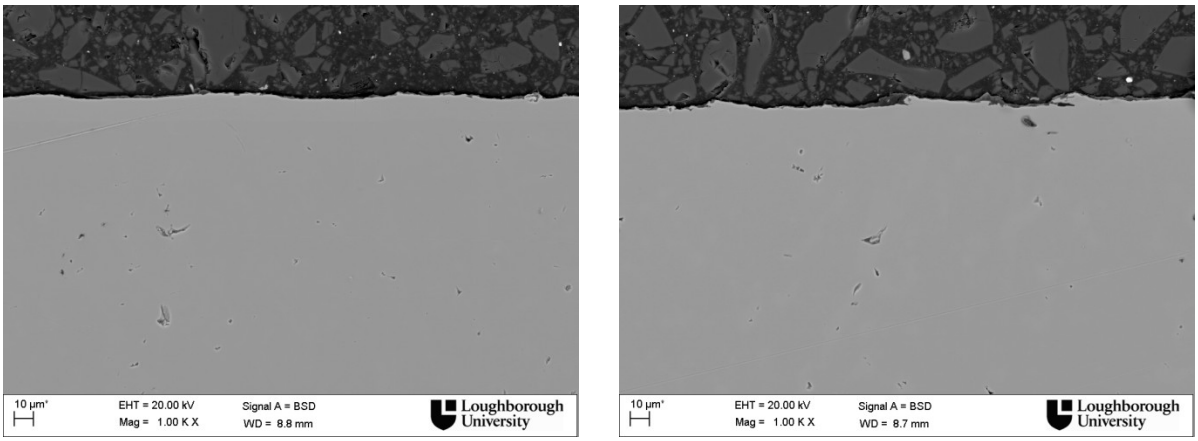

Figure 9-6: Backscatter images of CT (a) and UAT (b) machine work-pieces (a_p=0.5 mm, V=10 m/min, f=0.1 mm/rev)

The backscatter analysis excluded the presence of α-Ti in the sub-surface layer, therefore it was deemed necessary to try and investigate more in detail the layer which was showing in the [Figure 9-5]. The samples were therefore lightly etched with Kroll to try to evidence the sub-surface layer structures, and they were once again investigated at the SEM.

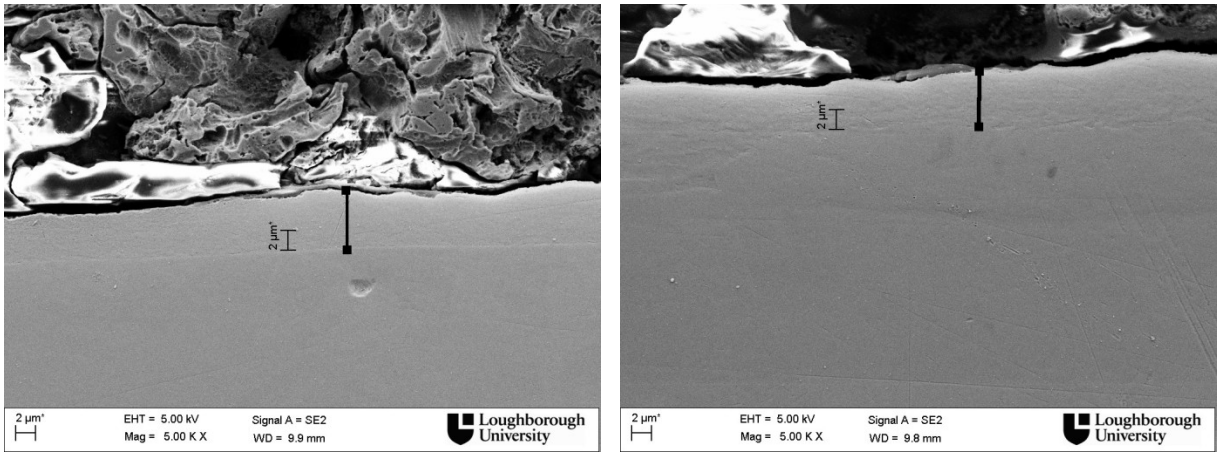

Figure 9-7: SEM images of uncoated etched sample (a_p=0.5 mm, V=10 m/min, f=0.1 mm/rev) for CT (a) and UAT (b)

In this image the layer is clearly defined and a structure is visible inside. Both the layers have same thickness of approximately 5 µm even if the UAT layer appears more lightly etched. The layer seemed consistent with a strongly deformed layer similar to the one visible in the secondary shear zone which could imply work-hardening due to surface and sub-surface deformations [MaMiNa, 2010a]. In this case, the different surface hardness of the CT and UAT samples could be explained by the different cutting conditions which have ultimately caused a different work-hardening of the sub-surface layer.

10 Discussion

10.1 Force reduction

For the cutting parameters used in the tests (cutting speed of 10 m/min, amplitude of vibration of 10 μm) the theoretical maximum reduction that is possible to obtain is approximately 73%. This is reasonably close with the results obtained from the experimental tests, which results were higher than expected. It is understood that the real case exhibited a much more complex behaviour than the one modelled in the mono-dimensional process used in [Astashev & Babitsky, 2007].

These consideration contrast with the explanations offered by the ultrasonic softening theory [Lagenecker, 1966], in which the softening effect was caused mainly by the apparent increased mobility of the defects in the material due to the added ultrasonic energy. While it was not possible to verify directly the magnitude of influence of each phenomenon, the ultrasonic-softening theory predictions are considered unreliable when applied to poly-crystalline materials.

Mechanistic models of cutting typically ascertain specific cutting pressures, which indicate energy consumption associate with material removal. Knowing the geometry of the cutting tool it was easy to visualize the cutting process in detail.

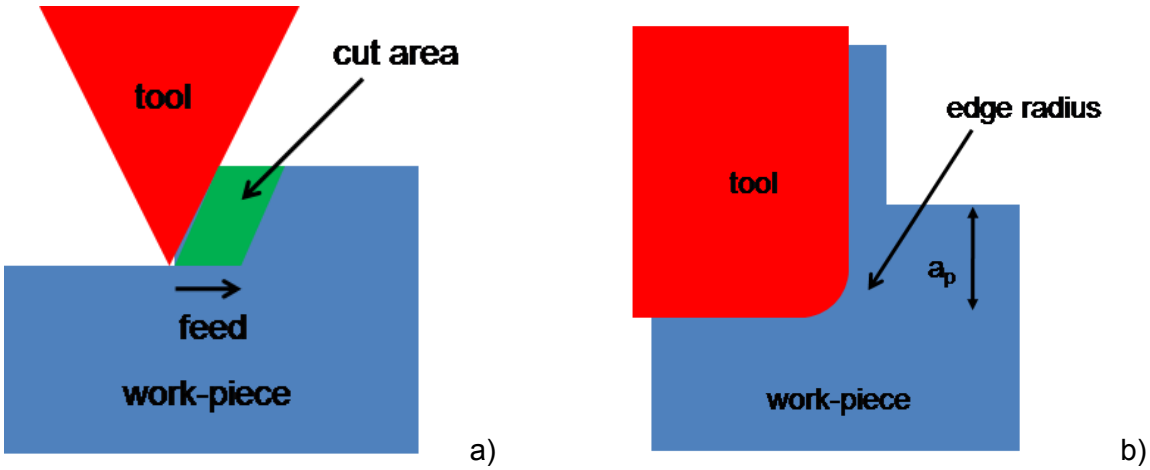

Figure 10-1: Schematics of the cutting areas: front a), side b)

Figure 10-1a shows that a cut area is the same for each pass since the feed is constant at 0.1 mm/rev; for simplicity, the cutting tool nose radius is considered very small when compared to a_p. Figure 10-1b shows the effect of tool-edge radius on the cutting process. It was understood that it was needed to account that at low a_p, the tool cutting edge radius was of similar magnitude as the depth-of-cut. In all these cases, the cutting process was more similar to ploughing.

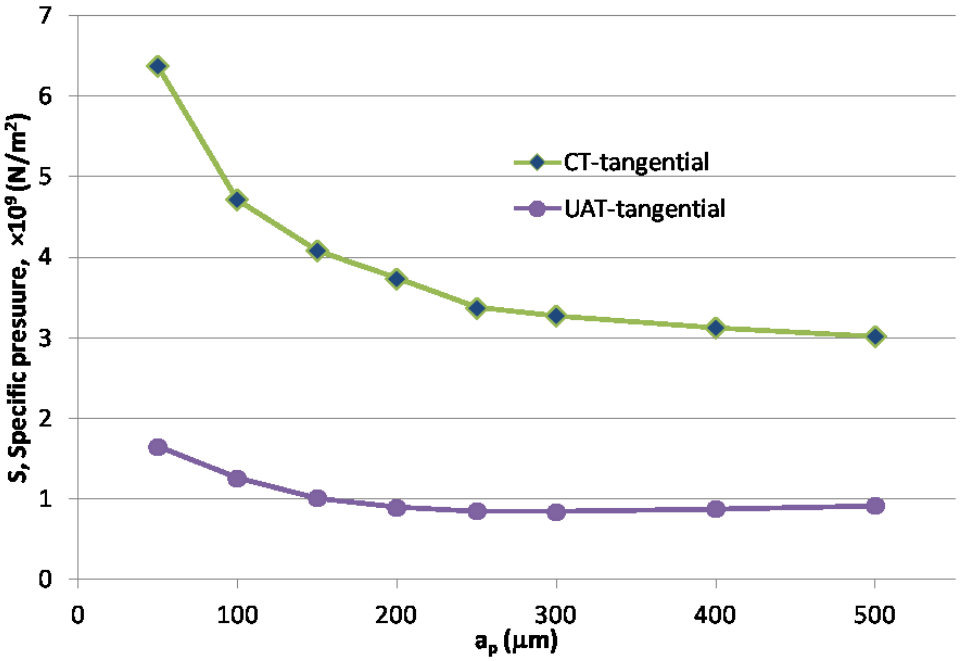

Figure 10-2: Specific cutting pressure at various cutting depths in CT and UAT at V=10 m/min, f=0.1 mm/rev.

Figure 10-2 is a plot of specific tangential cutting pressure, *S,* in CT and UAT at various depths of cut; the cutting speed was 10 m/min. Apparently, with increasing a_p the cutting forces tend asymptotically to fixed levels. The force magnitudes for two analysed techniques are noticeably different at lower a_p. This is due to a ploughing effect during cutting due to the large tool cutting edge radius (25 µm).

It is interesting to note that the average cutting forces in UAT for a_p = 500 µm are comparable to these in CT for a_p = 100 µm [see Figure 6-3]. This implies that, if tool wear and tool life remain the same in UAT, it could be possible to potentially increase MRR during vibration assisted machining by a factor higher than 3 (owing to the diamond shaped cutting tool geometry), with a cutting tool being exposed to the same level of cutting forces for respective cutting depths.

10.2 Cutting temperature

The studied titanium alloy combines low density, high strengths, ductility and low thermal conductivity. The alloy exhibits one of the highest ductility for all the titanium alloys. However, its machinability is poor. Cutting parameters have to be chosen carefully to avoid precipitation hardening, which would further impair its machinability. Since the cutting experiments were performed only in dry cutting conditions, it was needed to investigate the highest temperatures reached in the process zone.

Low thermal conductivity of the alloy renders difficult the diffusion into the chip thickness of the heat generated in the process zone [Sun *et al.*, 2009]; hence, heat is concentrated in front of the rake face of the tool. Helicoidal chips were produced during the machining operations of Ti 15-3-3-3; the posterior side of the chip was exposed to the camera objective shortly after leaving contact with the tool. It was understood that the temperatures measured were lower than the ones in the process zone. While direct measurement of the temperature in the process zone was out of reach for the technique used, chip temperatures were used to calibrate FE simulations thus retrospectively obtaining the desired information.

From simulations of the cutting process it was possible to verify the evolution of temperature in the process zone at different depths of cut. In [Muhammad *et al.*, 2012] the process zone temperatures were found to be very close to the chip's maximum measured temperatures. Figure 10-3 [Muhammad *et al.*, 2012] demonstrates that in UAT the zone that experiences higher temperatures is very close to the cutting edge, and the difference between CT and UAT appears to be small. These temperatures were far from that of α-formation (over 450°C) and it

could be concluded that no effects were introduced in the structure of the material. Still, total reliance on the simulations was deemed unsafe and further experimental examinations were performed on the work-piece surface to exclude hidden and unexpected effects on the structure of the alloy. This was deemed necessary since the UAT machining technique was not employed for the machining of this alloy.

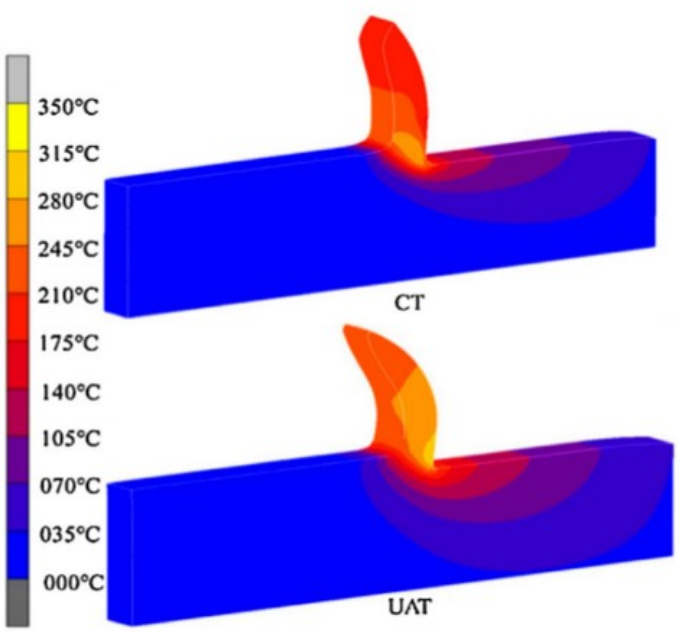

Figure 10-3: Distribution of temperature in cutting zone for CT and UAT (a_p = 0.2 mm, V = 10 m/min) [Muhammad *et al., 2012]*

10.3 Surface quality

In addition to cutting-force reduction UAT was known to improve also the surface quality of the machined work-piece. Burr suppression, and improved surface quality were observed in both 1D and 2D UAT machining of difficult-to-machine materials [Brehl & Dow, 2008]. Improvements in the machined surfaces were also observed in [Mitrofanov *et al.*, 2005] for a Ni-based alloy. Therefore, it was reasonable to expect surface quality improvements for Ti alloys.

Decreased surface roughness could be explained by the polishing effect of the cutting tool, which passed multiple times over the same areas, other effects were also to be considered, such as the different deformation rate of the material. However, it was understood that the reduction of regenerative chatter also played an important role in the observed roughness reduction [Xiao *et al.*, 2003]. Burr reduction, which was understood to account for over 60% in 1D UAT when compared to CT, was also an effective limiting factor in surface peak-to-valley levels, Burr formation is postulated to be the result of instantaneous compressive and bending stresses caused by cutting in the deformation zone at the edges of the cut. These stresses are greatly reduced by the use of VAM, since the tool forces are reduced compared to conventional cutting [Brehl & Dow, 2008]. Resulting surfaces are characterized by 20% to 60% reduction of surface roughness, by reduction of the R_z parameter and by increases of the S_{pd} parameter by over 50%. Changes in the tribological properties of the machined surfaces were also quantified by the changes in the skewness and kurtosis of the freshly produced surfaces.

Hardness measurements showed that UAT machined surfaces preserved hardness close to that of the virgin material. This desirable effect could be explained by the lower hardening effect exerted by a lower cutting force in UAT, lower than a conventional-cutting force predicted by [Astashev, 1992]. Lower forces were observed by [Shamoto & Moriwaki, 1992] in machining at very low speed and in simulations in several other works [Brehl & Dow, 2008] and [Muhammad *et al.*, 2012].

Indentation of the surface layer to a penetration depth of 5 μm (approximately the thickness of the etched layer observed in the metallographic tests) showed differences in hardness between CT and UAT machined surfaces. Additionally, CT

surfaces were observed to be 20% to 50% harder than the bulk material, while UAT surface's hardness was very close to it. Higher penetration depths of 15 μm showed lower differences ultimately questioning the presence of a hardened layer of less than 15 μm thickness. β-metastable Ti alloys consists of β-grains with an average grain size of 0.5-1 mm therefore it was necessary, for indentation tests to be statistically sound, to spread the pattern of indentation points so to reduce the likelihood of indenting only one or two grains. The precipitation of α-Ti was very unlikely due to relatively low temperatures reached in the process zone and the limited time the material was ultimately exposed to the raised temperature. However, the increased hardness raised concerns regarding the conditions of the sub-surface layers.

In order to investigate the sub-surface layers, a cross cut section was performed and traditional metallographic technique applied to the embedded sample. When α-precipitation is present, the structures of α-Ti appear like short needle precipitates, usually forming at the grain boundaries and non-uniformly distributed inside grains. The length of these formations is usually between 2 and 3 μm [Dodonov *et al.*, 2009]. These microstructures are difficult to resolve with the optical microscope; however, α-casing of these alloys is clearly distinguished in the etched sample. When the optical images of the etched sample [Figure 9-2] were compared to a typical α-casing etched sample [Figure 10-4], it became evident that the morphologies were very different.

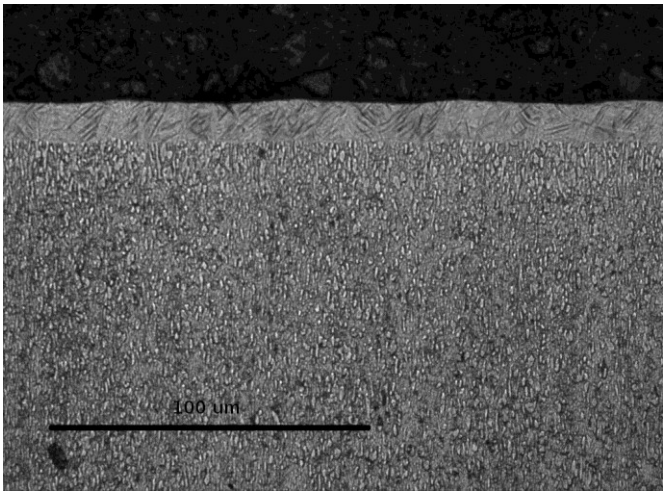

Figure 10-4: α-casing formations in Ti alloy

The possibility of α-precipitation in isolated chains not easily resolved with optical microscopy was to be taken into account. A SEM analysis of the etched sample could certainly offer better resolution but modern electron microscope usually allows performing a backscatter analysis. In this analysis α- and β-Ti would be clearly distinguishable with a very low threshold; it was hence selected as the choice analysis for its simplicity and sensitivity in detecting α-chains. A more efficient method would be Electron Backscatter Diffraction EBSD; however, it required long and tedious preparation of the sample, and it was definitely more time-consuming. The additional information it could provide were the orientation of the crystals thus detecting rotations in the lattice. This information is valuable for specialist material simulations and was therefore outside the scope of this work.

The absence of α-structures at the backscatter raised interest around the sub-surface layer, which was responding to the etching agent in a different way than the surrounding material. The observed effect was very clear in uncoated samples with CT showing a band of 5-6 μm immediately below the surface, which was etched in a different way than the bulk material; similar but lighter effect was observed in the UAT-machined sample. This was similar to a secondary-shear-zone etching

behavior, observed in [Siemers *et al.*, 2009; Rockiki *et al.*, 2010] for the same alloy. The sub-surface layer was showing similar etching properties to a strongly deformed layer, which was work-hardened in the process [Siemers, 2012; Korsunsky, 2012]. It was apparent that the work-hardening was different for CT and UAT; that was explained by the lower average cutting force in UAT, which ultimately led to lower passive forces and lower work-hardening in the material. It was possible that slightly higher temperatures also played a role in this phenomenon, but their contribution was estimated to be minimal. The sub-surface layer appeared therefore as a work-hardened layer of limited thickness, which could have limited influence on the employment of the finished component.

11 Conclusions

β-Ti alloys are difficult to machine materials. Their high hardness and chemical reactivity require large amounts of specialized coolant and cutting tools, which lower sustainability of the machining process [An *et al.*, 2011]. An improved UAT setup was developed and tested for machining of a beta Ti alloy; the machining operations were performed in the absence of coolant to match the requirements for green machining.

Substantial reductions in the average cutting forces, when compared to those in conventional turning with the same cutting parameters, were observed. Average cutting forces were observed to reduce in excess of 70% for depths of cut up to 0.5 mm. It is understood that such a result was desirable for high hardness alloys. Concomitant nearly full reduction of chatter was also observed as an interesting side effect. Ti-based alloys were known to show moderate to severe regenerative chatter when machined conventionally. Applying ultrasonic vibration reduced the freedom of the system and rendered the process more stable.

Higher temperatures were observed in UAT machining at all the levels of a_p tested, the process-zone temperature, however, remained below the transition temperature for this particular alloy. It was understood that the temperature difference was a parameter that appeared to be strongly material-dependant; hence, it was not possible to predict the results for different materials and even for different alloys.

A concomitant improvement was obtained in the surface quality of machine specimens. β-Ti alloys were known to generate poor quality surfaces when

conventionally cut. The studied alloy was known to produce a built-up edge on the cutting tool, chip welding, and smearing of the surface material when machined conventionally. A quantitative study of these effects was beyond the scope of this study; it was observed however, that built-up-edge formation and smearing of the surface was almost completely eliminate when machining in UAT.

Roughness of the machined surfaces was improved substantially, and depth-of-cut accuracy was improved greatly when machining in UAT. Other parameters of tribological importance showed that it was prudent to expect a different behaviour of CT- and UAT-machined surface for what concerns ability to retain a lubricant film and resistance to wear. Further tribological analyses were beyond the scope of this study.

Surface hardness was observed to increase in CT machined work-pieces while it remained close to that of the bulk material for UAT machined surfaces. This desirable effect was not expected since a higher strain rate of UAT should have produced a higher strain hardening of the material. Still, significantly lower average cutting forces generated lower parasitic forces with an ultimate effect of reducing hardening. In-depth investigations were performed to identify other possible effects of the ultrasonic vibration on the β-Ti structure. Cross-section samples were extensively analysed with optical and scanning electron microscopy in search of α-precipitates or oxygen capture with formation of α-casing structures. No visible changes were observed in the structure of sub-surface layers, which could justify the increased hardness of the CT samples. A presence of a strongly deformed hardened layer of approximately 5 μm was consistent with the increased hardness observed, and its influence was considered relatively modest because of low thickness of this layer.

The experiments demonstrated that there are some underlying physical mechanisms, which need to be revisited and looked at in some detail before their effect on the force reduction can be quantified. The progressive deformation model [Astashev & Babitsky, 2007] provides an explanation for most of the observed phenomena, leaving open questions only about the additional effects observed beyond the critical cutting velocity, which was attempted to explain with acoustic softening. Modern science does not have an adequate explanation to acoustic softening in metals and other materials. Additionally, fundamental experiments on the effect of ultrasonic vibration on the dislocation motion in metals are lacking. Still, some attempts of modelling the ultrasonic softening effect using a semi-empirical approach were made [Siddiq & Ghassemieh, 2008]. Thus, the obtained results for UAT will pose an interesting case for fundamental studies in ultrasonic processes and an eventual widespread adoption of this technology in the industry.

Future works

The necessity to reduce or eliminate coolants for green manufacturing increases the thermal load on the cutting tool, thus ultimately shortening its life if no adequate removal of heat is provided [Astakhov, 2004]. Even though UAT is a micro-chipping process, the initial observation demonstrated that the overall tool life was not seriously affected. However, if improved it could even further increase the sustainability of the machining process. It should be added, that special tools are potentially required in vibration-assisted cutting, and the expectation of using conventional tools in UAT (as has been the case so far) is, perhaps, not appropriate due to totally different regimes of tool-work-piece interaction. Further studies of tool wear and the overall tool life in UAT should be pursued in future, and UAT-dedicated

tools could be a serious advancement in the technique, which could speed-up its employment in the industry.

More investigations would be beneficial to achieve a deeper understanding of the UAT-cutting process. Ultrasonic-vibration effects on material's mechanical properties should be investigated. This would help to verify the influence of ultrasonic softening in the apparent reduction of material's hardness. Ultrasonic tests with amorphous material could ultimately rule out mobilization of dislocations effects. High-speed imaging techniques and 3D laser vibrometry could offer detailed information on a cutting cycle and vibratory modes. That data could be useful to further refine the current theoretical model of UAT. Introduction of UAT in the industry would be facilitated by further understanding of the physical mechanism underlying the process. That would help in designing UAT-cutting tools and optimizing cutting parameters.

Appendices

A1 Methodology

A methodology was developed to ensure consistent results of the machining test and to minimize the external influences that could introduce errors in the measured variables. A consistent reduction of the spread of results was observed when these guidelines were carefully followed showing importance that apparently secondary tasks or parts of the lathe could exert on the obtained results.

A1.2 Operations before machining

In order to ensure perfect reproducibility of tests and minimize every possible influence on the tests checklists were designed to ensure the best possible outcome from every machining run. Three different checklists were developed over the time, each of them dealing with a different module of the system. Early experimental tests on the Stage II prototype showed that the system behaved differently if used on a cold start or a warm one. In fact, a difference of 25 μm in the depth of cut was observed if the settings were performed on a cold lathe, which was subsequently allowed to warm up during the machining operations. Thus, it was evident that these errors should be kept to a minimum if precision in the depth of cut was required. It was also noted that the error in the work-piece centring was growing when the system was warming up after a cold start. The effect was later understood to derive from the bearing supporting the chuck of the lathe: they were designed with tolerances to prevent them to lock-up when warm. Moreover the lubricant layer,

which was almost completely resident on the bottom area of the bearing during a cold start, was observed to be spread evenly on the bearing surfaces once the system warmed up. It was observed that both the thermal expansion and the lubricant layer easily created a difference of 25 μm in the depth of cut, observed during cold and hot machining operations. This large difference gave the impulse for the development of a more organic flow of checks in the Stage III prototype.

A1.2.1 Mechanical checklist

The Stage III prototype was designed to address most of the shortcomings of the previous ones, in particular the inherent error in the setting of the depth of cut. With the accuracy of the new prototype, an error of 25 μm was unacceptable. A checklist was designed to minimize possible mechanical errors, which arise by machining with a cold lathe.

- Before each machining operation the lathe was to be run at medium speed for at least 20 minutes in order to let the lubricant in the bearings and the bearing themselves to be warmed up to operating temperature. It is important that the warm up happens at medium high speeds (it should be remembered that the four-jaw chuck installed can withstand up to 1000 rpm, but for safety reasons it was never allowed to go over 800 rpm if not for brief periods) because the low speeds are slower in warming up the lathe and bring the risk of achieving an incomplete warm-up of the machine.
- During the warm-up running, appropriate lubrication was also applied to the cross slide and feed mechanism by pulling the lubrication handle for two times while manually moving the cross slide across the slide. This would allow a consistent lubrication of the slide, which would smoothen up the feed

movement.

- Lubrication was then applied to the lathe micrometer if needed, and the micrometer was then extended to its extremities. This was to achieve a smooth setting of the depth of cut and minimize the micrometer's wear.
- The lathe inverter was then checked by sweeping the lathe speed from the minimum to maximum velocity and back. A less-than-optimal smoothness in the control of the speed could lead to errors in setting the cutting speed.
- All the safety devices of the lathe were then to be tested one by one to ensure that the machining operations could be stopped automatically or manually in case of need.
- Centring of the cutting insert was then performed with the aid of the centring point of the lathe.

All these operations require, if performed at a careful and relaxed speed, at least 10 minutes; the lathe was then let run for the following 15 minutes at its maximum speed. It is important to note that, in general, warming up the lathe with no work-piece installed resulted in the shortest total warm-up time. In fact, centring of the work-piece, would be lost anyway after the warm-up and new adjustment would be required. However, complete centring of the work-piece from scratch required more time than adjusting its lost centring. To minimize the non-machining times and optimize the process flow, the work-piece was removed from the lathe only when needed (for substitution, or measurements). Also, other operations of the following checklists were designed to be performed during the non-machining times in order to minimize the time the operator had to wait before the system was operational.

A1.2.2 Vibration checklist

The ultrasonic system, being the core technology of the UAT-system, was given full attention during the pre-machining operations. In fact, non-optimal tuning of the system or a failure in the amplification and transmission of the driving signal would not excite the resonant vibration in the ultrasonic head rendering the system ineffective. In order to address this, the ultrasonic system was set-up, checked in depth and run for at least 10 minutes during the pre-machining operations in order to warm up all its components to operating temperature, thus minimizing the frequency drift (the piezoelectric elements are sensitive to temperature changes and they seem to have a large temperature-to-frequency drift ratio). The following checklist, developed for the Stage III prototype ensures that generation of vibration is effective and the system is properly tuned and warmed up before starting the cutting operations.

- The laser vibrometer is installed firmly on the cross slide and its measuring spot is set up to the upper edge of the cutting insert. This is to prevent the necessity of moving the measuring spot for the machining operations. In fact the chip flow during the cutting operations could interrupt the laser beam, interrupting the measurement. Accumulation of dust and dirt on the lower area of the tool would lower the refractivity of the surface lowering the amplitude of the laser reflection below the level necessary to perform the measurement.
- The fixture of the cutting insert to the ultrasonic head is checked, its alignment and the torque of the fixing screw are ensured to be correct before starting vibration. An insufficient torque in the fixing screw could cause the loosening

of the tool when the ultrasonic vibration is turned on.

- The amplifier is then turned on and left running for 5 minutes to ensure that it reaches the operating temperature. At the same time this step allows enough time for a visual inspection of all the electrical connections.
- The impedance transformer is visually inspected to ensure that the ferrite core elements are not damaged or misplaced and that it is not warming up excessively (a sign that the isolation between the coils has failed).
- The signal generator is then turned on, making sure that its output is attenuated by the maximum factor. The output is gradually increased to its maximum value (10 V/p.p.) while observing the signal on the oscilloscope coming from the laser vibrometer measuring the displacement amplitude of the cutting insert's vibration.
- The optimal tuning of the system is then achieved by sweeping the signal generator frequency till the maximum amplitude of the vibration is observed. The system is then let running for 10 minutes to ensure that the transducer reaches the operating temperature performing the necessary frequency adjustments when necessary.
- At the end of the warm-up only the amplifier is switched off and temperature of each part of the system is roughly inspected: the ultrasonic head should result warm but not hot so should be the ferrite core of the impedance transformer. The cutting tool should have roughly the same temperature as the cutting head, an elevated temperature is a sign of friction between the tool holder and the tool itself, caused by an insufficient torque applied to the screw when fixing.

A1.2.3 Sensors checklist

The third and last checklist was developed to ensure perfect functioning of the data acquisition during the machining operations. This checklist is the one, which get started first, since it requires the charge amplifier to be turned on long before the other two checklists are started. The charge amplifier, in fact, warms up very slowly, requiring to be turned on up to 6 hours before the machining operations in order to reach the operating temperature and avoid excessive drift, which would introduce large errors in the force measurement readings.

- Approximately 2 hours (but up to 6 hours) before any measurement, the charge amplifier is turned on and left to reach its operating temperature (once it reaches it the current drift on the Picoscope slows to zero). The high-amplification low-noise operational amplifier present is, in fact, extremely sensitive to temperature and could show excessive drift if not properly warmed up.
- The leads connecting the dynamometer to the charge amplifier are inspected, the computer its turned on and the picoscope is connected.
- After approximately 5 minutes the dynamometer is gently tapped in the three different directions and its responses checked on the computer screen. If abnormalities are detected, a second inspection of the leads is then performed.
- The vibrometer is connected to the picoscope and the vibration signal is analysed, small frequency adjustments are performed.
- The cutting speed is detected with the laser tachometer by measuring directly on the mounted work-piece, and the lathe is readied for the machining

operations.

A3 Surface analysis

The following results are the raw data of the surface measurements for all the a_p in this study.

	Rz	Ra	Rsk	Rku	PSm	P3z	Ssk	Sku	Sa	Spd
	8.49	2.13	-0.0381	1.75	104	8.29	0.593	2.88	2.02	120
	7.92	1.92	0.434	1.89	89.9		0.28	2.96	1.89	106
	7.64	1.75	-0.344	1.82	74.3	7.33	-0.185	2.3	1.97	165
	9.53	1.65	0.507	2.94	134		0.213	2.04	3.14	352
100 CT	9.28	1.44	0.743	3.31	172	11.5	0.692	2.65	2.49	145
	7.19	1.82	0.505	1.79	63.9	6.28	0.133	2.55	1.91	399
	6.56	1.13	0.715	3.11	165	9.5	0.425	2.69	2.62	112
	8.54	1.96	0.721	2.29	105		0.28	2.25	1.69	213
	7	1.67	0.0178	1.81	103		-0.0333	2.44	2.1	142
STD	**1.02312**	**0.298012**	**0.39088**	**0.641004**	**37.59861**	**16.55391**	**0.280079**	**0.301515**	**0.458203**	**107.9542**
AVG	**8.016667**	**1.718889**	**0.3623**	**2.301111**	**112.3444**	**8.58**	**0.266411**	**2.528889**	**2.203333**	**194.8889**
	6.28	1.12	0.26	2.63	55.2	6.46	0.774	4.92	1.25	725
	6.03	0.933	0.849	3.34	75	5.83	0.674	3.52	1.2	719
	10.6	1.33	0.729	4.08	42.1		1.82	8.5	1.66	673
	7.52	1.53	0.412	2.17	73.5	8.09	0.994	4.22	1.36	1055
100 UAT	4.48	0.809	1.07	3.55	103	7.45	2.1	9.59	2.21	330
	6.32	1.09	0.24	2.41	55.4	6.03	0.798	4.73	1.51	668
	6.46	1.27	0.427	2.43	72.9	8.46	0.909	4.17	1.67	578
	5.66	0.789	0.349	3.18	56.3	6.83	0.604	3.59	1.59	350
	5.37	0.875	0.678	3.08	75.5	7.02	0.806	4.3	1.24	943
STD	**1.739656**	**0.256047**	**0.287781**	**0.624522**	**17.72619**	**7.626083**	**0.531252**	**2.197907**	**0.316719**	**238.3914**
AVG	**6.524444**	**1.082889**	**0.557111**	**2.985556**	**67.65556**	**7.02125**	**1.053222**	**5.282222**	**1.521111**	**671.2222**

	Rz	Ra	Rsk	Rku	PSm	P3z	Ssk	Sku	Sa	Spd
	8.66	1.91	0.0454	1.88	99.4	7.9	0.133	2.11	2.08	117
	6.58	1.58	0.0106	1.74	148	12	-0.0593	2.49	2.6	86.7
	7.44	1.97	0.444	1.75	97.9	9.69	0.0903	2.29	2.24	103
	6.43	1.57	-0.227	1.67	84.4	10.2	0.286	2.58	2.04	182
200 CT	6.81	1.02	-0.0093	3.15	116		-0.0278	3.01	1.74	154
	7.99	2.07	0.0725	1.6	96.1		0.301	2.28	2.09	120
	8	1.78	0.423	2	101	7.98	0.108	2.21	1.88	258
	8.89	2.04	0.334	1.97	98.1	8.75	0.184	1.91	2.1	108
	6.34	1.63	-0.115	1.68	103	8.96	-0.274	2.82	2.5	128
STD	**0.972754**	**0.32909**	**0.23811**	**0.474915**	**18.10668**	**7.877394**	**0.180998**	**0.34905**	**0.273059**	**52.66602**
AVG	**7.46**	**1.73**	**0.108689**	**1.937778**	**104.8778**	**9.354286**	**0.082356**	**2.411111**	**2.141111**	**139.6333**
	7.7	1.3	0.274	2.92	35.6	6.68	1.64	14.1	1.29	502
	5.55	0.901	0.7	3.58	52.6	6.17	0.465	3.5	1.18	1159
	3.86	0.698	0.106	2.38	37.1	5.91	0.0477	3.43	1.23	891
	5.61	0.883	0.793	3.13	57.1	6.56	0.571	4.03	1.27	630
200 UAT	4.01	0.719	0.795	3.13	45.4	4.95	0.287	3.41	1.03	806
	7.32	1.04	1.05	4.48	106	8.54	0.156	3.14	1.87	488
	10.3	1.17	1.91	7.52	57.1		0.403	4.73	1.09	793
	4.72	0.819	0.672	3.11	63.5	6.04	0.457	3.72	0.906	1331
	4.66	0.488	0.244	5.01	29.5	4.21	3.46	45	0.989	276
STD	**2.104834**	**0.250478**	**0.540913**	**1.575324**	**22.67521**	**9.670096**	**1.08719**	**13.77431**	**0.281696**	**334.8821**
AVG	**5.97**	**0.890889**	**0.727111**	**3.917778**	**53.76667**	**6.1325**	**0.831856**	**9.451111**	**1.206111**	**764**

	Rz	Ra	Rsk	Rku	PSm	P3z	Ssk	Sku	Sa	Spd
	4.52	0.907	0.447	2.15	162	6.67	-0.106	3.12	1.32	141
	5.16	1.17	0.0367	1.83	119	8.59	-0.104	2.54	2.02	117
	4.55	0.994	0.101	1.97	161	7.24	0.00758	3.08	1.5	95
	4.95	1.11	0.388	2.08	172	8.99	0.0501	2.4	1.91	123
300 CT	4.58	1.04	0.146	1.97	87.5	5.7	0.222	2.58	1.27	260
	5.28	1.11	0.0171	1.98	85.4	4.99	0.0828	2.41	1.18	321
	5.04	1.02	-0.309	2.22	347	10.6	-0.0796	2.29	2.26	100
	4.26	1.02	0.213	1.74	119	6.96	-0.162	2.61	1.74	118
	5.24	1.02	0.522	2.32	85.7	7.91	0.451	3.61	1.92	89.6
STD	**0.370566**	**0.077135**	**0.256373**	**0.184014**	**81.91418**	**1.723804**	**0.194355**	**0.4368**	**0.378517**	**81.71098**
AVG	**4.842222**	**1.043444**	**0.173533**	**2.028889**	**148.7333**	**7.516667**	**0.040209**	**2.737778**	**1.68**	**151.6222**
	5.93	0.88	1.37	5	59.1	6.58	0.882	6.37	1.51	249
	4.31	0.778	0.241	2.41	51.9	6.29	-0.0682	2.9	1.24	499
	6.05	0.897	0.446	3.06	74.8	7.46	0.328	3.54	1.36	309
	6.04	0.839	0.445	3.74	47.4	5.65	0.208	3.59	1.14	748
300 UAT	6.45	1.19	0.663	3.06	51.6	5.01	0.441	3.8	1.23	806
	5.31	0.831	0.874	3.06	52.4	4.75	-0.0106	3.3	1.03	1523
	5.99	1.06	0.475	2.62	57.4		0.708	3.99	1.34	602
	5.74	0.922	0.0965	2.79	85.4	7.13	0.389	3.54	1.94	642
	3.92	0.657	0.457	2.68	42.9	3.89	1.58	10.5	0.974	408
STD	**0.860334**	**0.155231**	**0.375145**	**0.78846**	**13.62158**	**1.23947**	**0.508625**	**2.418688**	**0.289767**	**380.2021**
AVG	**5.526667**	**0.894889**	**0.563056**	**3.157778**	**58.1**	**5.845**	**0.495244**	**4.614444**	**1.307111**	**642.8889**

	Rz	Ra	Rsk	Rku	PSm	P3z	Ssk	Sku	Sa	Spd
	5.38	1.01	0.56	2.54	76.6	5.75	-0.00523	2.45	1.49	222
	5.26	0.982	0.625	2.5	81.8	7.27	0.0432	2.93	1.74	64.2
	4.73	0.857	0.757	2.9	87.8	6.43	-0.006	3.71	1.24	300
	6.21	1.17	0.014	2.09	195	13.7	0.533	2.3	3.26	89.1
400 CT	5.73	0.991	0.626	2.51	87.9	5.22	-0.262	2.77	1.34	333
	5.27	0.939	0.673	2.96	87.5	5.56	-0.269	2.59	1.94	209
	4.32	0.868	0.389	2.29	88.6	8.01	-0.298	2.39	2.12	390
	5	0.938	0.236	2.21	55.3		0.213	2.62	1.42	654
	4.1	0.82	0.417	2.28	117	8.4	0.243	2.99	1.68	249
STD	**0.662956**	**0.104387**	**0.237593**	**0.298459**	**39.86869**	**2.744291**	**0.277523**	**0.429622**	**0.616157**	**175.9094**
AVG	**5.111111**	**0.952778**	**0.477444**	**2.475556**	**97.5**	**7.5425**	**0.02133**	**2.75**	**1.803333**	**278.9222**
	4.79	0.816	1	3.16	59.7	5.12	0.869	5.06	1.05	403
	5.45	1.09	0.574	2.46	62.2	5.63	0.269	3.09	1.06	1308
	5.89	1.17	0.608	2.55	60	6.82	0.195	2.92	1.39	1241
	5.24	0.875	0.0755	2.62	82.9	5.7	0.108	2.65	1.48	1233
400 UAT	4.13	0.882	0.655	2.45	57.9	5.68	0.851	4.27	1.16	932
	4.78	0.847	0.616	2.82	103	8.9	0.917	4.07	1.51	510
	4.76	0.959	0.312	2.41	54.4	5.58	0.434	3.39	1.18	285
	5.09	0.979	0.439	2.49	75.1	5.7	0.363	3.16	1.12	1173
	7.58	1.35	1.08	3.43	58.9	7.69	0.868	4.8	1.41	476
STD	**0.987907**	**0.176183**	**0.31189**	**0.359722**	**15.94224**	**1.246244**	**0.330966**	**0.865358**	**0.183833**	**417.4352**
AVG	**5.301111**	**0.996444**	**0.5955**	**2.71**	**68.23333**	**6.313333**	**0.541556**	**3.712222**	**1.262222**	**840.1111**

	Rz	Ra	Rsk	Rku	PSm	P3z	Ssk	Sku	Sa	Spd
	4.37	0.796	0.165	2.54	82.9	6.72	-0.109	2.56	1.57	145
	3.65	0.702	0.308	2.29	378	9.26	0.0127	2.11	2.22	490
	5	0.826	0.217	2.07	62	4.51	0.00807	2.79	1.4	429
	4.82	1.01	-0.314	2.04	65	5.83	-0.244	2.85	1.55	1041
500 CT	3.96	0.706	0.15	2.35	149	8.56	0.177	2.65	1.84	375
	5.79	0.912	-0.453	3.18	62.8	7.95	-0.0686	2.74	1.32	456
	5.66	1.03	0.46	2.94	223		0.699	4.45	3.07	145
	4.31	0.98	0.515	1.84	71.6	7.49	0.254	2.95	1.59	104
	4.6	0.872	0.24	2.29	101	6.5	-0.678	3.77	1.6	145
STD	**0.718768**	**0.123287**	**0.325112**	**0.432724**	**106.2295**	**1.535166**	**0.374197**	**0.701643**	**0.545507**	**295.4179**
AVG	**4.684444**	**0.870444**	**0.143111**	**2.393333**	**132.8111**	**7.1025**	**0.005686**	**2.985556**	**1.795556**	**370**
	7.28	1.12	0.41	3.06	49.3	7.11	0.629	3.58	1.39	1332
	6.09	1.11	0.118	2.28	107	9.1	-0.364	3.13	2.21	1452
	4.13	0.779	0.937	3.01	75.5	6.35	1.95	21.7	1.5	372
	7.03	1.24	0.665	3.47	74.5	7.15	0.427	2.85	1.6	620
500 UAT	5.7	1.11	0.954	2.76	82.9		0.626	3.81	1.59	697
	6.37	1.21	0.732	2.59	76.7	8.75	-0.0026	2.54	1.84	966
	8.43	1.31	0.836	3.78	102	7.29	0.132	3.35	1.3	671
	9.2	1.77	0.731	2.89	85.1	10	0.604	2.88	2.19	529
	6.75	0.859	0.884	4.43	74.1	9.1	0.448	2.88	1.77	338
STD	**1.488507**	**0.284022**	**0.273622**	**0.657161**	**16.88383**	**1.289152**	**0.641103**	**6.203589**	**0.324423**	**396.8434**
AVG	**6.775556**	**1.167556**	**0.696333**	**3.141111**	**80.78889**	**8.10625**	**0.494378**	**5.191111**	**1.71**	**775.2222**

References

AB Sandvik Coromant, Tofters Tryckeri AB, ed. (1994), Modern Metal Cutting, Sandvik Coromant, Technical Editorial dept..

Ahmed, N.; Mitrofanov, A.; Babitsky, V. & Silberschmidt, V. (2006), 'Analysis of material response to ultrasonic vibration loading in turning Inconel 718', Material Science and Engineering A 424, 318-325.

An, Q.; Fu, Y. & Xu, J. (2011), 'Experimental study on turning of TC9 titanium alloy with cold water mist jet cooling', International Journal of Machine Tools and Manufacture 51-6, 549-555.

Anon, M. (2001), 'Cutting and milling system utilizing ultrasonic vibrations', New Technology Japan 28-12, 35.

Arrazola, P.-J.; Garay, A.; Iriarte, L.-M.; Armendia, M.; Marya, S. & Maître, F. L. (2009), 'Machinability of titanium alloys (Ti6Al4V and Ti555.3)', Journal of Materials Processing Technology 209, 2223-2230.

Astakhov, V. (2004), 'The assessment of cutting tool wear', International Journal of Machine Tools & Manufacture 44, 637-647.

Astashev, V. (1992), 'Effect of ultrasonic vibrations of a single point tool on the process of cutting', Journal of Machinery Manufacture and Reliability 5, 65-70.

Astashev, V. & Babitsky, V. (1998), 'Ultrasonic cutting as a non-lineal (vibro-impact) process', Ultrasonics 36, 89-96.

Astashev, V. & Babitsky, V. (2007), Ultrasonic Processes and Machines, Springer.

Babikov, O. (1960), Ultrasonics and its industrial applications, Consultants Bureau.

Babitsky, V.; Kalashnikov, A.; Meadows, A. & Wijesundara, A. (2003), 'Ultrasonically assisted turning of aviation materials', Journal of Materials Processing Technology 132, 157-167.

Babitsky, V.; Mitrofanov, A. & Silberschmidt, V. (2004), 'Ultrasonically assisted turning of aviation materials: simulations and experimental study', Ultrasonics 42, 81-86.

Basti, A.; Obikawa, T. & Shinozuka, J. (2007), 'Tools with built-in thin film thermocouple sensors for monitoring cutting temperature', International Journal of Machine Tools and Manufacture 47, 793-798.

Boothroyd, G. & Knight, W.; 7852-9, I. 0.-8247., ed. (1989), Fundamentals of metal machining and machine tools, Marcel Dekker.

Brehl, D. & Dow, T. (2008), 'Review of vibration-assisted machining', Precision Engineering 32, 153-172.

Byrne, G. & Scholta, E. (1993), 'Environmentally Clean Machining Processes — A Strategic Approach', CIRP Annals - Manufacturing Technology 42-1, 471-474.

Chandrasekaran, H. (1976), 'Friction in machining - Comparison of rake and flank wear-land friction', Wear 36, 133-145.

Childs, T.; Richings, D. & Wilcox, A. (1972), 'Metal cutting: Mechanics, surface physics and metallurgy', International Journal of Mechanical Sciences 14, 359-368.

David, J. & Cheeke, N., (2002), Fundamentals and applications of ultrasonic waves, CRC Press.

Davies, M.; Cooke, A. & Larsen, E. (2005), 'High bandwidth thermal microscopy of

machining AISI 1045 Steel', CIRP Annals - Manufacturing Technology 54, 63-66.

Devine, J. (1979), 'Ultrasonically assisted metal removal', Society for the Advancement of Materials Process Engineering 10, 485-496.

DMG (2010), 'DMG D4839/0210ND1; Ultrasonic Series; ULTRASONICS hard machining and milling on one machine'.

Dodonov, A.; Siemers, C. & Rosler, J. (2009), 'Analyses of the processing and machining characteristics of Ti15V3Al3Sn3Cr alloy''International Conference on Modern Practice in Stress and Vibration Analyses'.

Donachie, M. (2000), Titanium: a technical guide, ASM International.

Ezugwu, E. (2005), 'Key improvements in the machining of difficult-to-cut aerospace superalloys', International Journal of Machine Tools and Manufacture 45-12-13, 1353-1367.

Ezugwu, E.; Bonney, J. & Yamane, Y. (2003), 'An overview of the machinability of aeroengine alloys', Journal of Materials Processing Technology 134-2, 233-253.

Frederick, J., (1965), Ultrasonic engineering, John Wiley & Sons Inc..

Gadelmawla, E.; Koura, M.; Maksoud, T.; Elewa, I. & Soliman, H. (2002), 'Roughness parameters', Journal of Materials Processing Technology 123-1, 133-145.

Gao, G.; Zhao, B.; Jiao, F. & Liu, C. (2002), 'Research on the influence of the cutting conditions on the surface microstructure of ultra-thin wall parts in ultrasonic vibration cutting', Journal of Materials Processing Technology 129, 66-70.

GfE; Metalle & Materialien (2011), 'http://www.gfe.com/', GfE Metalle Materialien.

Grzesik, W. & Nieslony, P. (2000), 'Thermal characterization of the chip-tool interface

when using coated turning inserts', Journal of Manufacturing Processes 2, 79-87.

Guzzo, P.; Shinohara, A. & RaslanI, A. (2004), 'A comparative study on ultrasonic machining of hard and brittle materials', Journal of the Brazilian Society of Mechanical Sciences and Engineering 26, 56-61.

Han, L.; Xu, W. & Tso, S. (1998), 'Ultrasonically assisted and piezoelectric actuators integrated cutting tool', Japanese Journal of Applied Physics 37, 4616-4619.

Hoffmeister, H.-W. (2010), private communications.

Hope, D. (1977), 'Cutting fluids - pet or pest?: A review of staining and corrosion tendencies and effects on machine tool paints and seals', Tribology International 10-1, 23-27.

Hsu, C.; Lin, Y.; Lee, W. & Lo, S. (2008), 'Machining characteristics of Inconel 718 using ultrasonic and high temperature-aided cutting', Journal of Material Processing Technology 198, 359-365.

Inman, D. J. (2008), Engineering Vibration, Pearson Prentice Hall.

Isaev & Anochin (1961), 'Vestnik Mashinostroenya', Vestnik Mashinostroenya 5, 56.

Jin, M. & Murakawa, M. (2001), 'Development of a practical ultrasonic vibration cutting tool system', Journal of Materials Processing Technology 113, 342-347.

Kim, J. & Choi, I. (1997), 'Micro surface phenomenon of ductile cutting in the ultrasonic vibration cutting of optical plastics', Journal of Materials Processing Technology 68, 89-98.

Kim, J. & Choi, I. (1998), 'Characteristics of chip generation by ultrasonic vibration cutting with extremely low cutting velocity', International Journal of Advanced Manufacturing Technology 68, 89-98.

Kim, J. & Lee, E. (1996), 'A study of ultrasonic vibration cutting of carbon fibre reinforced plastics', International Journal of Advanced Manufacturing Technology 12, 78-86.

Kistler (2011), 'http://www.kistler.com/', Kistler Kiag.

Klocke, F. & Eisenblätter, G. (1997), 'Dry cutting', CIRP Annals - Manufacturing Technology 46-2, 519-526.

Klocke, F. & Rubenach, O. (2000), 'Ultrasonic-assisted diamond turning of glass and steel', Industrial Diamond Review 60, 227-239.

Kong, C. Y.; Soar, R. C. & Dickens, P. M. (2004), 'Ultrasonic consolidation for embedding SMA fibres within aluminium matrices', Composite Structures 66, 421-427.

Korsunsky, A. (2012), private communications.

Korzynski, M.; Zarski, T. & Korzynska, K. (2011), 'Surface layer condition and the fatigue strength of an AZ91 alloy after ball peening', Journal of Materials Processing Technology 211, 1982вЂ“1988.

Kremer, D. (1995), 'Ultrasonically assisted machining', Mecanique Industrielle et Materiaux. 48, 15-21.

Kubota, M.; Tanura, J. & Shimamura, N. (1977), 'Bulletting of Japanese Society of Precision Engineering', Proceedings of the 4th International Conference on Progress of Cutting and Grinding 1(11), 327-330.

Kumabe, J. (1979), 'Vibratory cutting', Dzikke Sjuppan, Tokyo.

Kumabe, J.; Fuchizawa, K.; Soutome, T. & Nishimoto, Y. (1989), 'Ultrasonic superposition vibration cutting of ceramics', Precision Engineering Nanotechnology

11, 71-77.

Kumabe, J. & Hachisuka, M. (1984), 'Super-precision cylindrical machining', Precision Engineering 6, 67-72.

Leach, R. & Haitjema, H. (2010), 'Bandwidth characteristics and comparisons of surface texture measuring instruments', Measurement Science and Technology 21.

Lucas, M.; Graham, G. & Smith, A. (1996), 'Enhanced vibration control of an ultrasonic cutting process', Ultrasonics 34, 205-211.

Machai, C. & Biermann, D. (2011), 'Machining of β-titanium-alloy Ti–10V–2Fe–3Al under cryogenic conditions: Cooling with carbon dioxide snow', Journal of Materials Processing Technology 211, 1175вЂ“1183.

MaMiNa (2010a), 'Chip Formation of Titanium Alloy', Internal technical report, MaMiNa - Scientific Programme.

MaMiNa (2010b), 'Material Properties of Titanium Alloy', Internal technical report, MaMiNa - Scientific Programme.

Markov, A. (1996), 'Optimal ultrasonic cutting of hard-to-work materials', Russian Engineering Research C/C of Vestnik Mashinostroeniia And Stanski Instrument 16, 26-31.

Markov, A. (1966), Ultrasonic machining of intractable materials, London Iliffe Books Ltd..

Mativenga, P. & Rajemi, M. (2011), 'Calculation of optimum cutting parameters based on minimum energy footprint', CIRP Annals - Manufacturing Technology 60-1, 149-152.

Maurotto, A.; Roy, A.; Babitsky, V. & Silberschmidt, V. (2012), 'Analysis of

machinability of Ti and Ni based superalloys', Solid State Phenomena 188, 330-338.

Maurotto, A.; Roy, A.; Babitsky, V. & Silberschmidt, V. (2010), 'Recent developments in ultrasonically assisted machining of advanced alloys''Proceedings of 4th CIRP International Conference on High Performance Cutting Vol. 2 ; 0 ; 81-84'.

Merchant, M. (1945), 'Mechanics of the metal cutting process', Journal of Applied Physics 16, 318-324.

Mitrofanov, A. (2004), 'Modelling the ultrasonically assisted turning of high-strength alloys', PhD thesis, Wolfson School of Mechanical and Manufacturing Engineering, Loughborough University, UK.

Mitrofanov, A.; Ahmed, N.; Babitsky, V. & Silberschmidt, V. (2005), 'Effects of lubrication and cutting parameters on ultrasonically assisted turning of Inconel 718', Journal of Materials Processing Technology 162-163, 649-654.

Mitrofanov, A.; Babitsky, V. & Silberschmidt, V. (2005), 'Thermomechanical finite element simulations of ultrasonically assisted turning', Computational Materials Science 32, 463-471.

Mitrofanov, A.; Babitsky, V. & Silberschmidt, V. (2003), 'Finite element simulations of ultrasonically assisted turning', Computational Materials Science 28, 645-653.

Mori Seiki (2012), private communications.

Moriwaki, T. & Shamoto, E. (1991), 'Ultraprecision diamond turning of stainless steel by applying ultrasonic vibration', 'Annals of the CIRP', 559-562.

Moriwaki, T.; Shamoto, E. & Inoue, K. (1992), 'Ultraprecision ductile cutting of glass by applying ultrasonic vibration''Annals of CIRP', 141-144.

Muhammad, R.; Maurotto, A.; Demiral, M.; Roy, A. & Silberschmidt, V. (2011a), '3D

finite element analysis of ultrasonically assisted turning of modern alloys"International Conference on Computational and Experimental Engineering and Sciences'.

Muhammad, R.; Maurotto, A.; Demiral, M.; Roy, A. & Silberschmidt, V. (2011b), 'Numerical study on hot ultrasonically assisted turning of Ti alloy"IWCMM 2011'.

Muhammad, R.; Maurotto, A.; Roy, A. & Silberschmidt, V. (2011c), 'Characterization of thermomechanical loads in vibro-impact machining of advanced alloys"International Conference on Advances in Experimental Mechanics: Integrating Simulation and Experimentation for Validation'.

Muhammad, R.; Maurotto, A.; Roy, A. & Silberschmidt, V. (2011d), 'Analysis of forces in vibro-impact and hot vibro-impact turning of advanced alloys', Applied Mechanics and Materials 70, 315-320.

Muhammad, R.; Ahmed, N.; Roy, A. & Silberschmidt, V. (2012), 'Numerical Modelling of Vibration-Assisted Turning of Ti-15333', Procedia CIRP 1, 347-352.

Muraka, P.; Barrow, G. & Hinduja, S. (1979), 'Influence of the process variables on the temperature distribution in orthogonal machining using the finite element method', International Journal of Mechanical Sciences 21, 445-456.

Oxley, P.Ellis Horwood, I.; (1989), Mechanics of machining, Chichester.

O'Sullivan, D. & Cotterell, M. (2001), 'Temperature measurement in single point turning', Journal of Materials Processing Technology 118, 301-308.

Polytech (2011), 'http://www.polytec.de/uk/', Polytech GmbH.

Puskar, A.; (1982), The use of high intensity ultrasonics, Elsevier scientific publishing company.

Rokicki, P.; Nowag; K.; Spotz; Z.; Fusova; L.; Saksl; K.; Ghisleni, R. & Siemers, C. (2010), 'Microstructural characteristic of Ti-15V-3Al-3Sn-3Cr chips', Rudy i metale nieżelazne 55, 452-456.

Rowe, G. & Spick, P. (1967) in Trans ASME 89B.

SECO (2011), 'http://ecat.secotools.com/', SECO - Web Catalog.

Shamoto, E. & Moriwaki, T. (1999), 'Ultaprecision diamond cutting of hardened steel by applying elliptical vibration cutting', CIRP Annals - Manufacturing Technology 48/1, 441-444.

Shamoto, E.; Ma, C. & Moriwaki, T. (1999), 'Ultraprecision ductile cutting of glass by applying ultrasonic elliptical vibration cutting', Precision Engineering Nanotechnology 1, 408-411.

Sharman, A.; Bowen, P.; Aspinwall, D. & Dewes, C. (2001), 'Workpiece surface integrity considerations when finish turning gamma titanium aluminide', Wear 249, 473-481.

Shoh, A. (1975), 'Industrial applications of ultrasound—a review: 1. High-power ultrasound', IEEE Transactions on Sonics and Ultrasonics 22-2, 60-71.

Siemers, C. (2012), private communications.

Siemers, C.; Zahra; B.; Leemet, T. & Roesler, J. (2009), 'Development of Advanced beta-Titanium Alloys''Proceedings of the 8th International Advanced Metal Materials and Technologies Conference' Beijing, China.

Singh, R. & Khamba, J. (2007), 'Investivation for ultrasonic machining of titanium and its alloys', Journal of Materials Processing Technology 183, 363-367.

Singh, R. & Khamba, J. (2006), 'Ultrasonic machining of titanium and its alloys: A

review', Journal of Materials Processing Technology 173, 125-135.

Skelton, C. (1969), 'Effect of ultrasonic vibration on the turning process', International Journal of Machine Tool Design and Research 9, 363-374.

Su, Y.; Wang, L.; Luo, L.; Jiang, X.; Guo, J. & Fu, H. (2009), 'Deoxidation of Titanium alloy using hydrogen', International Journal of Hydrogen Energy 34, 8958-8963.

Sun, S.; Brandt, M. & Dargusch, M. (2009), 'Characteristics of cutting forces and chip formation in machining of titanium alloys', International Journal of Machine Tools and Manufacture 49, 561-568.

Sun, J. & Guo, Y.B. (2009), 'A comprehensive experimental study on surface integrity by end milling Ti-6Al-4V', Journal of Materials Processing Technology 209-8, 4036-4042.

Suzuki, H.; Hamada, S.; Okino, T.; Kondo, M.; Yamagata, Y. & Higuchi, T. (2010), 'Ultraprecision finishing of micro-aspheric surface by ultrasonic two-axis vibration assisted polishing', CIRP Annals - Manufacturing Technology 59, 347-350.

Takeyama, H. & Lijima, N. (1988), 'Machinability of glassfiber reinforced plastics and application of ultrasonic machining''Annals of CIRP'.

Thoe, T.; Aspinwall, D. & Wise, M. (1998), 'Review on ultrasonic machining', International journal of Machine tools and Manufacturing 38, 239-255.

Thomas, P. & Babitsky, V. (2007), 'Experiments and simulations on ultrasonically assisted drilling', Journal of Sound and Vibrations 308, 815-830.

Ugarte, A.; M'Saoubi, R.; Garay, A. & Arrazola, P. (2012), 'Machining behaviour of Ti-6Al-4 V and Ti-5553 alloys in interrupted cutting with PVD coated cemented carbide', Procedia CIRP 1, 202-207.

Voronina, S. & Babitsky, V. (2008), 'Autoresonant control strategies of loaded ultrasonic transducer for machining applications', Journal of Sound and Vibrations 313, 395-417.

Wang, L.-J. (1992), 'The tree states of unseparating zone in ultrasonic vibration cutting', Science in China 35(A), 1110.

Wang, X.; Zhou, M.; Gan, J. & Ngoi, B. (2002), 'Theoretical and experimental studies of ultraprecision machining of brittle materials with ultrasonic vibration', International Journal of Advanced Manufacturing Technology 20, 99-102.

Weber, H. & Piltz, J. H. R. (1984), 'Turning of machinable glass ceramics with an ultrasonically vibrated tool''Annals of CIRP', 85-87.

Weinert, K.; Inasaki, I.; Sutherland, J. & Wakabayashi, T. (2004), 'Dry Machining and Minimum quantity lubrication''CIRP Annals - Manufacturing Technology, 53-2, 511-537'.

Xiao, M.; Sato, K.; Karube, S. & Soutome, T. (2003), 'The effect of tool nose radius in ultrasonic vibration cutting of hard metal', International Journal of Machining Tools & Manufacturing 43, 1375-1382.

Yang, J.; Zhang, Y. & Yang, S. (1998), 'Ultrasonic vibration turning of aluminum matrix composites', Progress of Cutting and Grinding, Urumqi and Turpan, China; CHINA; 5-9 Oct. 1998. pp. 327-330

Zhou, M.; Eow, Y.; Ngoi, B. & Lim, E. (2003), 'Vibration-assisted precision machining of steel with PCD tools', Materials and Manufacturing Processes 18, 825-834.